AD NUMBER: AD0837604
LIMITATION CHANGES
TO: Approved for public release; distribution is unlimited.
FROM: Distribution authorized to US Government agencies and their contractors; Export Controlled; Critical Technology; 1 Jul 1968. Other requests shall be referred to Rome Air Development Center, Griffiss AFB, NY 13440.
AUTHORITY
RADC, USAF ltr dtd 31 Jan 1974

RADC-TR-68-49
Final Report

DESIGN STUDY OF A LIGHT MODULE FOR A PHOTOGRAMMETRIC CAMERA CALIBRATION RANGE

Edward B. Jay

Aerospace Controls Corporation

TECHNICAL REPORT NO. RADC-TR-68-49
July 1968

Rome Air Development Center
Air Force Systems Command
Griffiss Air Force Base, New York

DESIGN STUDY OF A LIGHT MODULE FOR A PHOTOGRAMMETRIC CAMERA CALIBRATION RANGE

Edward B. Jay

Aerospace Controls Corporation

AFLC, GAFB, N.Y., 5 Aug 68-73

FOREWORD

This final technical report was prepared by Aerospace Controls Corporation, 215 West 131 St., Los Angeles, California under Air Force Contract F30602-67-C-0350, Project 698DB Task 698DB00. The number assigned to the report by the contractor was P-575. The work was administered under the direction of the Rome Air Development Center, EMIRA, Griffiss Air Force Base, N. Y. 13440, Frank Scarano, project engineer.

The studies herein were initiated in June, 1967 and concluded in January 1968. The research activity was carried out by Edward B. Jay, Chief Physicist.

Aerospace Controls Corporation is indebted to the Eastman-Kodak Company for permission to use Figures 17, 18 and 19 extracted from Kodak Publication Number M-29, "Kodak Data for Aerial Photography".

This technical report has been reviewed and is approved.

Approved: Frank A. Scarano
FRANK A. SCARANO
Project Engineer

Approved: Howard Davis
JAMES J. DIMEL
Colonel, USAF
Chief, Intel & Infor Proc Div

FOR THE COMMANDER: Irving J. Gabelman
IRVING J. GABELMAN
Chief, Advanced Studies Group

ABSTRACT

A design study of a light module for a night photogrammetric camera calibration range was performed. It was determined that a ground-based light source can be used to spatially calibrate aerial cameras to within three microns at the film plane. This is accomplished by incorporating a low energy (2.5 joule), pulsed, xenon flash lamp and various factory-stocked films for the calibration procedure.

A photogrammetric test range designed on the principles discussed herein appears to be quite feasible and useful in calibrating almost every type of aerial camera.

BLANK PAGE

TABLE OF CONTENTS

Section	Title	Page
I.	INTRODUCTION	1
II.	ATMOSPHERIC EFFECTS	4
	A. Attenuation	4
	B. Absorption by Atmospheric Particles	19
	C. Contrast Degradation	19
	1. Scattering	19
	2. Degradation Due to Turbulence Effects	24
III.	CASA GRANDE CLIMATOLOGICAL CONDITIONS	47
	A. Temperature	47
	B. Precipitation and Humidity	48
	C. Cloud Cover Statistics	49
	D. Wind Conditions	49
	E. Conclusion	49
IV.	FILM CHARACTERISTICS	52
	A. Spectral Characteristics	53
	B. Sensitivity	59
	C. Graininess	60
	D. Contrast	67
	E. Choice of Film	68

Table of Contents (cont.)

V.	COMPARISON OF TEST RANGE CONCEPTS	77
	A. Passive Test Range	77
	B. Active Test Range	84
VI.	DESIGN OF THE PHOTOGRAMMETRIC TEST RANGE LIGHT MODULE	86
	A. Source Energy and Power Requirements	87
	B. Lamp/Camera Synchronization and Source Average Power	89
	C. Selection of Lamp	90
	D. Control of System	93
	E. Light Collector Design	98
	F. Pulse Circuitry	101
	1. General Design	103
	G. Prime Power Supply	126
VII.	CONCLUDING REMARKS	130
	References	131

LIST OF FIGURES

Number	Title	Page
1	Rayleigh scattering cross-section versus wave-length	7
2	Representative profile, aerosol number density vs altitude	9
3	Aerosol attenuation coefficients at sea level	10
4	Atmospheric transmission from h=0 to h=11 km. Includes Rayleigh and MIE scattering and Ozone absorption.	12
5	Ratio of scattered to coherent intensity vs optical thickness τ	17
6	Cloud transmittance vs optical thickness	18
7	Fog-rain attenuation $\lambda = 0.63\mu$	20
8A	Atmospheric transmission, 0.3 to 1.3 microns	21
8B	Atmospheric transmission, 1.2 to 5.0 microns	22
9	Fine structure of atmosphere around 6943Å (after Long)	23
10	Polar diagrams for the scattering of linearly polarized light by a spherical particle	25
11	Power reduction in an optical hetrodyne receiver caused by loss of phase coherence (after Fried)	29
12	Dependence of coherence length, γ_o, on zenith angle, ϕ, and wavelength, λ, (after Fried)	31
13	Diameter of wavefront, ρ, vs standard deviation in angle of arrival, σ_θ, for intermediate turbulence	33
14	Beam spreading in intermediate turbulence	36

Number	Title	Page
15A	Range, R, vs rms deviation in normalized differential power received, σ_p, for intermediate turbulence	43
15B	Range, R, vs rms deviation in normalized differential power received, σ_p, for intermediate turbulence	44
15C	Range, R, vs rms deviation in normalized differential power received, σ_p, for intermediate turbulence	45
16	Normal rainfall in Phoenix, Arizona	50
17	Spectral characteristics of Various films	54
18	Characteristic curves of various films	61
19	Contrast of films vs time	69
20	Air-ground communications link	96
21A	Block diagram - Airborne System	97
21B	Block diagram - Ground Control Station	97
21C	Block diagram - Mountaintop Relay Station	97
22	Block diagram of site communications system	99
23	Block diagram of pulse circuitry	105
24	Pulse forming network	107
25	Pulse forming network	108
26	Lamp triggering circuitry	110
27	Thyratron trigger circuit	112
28	DC-DC Converter	114
29	Hysteresis curve of transformer	115
30	Circuit voltage and current waveforms	117
31	Transformer equivalent circuit	118

Number	Title	Page
32	Common collector auto transformer configuration	121
33	Dual transformer power converter	123
34	Collector current of single transformer circuit	124
35	Collector current of V_{Dual} transformer circuit	125
36	Charge and discharge curves of a lead cell and an Edison cell.	129

Evaluation - TR-68-49
Aerospace Controls Corp.
F30602-67-C-0350

This report constitutes a comprehensive investigation into the many factors that affect the imaging of a ground light upon the film of an aerial camera with the objective of achieving an image that will be measurable on the film to an accuracy of 3 microns r.m.s. for aircraft overflying at altitudes up to 100,000 feet. The various factors investigated include: (a) atmospheric effects, including contrast degradation and attenuation; (b) climatological conditions; (c) film characteristics. The light module design considered: (a) lamp/camera synchronization; (b) source power requirements; (c) remote control from the air and ground; (d) light collector design; (e) spectral characteristics; (f) pulse circuit design.

Both an active and passive system were investigated. The passive system would have utilized an airborne strobe-light in conjunction with ground-based reflectors. The active system would employ ground-based lights. Although the passive system was discarded after examining the magnitude of important system parameters, this report includes an excellent analysis of a passive system, including reflector design and source energy requirements.

The design analysis of the active system points to what may amount to a costly light package for the camera calibration range. The severe specifications to which the design analysis was addressed may make the costs prohibitive. An alternate choice would be to provide power lines in the area. This would eliminate the need for batteries, pulsing circuits, synchronization, and other requirements. It may well be that the costs of providing power lines in the range would be offset by the savings of a more simplified system employing a continuous light source. This will have to be considered before any considerable funds would be allocated for the type of system described in this report.

Frank A. Scarano

FRANK A. SCARANO
Project Engineer
Recon Engineering Section

I. INTRODUCTION

A photogrammetric camera calibration range is being constructed at Casa Grande, Arizona intended for use in calibrating aerial cameras. The United States Air Force desires to add the necessary equipment to this range to permit camera calibration during the night hours.

The Casa Grande Range consists of 272 geodetic points each constructed in the shape of a maltese cross. For night illumination two approaches were considered -- an active and a passive approach. The active approach incorporates light fixtures fixed on or near each of the 272 points. The passive approach utilizes reflectors fixed at or near the various points with an airborne illumination system in the camera carrying aircraft.

While it would be desirable to have lights or reflectors on each of the 272 points, it is not necessary to employ all at any one particular time for a particular calibration. The number of lights required and the pattern in which they are lighted depends upon several factors including the type of camera being calibrated, the aircraft altitude, film type, etc.

The camera carrying aircraft will also carry a strobe light (or equivalent source) used to determine position of the aircraft against a stellar background the instant the camera shutter is opened. Ground-based ballistic cameras will be utilized to track the aircraft.

The approach taken in determining the design of the light module is relatively straightforward, and is reflected in the Table of Contents. The problems associated with determining the center of the image to within three microns are analyzed first. These problems arise due to the characteristics

of the atmosphere and are partially compensated for by the proper choice of the spectral region in which the system shall operate. Through the choice of specific films and light sources, the problems may be almost totally negated, at least for ground-based lights.

In the case of ground-based reflectors and an airborne source, the difficulties associated with the atmospheric characteristics are such that image resolution is too poor for accurate calibration of the cameras. Hence, after showing the feasibility of utilizing ground-based light sources, the conceptual design of an active photogrammetric test range is presented. The choice of lamps, energy collectors, power supplies, and system logic (turn-on and turn-off from remote location) coupled with environmental considerations is detailed.

The general requirements for the active lighting system are:

1) Self-sustaining, with minimum maintenance requirements, as the lights shall be located in a remote area. It is required that it function trouble-free for a minimum of thirty days and require minimal maintenance thereafter.

2) Vandal proof - no individuals other than authorized personnel shall be able to disassemble the fixture.

3) Bullet proof - to the extent that it may be fired upon by individuals with ordinary hunting rifles.

4) Lightweight - less than 100 pounds, and able to be easily carried by one man.

5) Remote control - intensity and on-off control.

6) Regenerative power supply - e.g., batteries, solar cells, etc.

7) Plug-in feature - such that it may be mounted upon a fixed base and removed in minutes.

8) Environmental protection - such that it will withstand the elements of the Casa Grande, Arizona region for a period of at least five years without degradation of performance.

The detailed requirements are:

1) The light source shall be of such a size that it will be imaged as a circle less than 100 microns in diameter upon the recording film of aircraft overflying at altitudes up to 100,000 feet with typical reconnaissance and mapping cameras.

2) The light and all associated equipment shall be an integral unit, and self-sustaining. It shall operate from its own built-in power supply and have no dependence upon any external sources.

3) The lights on the range shall be of a size, intensity, and spectral value such that the true center point of the images they produce on selected films shall be measurable to an accuracy of three microns RMS or less. The type of film to be employed for calibration tests may be specified.

4) The lights shall be remotely controlled such that they may be turned on or off from the test aircraft or by an operator on the ground.

II. ATMOSPHERIC EFFECTS

The earth's atmosphere contains a large number of various sized particles which, due to their presence, can be expected to degrade system performance. Scattering of light from these particles reduces the received signal energy and degrades the image contrast at the film plane of the airborne camera. Further, the signal may be attenuated due to absorption by the molecules which make up the atmosphere.

Even the clear atmosphere is a turbulent, inhomogeneous region in which the refractive index is a function of position and time. It may be considered to consist of a large number of regions with varying dimensions, called eddies, over which the refractive index deviates from the average. When the light propagates through such a medium, its interaction with the inhomogeneities produces random fluctuations in the amplitude and phase of the signal. This randomness tends to degrade the light through a variety of effects. As a consequence of these atmospheric characteristics, the image at the focal plane can be expected to be reduced in energy, its contrast degraded, and its actual recorded position on the film to deviate from the position calculated assuming straight line exoatmospheric propogation.

In this section these effects are discussed and their results are examined. Also, attenuation due to the presence of rain and clouds is discussed.

II.A. Attenuation

Attenuation of the signal arises from scattering and absorption of the light from the constituent particles in the atmosphere, scattering from turbulence regions, and absorption by rain and clouds.

II.A.1. Attenuation Due to Scattering

Scattering due to very small particle, or molecular scattering is called Rayleigh scattering. Rayleigh scattering varies as λ^{-4} and produces large attenuation at short wavelengths. Scattering by particles large compared to the signal wavelength (e.g., from aerosol particles) is called Mie scattering and is much less wavelength dependent. Scattering of the light from turbulence regions is not very wavelength dependent but is important since large portions of the beam are lost due to reflection. A theoretical discussion of turbulence caused scattering is presented. To determine the amount of attenuation due to scattering from atmospheric constituents a model of the atmosphere must be developed. Elterman has developed such a model, which is augmented with empirical data peculiar to Casa Grande, and his model is utilized in the following analysis.

II.A.1.a. Rayleigh Scattering

Rayleigh scattering -- the scattering of radiation from particles small compared to the wavelength -- dominates as the cause of attenuation at short wavelengths. The Rayleigh attenuation coefficient, β_R , is a function of altitude, h, and wavelength, λ , and is given by

$$\beta_R = \sigma_R N_R(h) \times 10^5 \qquad (1)$$

Where:

σ_R = Rayleigh scattering cross-section given by

$$\sigma_R = \frac{8\pi^3 (n^2 - 1)^2}{3\lambda^4 N_s^2} \cdot \frac{6 + 3\delta}{6 - 7\delta} \qquad (2)$$

Where:

n = refractive index of air at sea level

δ = depolarization factor

N_s = molecular number density at sea level

N_R = molecular number density at any altitude

λ = signal wavelength

The term $(6 + 3\delta)/(6 - 7\delta)$ accounts for the depolarization due to the anisotrophy of the atmosphere. Figure 1 shows σ_R as a function of λ.

The probability that a photon travels a distance R, through the atmosphere without encountering a collision with a Rayleigh scatterer is given by

$$\bar{P}_R = e^{-\beta_R R} \tag{3}$$

where $\bar{P}_R$ is this probability. The product B_R^R is commonly termed the "Rayleigh optical thickness". For large numbers of photons, the statistics are such that $\bar{P}_R$ becomes the transmissivity of the atmosphere insomuch as Rayleigh scattering is concerned.

With respect to altitude, R may be written as

$$R = h \sec \theta \tag{4}$$

h being the altitude and θ the zenith angle.

II.A.1.b. Mie Scattering

Mie scattering is caused by aerosol, or large particle scattering and is not as wavelength dependent as Raleigh scattering.

As with Rayleigh scattering, the fundamental parameter for determining the loss due to Mie scattering is the aerosol attenuation coefficient, β_a. It has

Figure 1

Rayleigh scattering cross-section versus wave-length

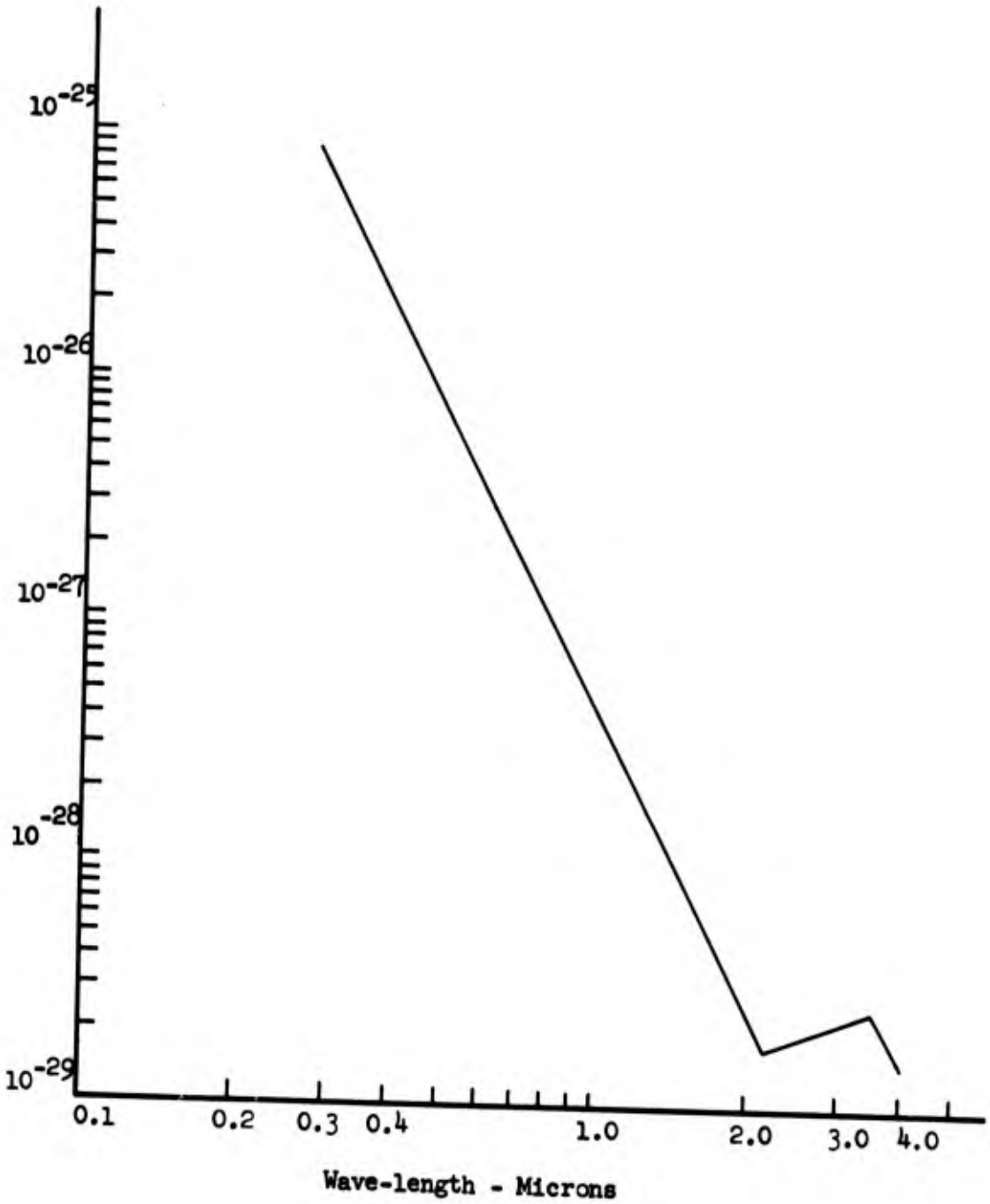

been found by Junge that the size distribution of aerosol particles tends to remain relatively constant with altitude. This allows the relation

$$\beta_a(h) = \beta_a(0) \frac{N_a(h)}{N_a(0)} \tag{5}$$

Where:

$\beta_a(0)$ = aerosol attenuation coefficient at sea level (for a particular meteorological range)

$N_a(h)$ = aerosol number density at an altitude h

$N_a(0)$ = aerosol number density at sea level

Figure 2 shows $N_a(h)$ as a function of h. This curve is relatively well representative of the conditions at Casa Grande. Figure 3 shows the aerosol attenuation coefficients at sea level as a function of wavelength.

As with Rayleigh scattering, the probability of no collision of a signal photon with a scatterer, and hence, the transmissivity, is given by

$$P_a = e^{-\beta_a R} \tag{6}$$

II.A.1.c. Total Particle Scattering Attenuation

The total scattering attenuation coefficient, $\beta_t(\lambda, h)$, is simply the sum of the Rayleigh and Mie coefficients for each wavelength and altitude:

$$\beta_t(\lambda, h) = \beta_R(\lambda, h) + \beta_a(\lambda, h) \tag{7}$$

To determine the total extinction coefficient, τ_{ext}, from ground to some altitude, h, requires summing the product of attenuation coefficients and increments of altitude, Δh.

Figure 2

Representative profile, aerosol number density vs altitude

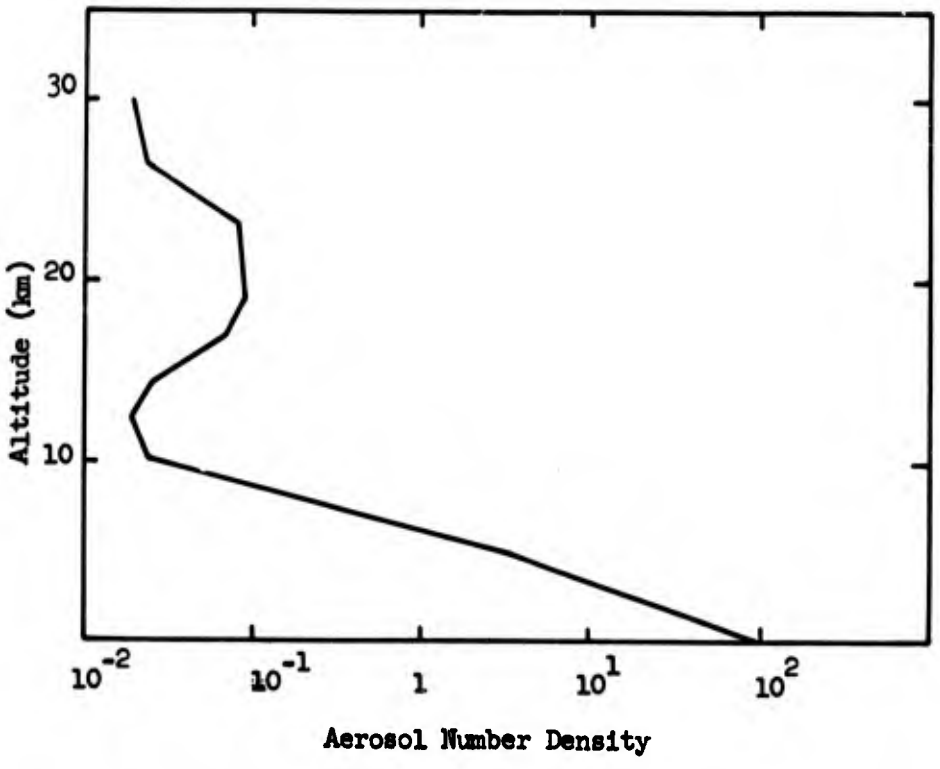

Figure 3

Aerosol attenuation coefficients at sea level

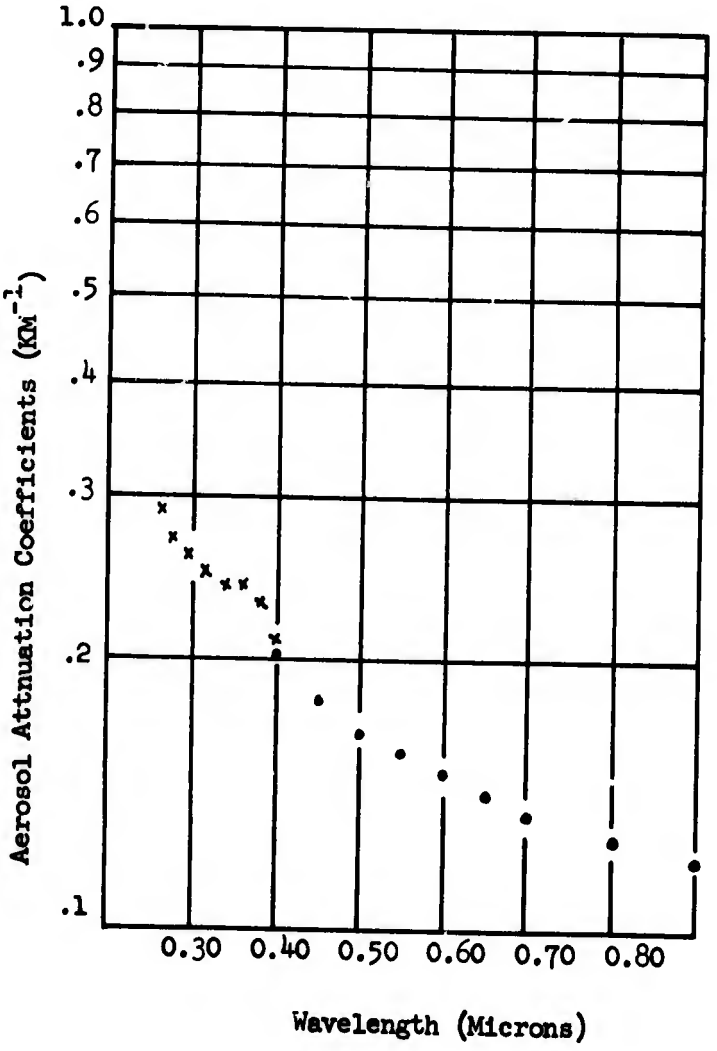

$$\tau_{ext}(h) = \sum_{o}^{h} \beta_t (\lambda, h) \Delta h \tag{8}$$

As before, if $e^{-\tau}$ is the probability of no scattering, then the altitude variation in atmospheric transmissivity may be written as

$$T_{o-h} = \exp - \left[\sec \theta \sum_{o}^{h} \beta_t (h) \Delta h\right] \tag{9}$$

or

$$T_{o-h} = \exp - \left[\sec \theta \sum_{o}^{h} \left[\sigma_R N_R(h) \times 10^{-5} + \beta_a (0) \frac{N_a (h)}{N_a (0)}\right]\right] \tag{10}$$

Figure 4 (after Elterman) shows Eq. (10) graphically as a function of wavelength for an altitude of 35,000 feet and a zenith angle of 0°. The contribution of scattering above this altitude is negligible and is thus ignored in any of the calculations in this report.

II.A.1.d. Scattering Attenuation from Turbulence Regions

Due to refractive index discontinuities associated with turbulent regions in the atmosphere, a portion of the incident light will be reflected (back-scattered) giving rise to attenuation. The amount of loss is a function of altitude, temperature, wind speed and wind speed gradients. Since the turbulent regions can be manifested in many sizes and shapes, and thus must be represented by a large variety of mathematical models, it is extremely difficult to quantitatively assess the loss. It is possible however, to express in general form, the reflection coefficients associated with refractive index discontinuities.

Figure 4

Atmospheric Transmission from h=o to h=11 km. Includes Rayleigh and MIE scattering and Ozone absorption.

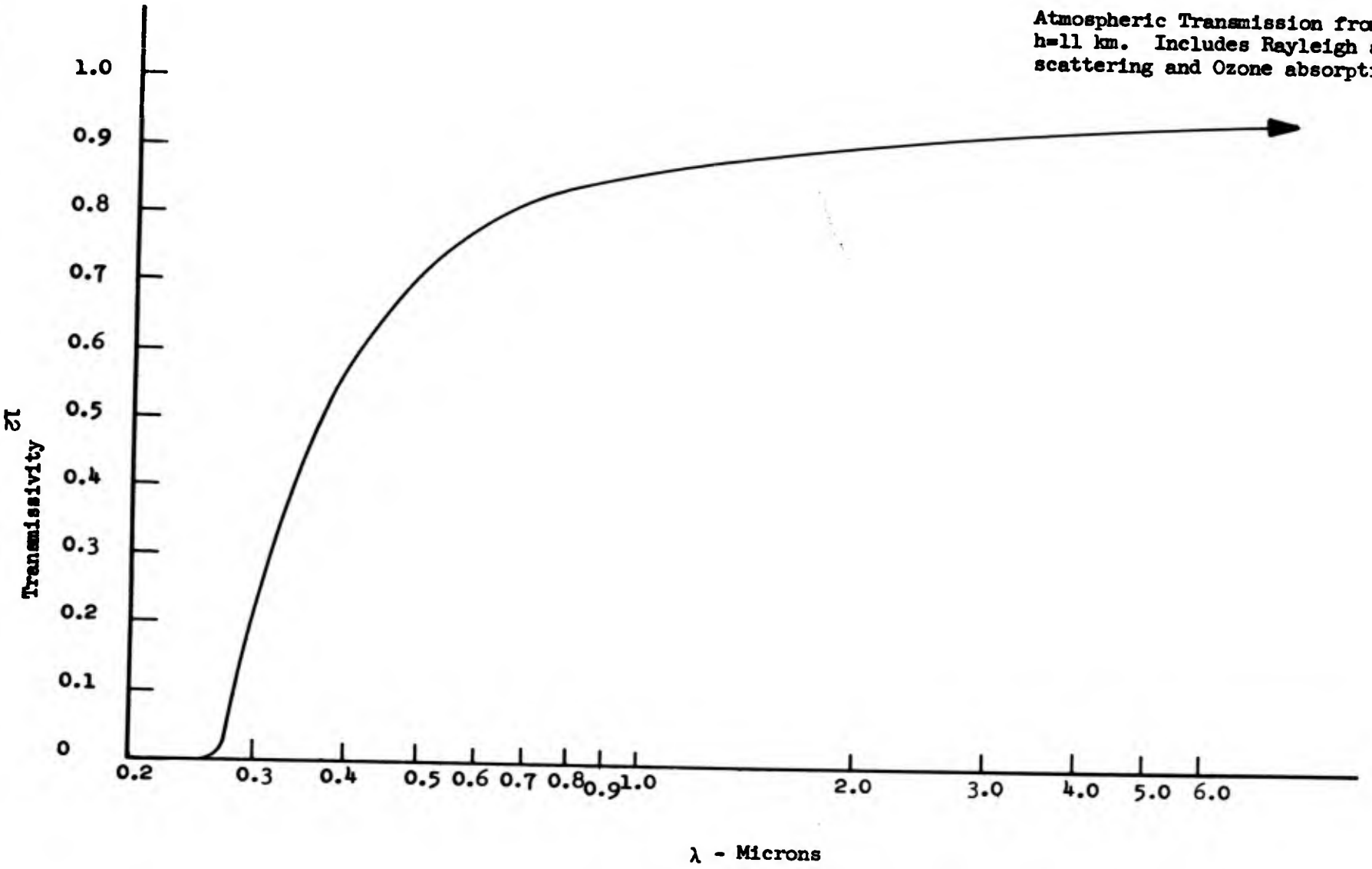

The refractive index, n, of a gas may be approximated by

$$n = \sqrt{\frac{2N e^2}{m (\nu_o - \nu)^2}} + 1 \qquad (11)$$

Where:

N = molecular number density

e = electron charge

m = mass

ν_o = resonant frequency of the molecules

ν = source frequency

Since N is a function of altitude and temperature, so must be n. The variation in n, δn, with respect to a variation in N, δN, is

$$\delta n = \frac{\alpha \, \delta N}{\sqrt{2N\alpha + 1}} \qquad (12)$$

where

$$\alpha = \frac{e^2}{m(\nu_o^2 - \nu^2)} \qquad (13)$$

A change δN can be brought about by turbulent wind conditions or thermal inversion layers and thus may be expressed by

$$\delta N = \delta N (T, \Delta T, h, s_w, \nabla s_w) \qquad (14)$$

With s_w the wind speed and ∇s_w its gradient. Further, since δN is generally a function of position for a turbulent region,

$$\delta N = \delta N (X, y, Z, T, \Delta T, h, s_w, \nabla s_w) \qquad (15)$$

Evaluating the functional form of δN is not possible and consequently is not

discussed further; however, the development of pertinent equations is presented here.

The reflection coefficient, ρ, of a gas of refractive index n, is given by

$$\rho_i = \frac{(n - \cos \theta_i)^2}{(n + \cos \theta_i)^2} \tag{16}$$

for a medium which is not highly absorptive, and where θ_i is the angle of incidence of the i'th ray undergoing reflection.

The energy reflected from the i'th ray, E_{R_i}, is simply

$$E_{R_i} = E_{o_i} \rho_i \tag{17}$$

with E_{o_i} the energy incident on the turbulence region. Now ρ_i is given in Eq. (16), and, by combining this with Eq. (11) gives

$$\rho_i = \frac{(\sqrt{2N\alpha + 1} - \cos \theta_i)^2}{(\sqrt{2N\alpha + 1} + \cos \theta_i)^2} \tag{18}$$

we obtain, after summing over all angles θ_i, (from normal incidence to the half-angular width of the beam, $\omega/2$), the total reflected energy, E_R. Of course the variation in N must be considered to obtain a truly quantitative result (c.f. Eq. (14)). If ρ_i is evaluated at a given altitude and temperatures, then by integrating Eq. (17) over x, y, z and the wind conditions, this quantitative result is achieved. Thus, the general expression for the amount of energy is given by

$$E_{R/T,h} = E_o \sum_{\theta_i=o}^{\omega/2} \iiint\iint \frac{(\sqrt{2N\alpha + 1} - \cos \theta_i)^2}{(\sqrt{2N\alpha + 1} + \cos \theta_i)^2} \, dx \, dy \, dz \, ds_w \, d(Vs_w) \tag{19}$$

For regions which exhibit high absorption, this result is altered to the extent that it is far more complicated. The real situation, where a broadband source is used is extremely complicated.

To make an approximation of the loss incurred by reflection of the signal by turbulence regions, Eq. (19) was solved for a single case. A ten percent change was assumed in the molecular number density, δN (at 20,000 feet) and a loss of 4.75 percent resulted. To solve the problem, E_R was averaged over all angles within the beam width, s_w and ∇s_w were not considered in the problem (these determine the functional form of δN), and a uniform spatial distribution in δN was assumed over the turbulence region.

II.A.1.e. Scattering by Rain and Clouds

As is expected gross attenuation results when rain or clouds are present between the source and camera. In the wavelength range of 0.4μ to 1.0μ, the water particles are nonabsorbent, so that all of the energy is scattered.

With respect to clouds, the intensity of light exiting from the cloud is composed of both direct (transmitted light) and scattered light. The intensity of the exiting light can be expressed as

$$I_t = I_o e^{-\tau \sec\theta} + I_s \qquad (20)$$

Where:

I_t = total light intensity exiting the cloud

I_o = incident light intensity

I_s = scattered light

τ = optical thickness of the cloud

θ = angle of incidence measured from the vertical

The term $I_o e^{-\tau \sec\theta}$ pertains to the part of the transmitted light that remains coherent upon passage through the cloud*. Defining $I_{coh} = I_o e^{-\tau \sec\theta}$, Eq. (20) becomes

$$\frac{I_s(\tau)}{I_{coh}(\tau)} = T(\tau)\, e^{-\tau \sec\theta} - 1 \qquad (21)$$

This ratio is plotted in Figure 5.

The optical thickness τ, is related to the attenuation coefficient, β, and the cloud thickness z, by $\tau = \beta z$. The value of β has been calculated using measured values of droplet size and density distributions. For a cloud with an average density of 100 drops per cubic centimeter, a radius of 0.7μ, the attenuation coefficient is approximately 16 km^{-1}. Experimental data gives for dense fog, β between 13-16 km^{-1}. (A good estimate would be 1 $km^{-1} \leq \beta \leq$ 100 km^{-1}, depending upon the density.) The thickness of clouds varies, but average about 200 meters for stratocumulus and 2 km for cumulonimbus. Using these facts, one finds that for thin, low density ($\beta \approx 1$ km^{-1}) clouds, τ is of the order of 0.2, indicating that a major portion of the light is coherent (thus transmitted). On the other hand, for fairly dense clouds ($\beta \approx 16$ km^{-1}) of average thickness, τ will be approximately 3 and most of the light will be scattered. Figure 6 shows the transmittance of clouds as a function of τ.

---

*If the original beam incident on the cloud is spatially coherent, the direct beam exiting from the cloud will also be. The scattered portion may be partially coherent, but the degree is unknown.

Figure 5

Ratio of scattered to coherent intensity vs optical thickness τ

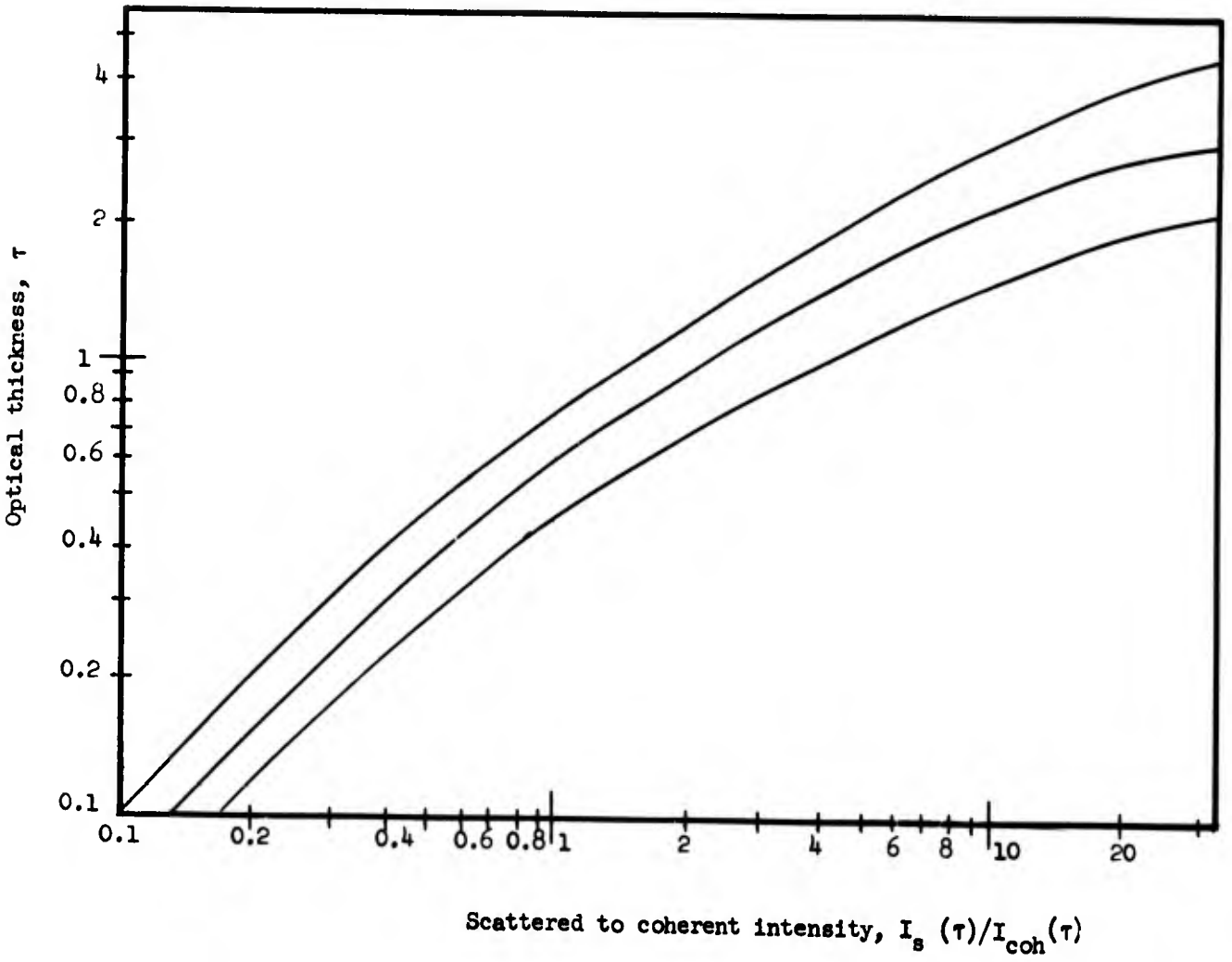

Figure 6

Cloud transmittance vs optical thickness

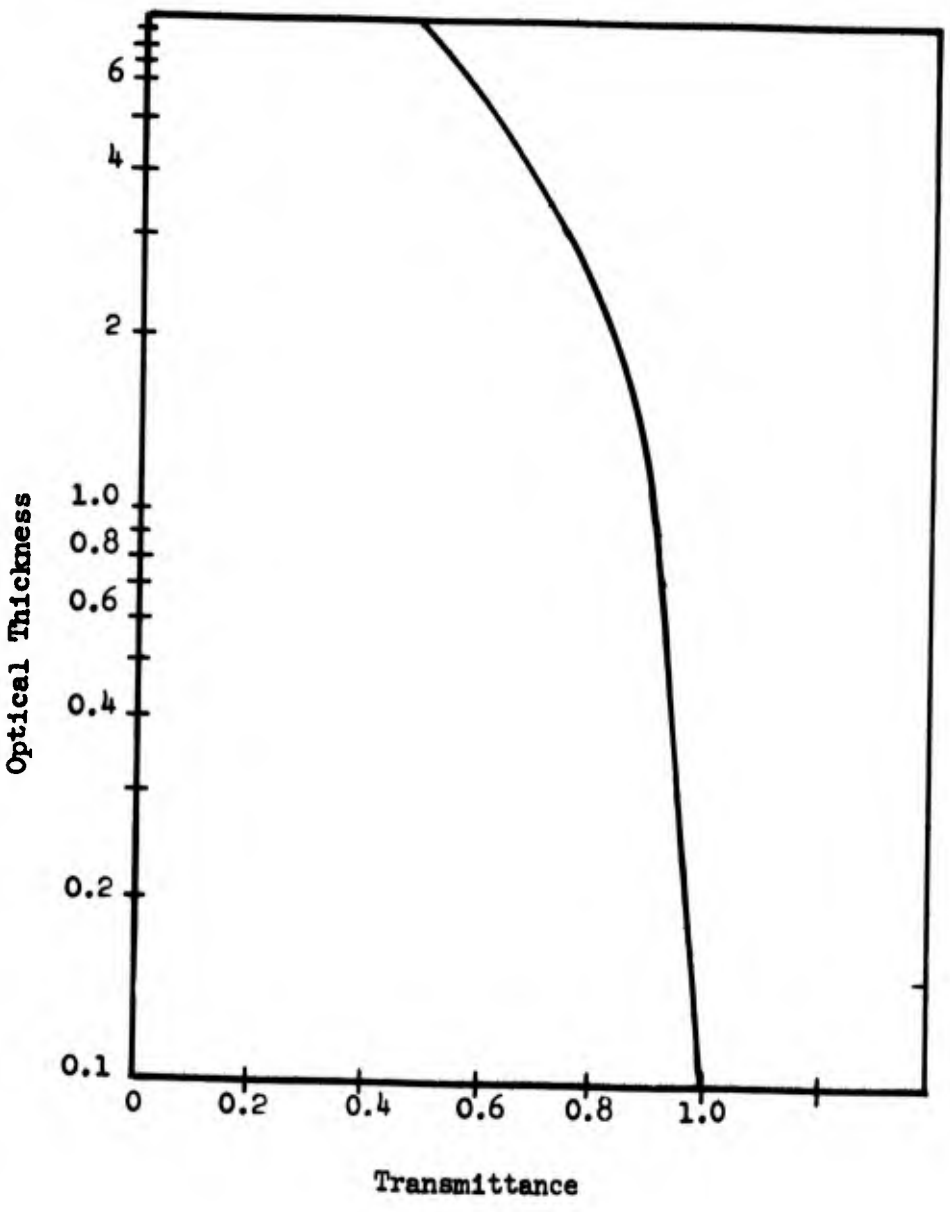

Because of the large size of rain drops relative to the signal wavelength, light which undergoes collisions will generally be backscattered (a result of geometrical optics). Consequently, in the presence of rain, large amounts of attenuation will be realized. This is illustrated in Figure 7.

II.B. Absorption by Atmospheric Particles

Attenuation of optical signals by the atmosphere arises as a consequence of absorption by molecular atmospheric constituents. The entire wavelength region from 0.3μ to 15μ contains thousands of sharp absorption lines due to the presence of H_2O, CO_2, N_2O, CH_2, O_2, O_3, CO, and their isotopes. At low resolution these lines are smoothed such that they are manifested as absorption bands. This is apparent in Figure 8 where a low resolution picture of atmospheric transmissivity is shown. At high resolution the individual lines are quite detectable, as may be seen in Figure 9. It should be noted that these curves are based on excellent sea level visibility (> 50 miles) and typical atmospheric water vapor content.

II.C. Contrast Degradation

II.C.1. Scattering

Scattering of photons by atmospheric particles reduces the image contrast. Scattering angles are not uniformly distributed but rather have probability distributions which depend on the size of the scatterers. For very small dielectric particles (or particles with low conductivity), the reflected photons are symmetrical about the plane through the center of the scatterer, at right angles to the direction of propagation of the incident light. There

Figure 7

Fog-rain attenuation
$\lambda = 0.63\mu$

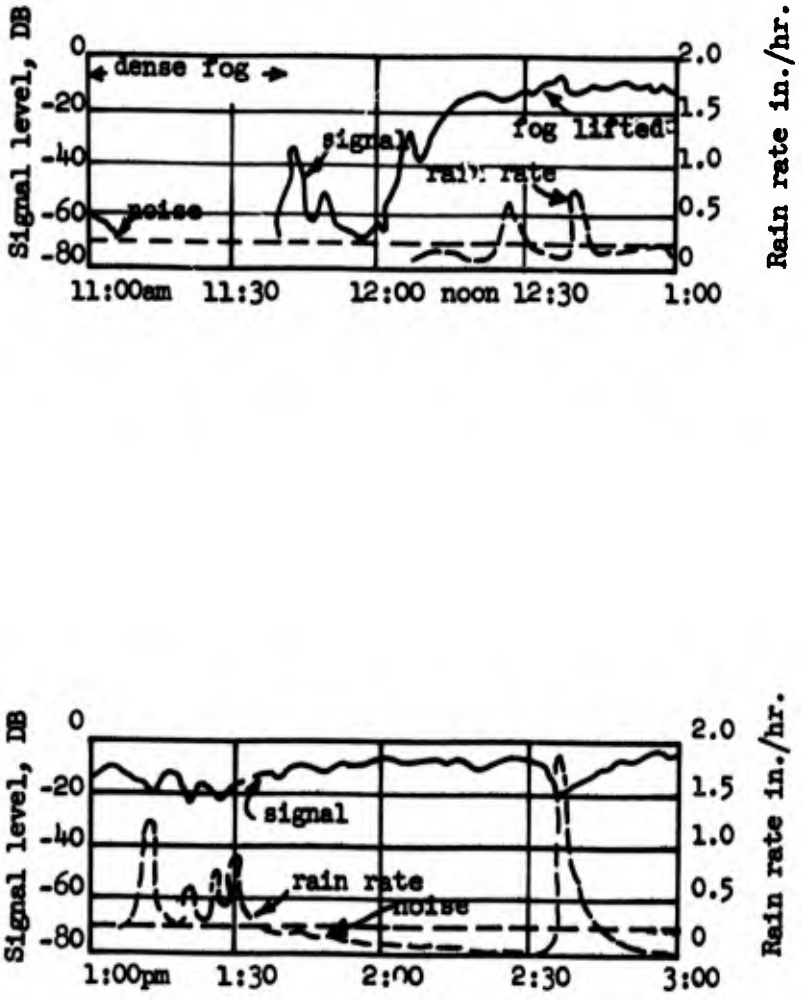

Figure 8A

Atmospheric transmission, 0.3 to 1.3 microns

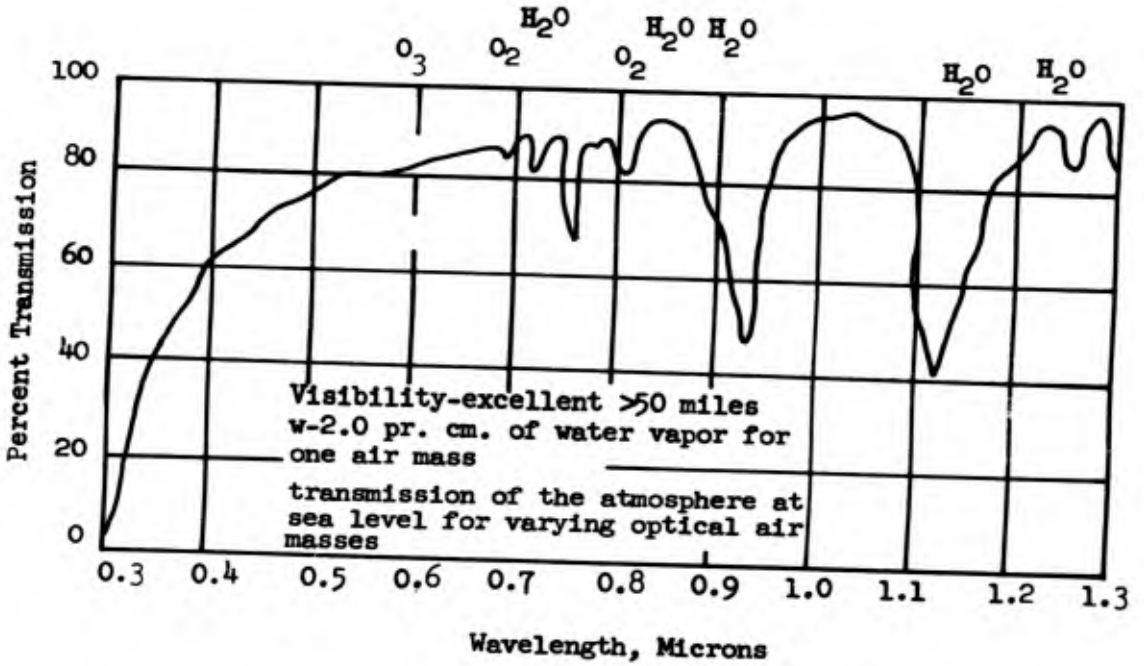

Figure 8B

Atmospheric transmission,
1.2 to 5.0 microns

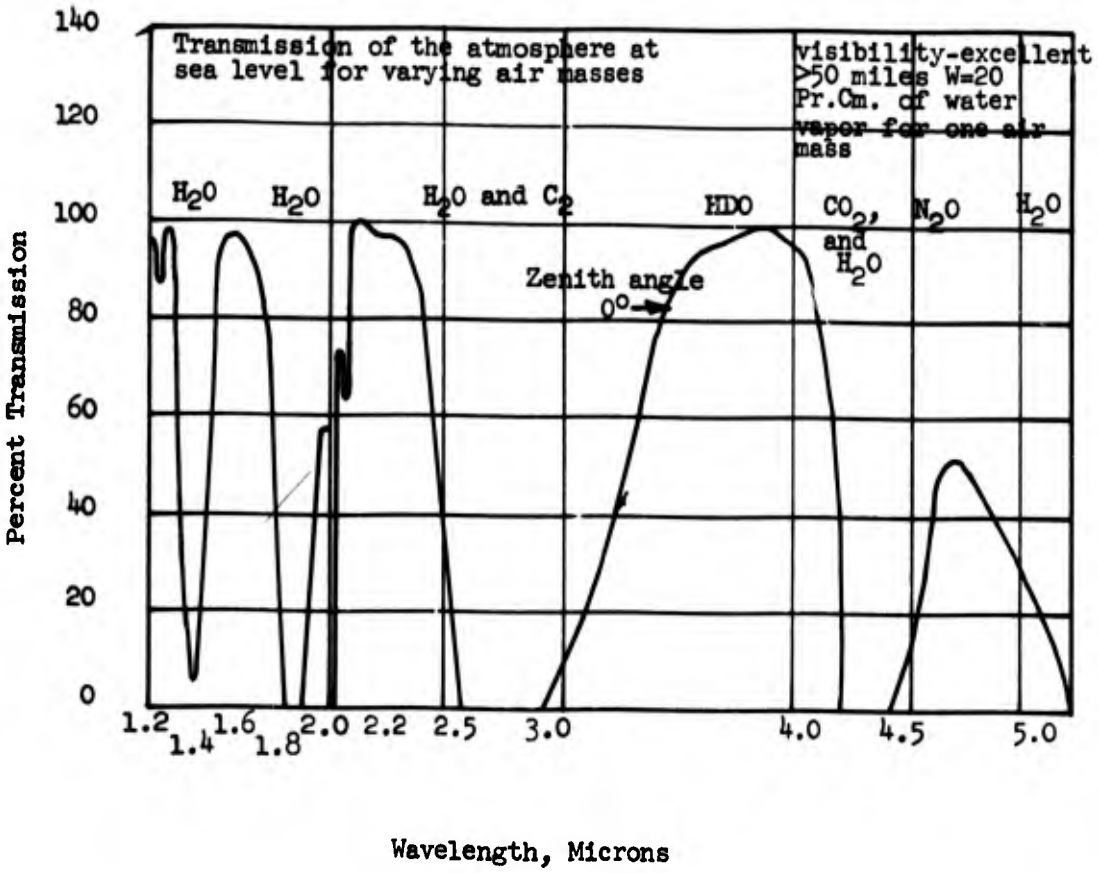

Figure 9

Fine structure of atmosphere around 6943Å (after Long)

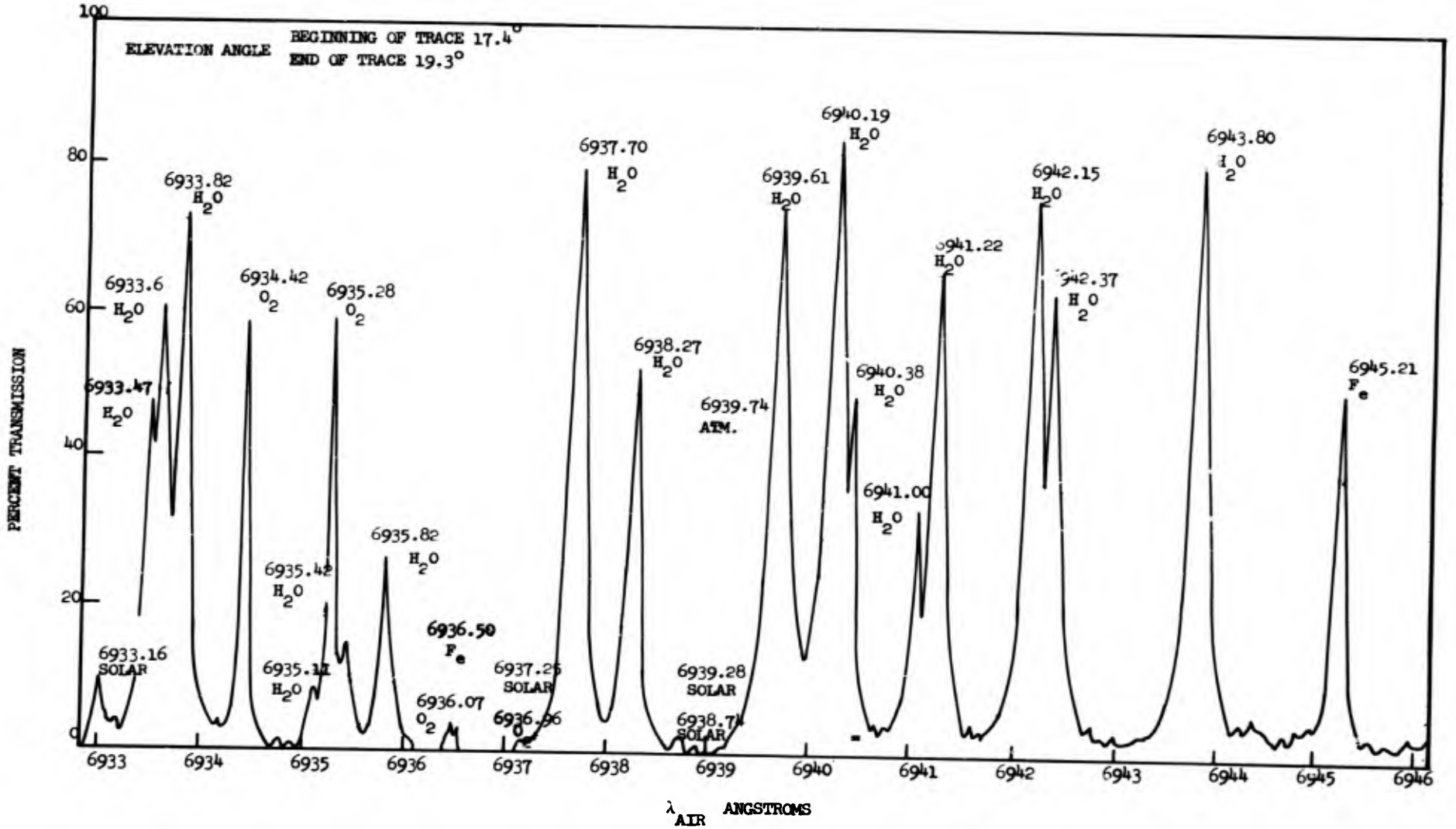

is an intensity maximum in the forward direction ($\phi = 0$) and in the reverse direction ($\phi = 180^{\circ}$), and there is a minimum in the plane of symmetry ($\phi = 90^{\circ}$). As the particle size increases, the symmetry is destroyed, more light being forward scattered. As the radius of the particle is further increased, the photons are almost all scattered in the forward direction, Figure 10 shows the intensity distribution as a function of particle size. It should be noted that, as the particle size becomes large relative to λ, most of the incident radiation is backscattered. This is expected from geometrical optics.

As a consequence of the fact that photons are not always scattered in the $\phi = 0$ direction, the energy associated with the light signal is distributed in some manner other than uniformly in the forward direction. Some of the energy is scattered from the direction of propagation of the light. This gives rise to the scattering loss discussed in the previous section. Light that is scattered in the direction $\phi = \pm\Delta\phi$ results in the degradation of image contrast since the energy from a point on the source is distributed over some spatial region.

To determine the probability distribution of photon scattering angles is straightforward. The total scattering process consists of several collisions resulting in a large number of deflections and, because of this, it is sufficient to describe the overall angular distribution of scattered photons as being Gaussian by virtue of the Central Limit Theorem.

II.C.2. Degradation Due to Turbulence Effects

The properties of the atmosphere give rise to limitations in addition to

Figure 10

Polar diagrams for the scattering of linearly polarized light by a spherical particle

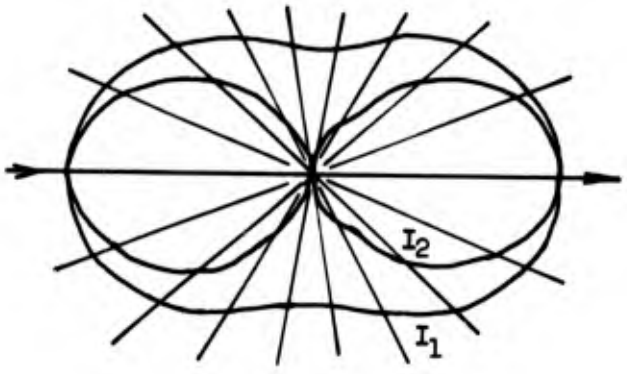

r → 0

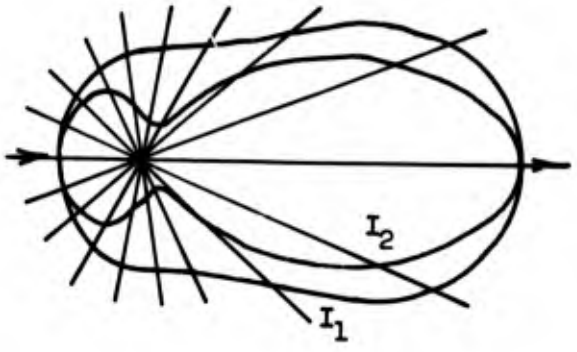

r = 80μμ

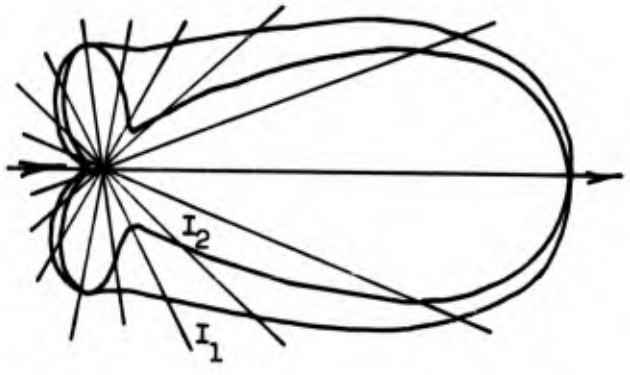

r = 90μμ

I_1, I_2 = Planes of Polarization

those imposed by attenuation due to absorption and scattering. Beam directivity and coherence are degraded by the presence of atmospheric turbulence. The randomness which arises when the signal interacts with atmospheric turbulence regions leads to a variety of effects which degrade the performance of the system. The effects are related; however, for clarity we list them separately:

1. Loss of spatial coherence: destruction of the phase coherence across the beam, the phase changing rapidly with position, leads to blurring of the image.
2. Beam spreading: small angle scattering by the inhomogeneities will spread the signal energy over a larger region.
3. Beam steering: the entire beam may be deviated from the line of sight.
4. Image dancing: variations in the angle of arrival of the received wave front will cause the image to be focused at different points in the focal plane of the receiving aperture.
5. Scintillation: small angle scattering produces local fluctuations in the amplitude, so that over the beam there will appear areas bright and dark compared to the average. This leads to fluctuations in received power which are strongly dependent on the dimensions of the receiver aperture.

All of the above effects are determined by amplitude and phase fluctuations, and to gain quantitative information requires the solution of the wave equation with boundary conditions appropriate for the particular type of beam. This problem has never been solved; however, there has been considerable work on closely related problems. In what follows, arguments based upon both geometrical and wave optics will be presented, and the theoretical results

will be compared with empirical data where available.

II.C.2.a. Qualification of Theory

To ascertain the importance of range in determining the effect of the turbulence on the properties of the beam, requires some knowledge of the dimensions of refractive index inhomogeneities. When the dimensions, ℓ, of the inhomogeneities are large compared to the diameter of the beam, the major effect of the turbulence will be to refract the beam as a whole, so that over ranges large compared to ℓ and D (the diameter of the beam), the beam will suffer a large number of deviations. On a plane perpendicular to the geometrical axis of the transmitter, the projected location of the center of the beam executes a two-dimensional random walk (this is predicated on the randomness of the turbulence inhomogeneities). If the turbulence is isotropic the deviation of the center of the beam from the geometrical axis of the transmitter will be Rayleigh distributed. The moments of the distribution will be discussed below.

When the dimensions of the inhomogeneities are comparable to the beam diameter, the picture is considerably different. In a first approximation, the inhomogeneities will act as lenses which tend to focus and de-focus all or part of the beam, causing a granular structure of the wave front. In the receiver plane the variation about the geometrical axis of the transmitter will usually be small. Also, if the inhomogeneities have dimensions comparable to the transmitting aperture, the diffraction and scattering effects will not lead to noticeable variations in the beam diameter. If the range over which the signal is being transmitted is large the scintillation

(amplitude fluctuations) across the beam will be small.

In the case where the beam diameter is large compared to the inhomogeneities, small portions of the beam will be independently diffracted and scattered (focused and de-focused). Here the magnitudes of the scattering (diffraction) angles are such as to give rise to a spreading of the beam. Furthermore, these processes can change the phase coherence of the beam appreciably, and strong amplitude fluctuations may occur within the beam. At large ranges along with a spreading of the beam, we may expect a badly distorted wave front in which intensity fluctuations are quite strong.

II.C.2.b. Loss of Spatial Coherence

Spatial coherence is degraded by phase changes in a direction perpendicular to the propagation direction. Due to local refractive index variations in the path of the rays collected by the aperture, the initially plane wavefront becomes distorted so that the aperture is no longer an equiphase surface. This effect leads to image blurring.

In order to illustrate the effects of loss of spatial coherence at the aperture plane of an optical receiver, a power reduction factor ρ, is defined as the ratio of the power received when the wave is partially coherent to that received when it is totally coherent. ρ may be expressed for optical heterodyne detection systems as

$$\rho = \frac{1}{z^2} \Psi(z) \qquad (22)$$

where (z), plotted in Figure 11 (Fried) contains the dependence of signal-to-noise ratio on receiver diameter and z is the receiver aperture diameter in

Figure 11

Power reduction in an optical hetrodyne receiver caused by loss of phase coherence (after Fried).

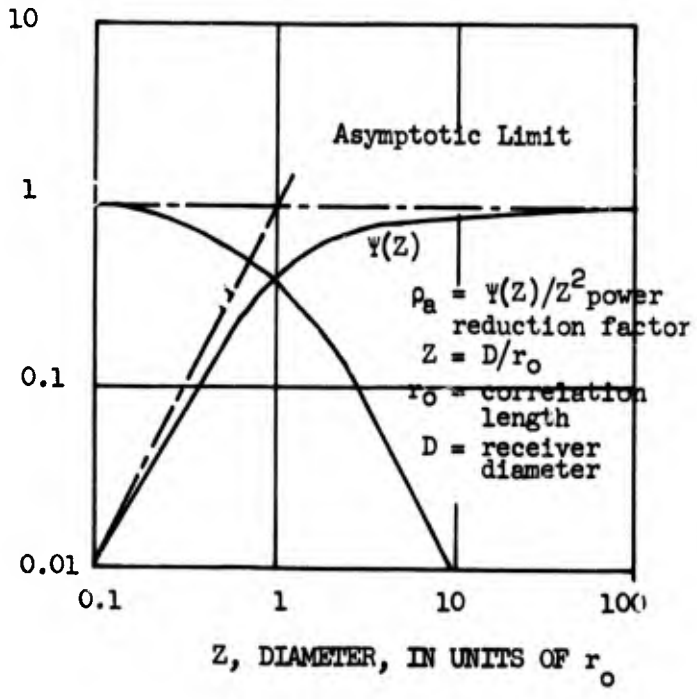

units of coherence length r_o, given approximately by

$$r_o(\lambda, \phi) = r_o(\lambda_o, 0) \left[\frac{\lambda}{\lambda_o}\right]^{6/5} [\cos \phi]^{3/5} \qquad (23)$$

Where:

λ = wavelength

ϕ = zenith angle

$r_o(x_o, 0)$ = coherence length for wavelength λ_o and zenith angle ϕ

Physically, r_o is a measure of the spatial coherence in a plane perpendicular to the propagation direction. The power reduction factor ρ decreases as z^2 for $z > 1$. The power reduction factor is plotted in Figure 11 as a function of normalized receiver aperture diameter. The coherence length r_o is plotted in Figure 12 as a function of wavelength for various receiver altitudes and transmission path zenith angles.

It can be seen that the useful aperture diameter may be quite small for wavelengths in the visible and near infrared. The advantage of using longer wavelengths can be seen when the $\lambda^{6/5}$ dependence of the coherence length is considered.

II.C.2.c. Beam Steering and Spreading

Two effects which depend strongly upon the intensity of the turbulence, and hence the inhomogeneity dimensions, are beam steering and spreading. When the wave front is not distorted appreciably by the turbulence, the effect of beam steering will be most noticeable, for it is then that the beam will be refracted as a whole. However, as the intensity of the turbulence increases, and the small scale inhomogeneities become important, the wave front is

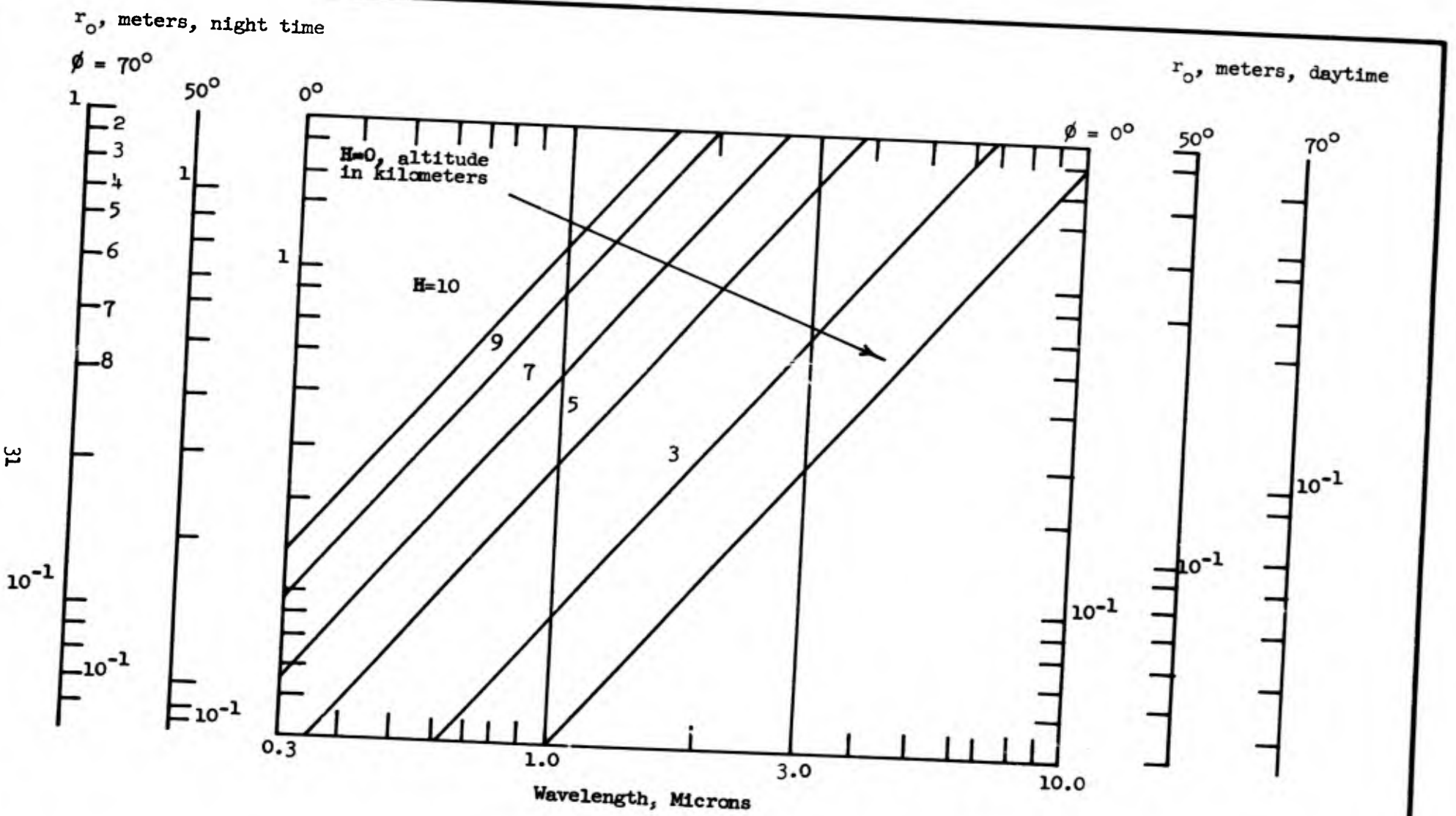

Figure 12

Dependence of coherence length, r_o, on zenith angle, ϕ, and wavelength, λ, (after Fried).

increasingly distorted, and consequently the beam appears to come from a spatially incoherent source as discussed above, so that the beam energy is spread over a larger area in the receiver plane. Although the beam may not be steered off the receiving aperture, the received power will still be reduced by the spreading of the beam.

When the receiver is far from the transmitter, beam steering will be negligible if the rms angular deviation* $\delta\theta = \sigma_\theta/\sqrt{2}$ of the undistorted wave front remains small (a factor of 3) compared to the (half) angular divergence of the transmitted signal. Figure 13 plots values of σ_θ for an undistorted wave front of various dimensions as a function of ρ. If the wave front is distorted by the turbulence, beam spreading will be important only when the rms angular deviation $\delta\theta = \sigma_\theta/\sqrt{2} = \pi/\sqrt{2}\,K\rho_o$ associated with a phase coherent portion of the wave front with dimension r_o, is comparable to, or greater than, the (half) angular divergence of the beam. Figure 13 can be used to obtain values of σ_θ in this case. For comparison with experiment, Goodwin has found that over an 18 mile path with a laser operating at 0.6328μ the angular deviations usually remain less than about 50 microradians under intermediate turbulence conditions, which indicates an rms deviation in angle of arrival of 24 to 35 microradians, and hence agreement

---

*Making the approximation that the correlation distance for the derivative of the angle with respect to position along the path is microscopic compared to the total range, it can be shown that the lateral displacement of a "ray" has an rms deviation $\sigma = R\sigma_\theta/\sqrt{2}$ along an axis in the receiver plane, and hence we make the association $\delta_\theta = \sigma_\theta/\sqrt{2}$.

Figure 13

Diameter of wavefront, ρ, vs standard deviation in angle of arrival, σ_θ, for intermediate turbulence.

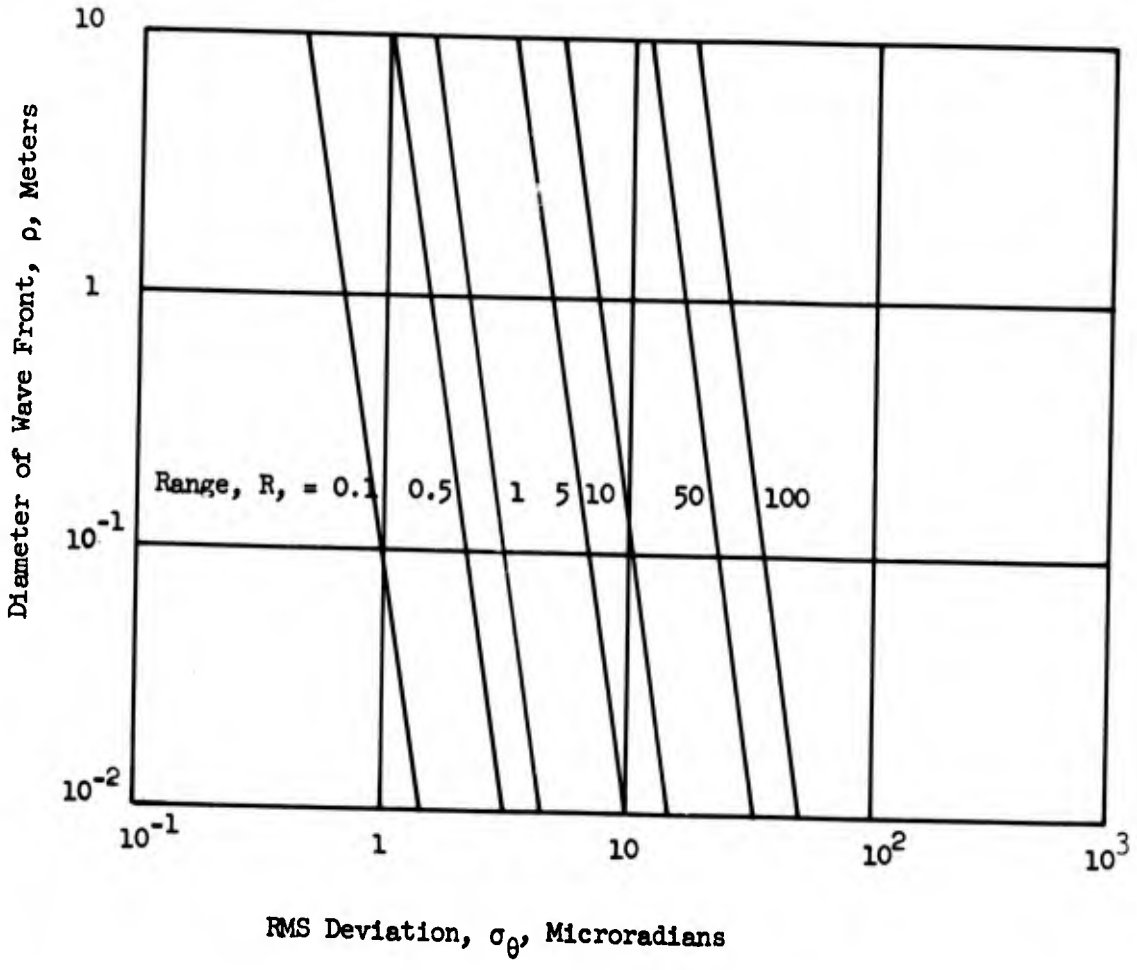

with the theory is quite satisfactory.

The simplest way to correct for beam steering (with a reduction in intensity), given that the aperture sizes are fixed, is to use diverging optics so that the effective (half) angular divergence α of the beam is large compared to δ_θ: since the angular deviation is Rayleigh distributed, it will be less than δ_θ, $2\delta_\theta$, and $3\delta_\theta$ for approximately 39, 86, and 99.9 percent of the time, respectively, and hence the beam divergence α should have corresponding values to insure that the receiver aperture will be illuminated the given percentage of time.

In considering beam spreading, it is useful to account for the reduction in received power. This problem cannot be solved precisely here, but a good estimate can be obtained by assuming a uniform intensity, I_o, over the transmitting aperture. We will use the approximation of geometrical optics insofar as the transfer function will be taken to be gaussian. If we let the line of sight pass through the origin or coordinates in the receiver plane located at range R, then the intensity at position (x, y) in this plane will be given by

$$I(x,y) = I_o \iint p(x - x', y - y')\, dx'\, dy' \qquad (24)$$

where the integration is over a circle of diameter D and

$$p(x,y) = \frac{1}{\pi(R\sigma_\theta)^2} \exp\left[-\frac{(x^2 + y^2)}{(R\sigma_\theta)^2}\right] \qquad (25)$$

the fraction η of the total power which is incident upon a circle of diameter d centered about the origin in the receiver plane is given by

$$\eta = \frac{4}{\pi D^2} \iint dx\, dy \iint p(x - x', y - y')\, dx'\, dy' \qquad (26)$$

Changing to polar coordinates, this may be written as

$$\eta = \frac{16}{D^2\sigma^2} \int_o^{d/2} \exp(-r^2/2\sigma^2)\, rDr \int_o^{D/2} \exp(-p^2/2\sigma^2)\, I_o \frac{rp}{\sigma^2}\, pdp \tag{27}$$

where I_o is a modified Bessel function of the first kind, of zero order, which has the series expansion

$$I_o(Z) = \sum_{k=o}^{oo} \frac{(Z/2)^{2k}}{(k!)^2} \tag{28}$$

Using this fact, we can write in the following form

$$\eta = \frac{1}{t} \sum_{k=o}^{oo} P(k+1, t)\, P(k+1, s) \tag{29}$$

where

$$P(K+1, t) = \sum_{n=k+1}^{oo} \frac{t^n}{t!}\, e^{-t} \tag{30}$$

defines the cumulative Poisson distribution to be found in Molina's Tables, and $t = (D/2R\sigma_\theta)^2$, $s = (d/2R\sigma_\theta)^2$. Simple expressions which are accurate to two figures are obtained in the following limits

$$\eta = 1 - e^{-s} = \left[1 - \exp - (d/2R\sigma_\theta)^2\right],\ t < 0.01;$$
$$\eta = \frac{s}{t}(1 - e^{-t}) = \left[\frac{d}{D}\right]^2 \left[1 - \exp - (D/2R\sigma_\theta)^2\right],\ s < 0.01 \tag{31}$$

For most cases of interest, only a few terms are needed to get good accuracy and in Figure 14 η versus s is plotted for several values of t. Once the transmitter diameter and the quantity $2R\sigma_\theta$ are known, the curves in Figure 14 can be used to calculate the required diameter necessary to insure that a certain fraction of the total power will be received; alternately, if the

Figure 14

Beam spreading in intermediate turbulence

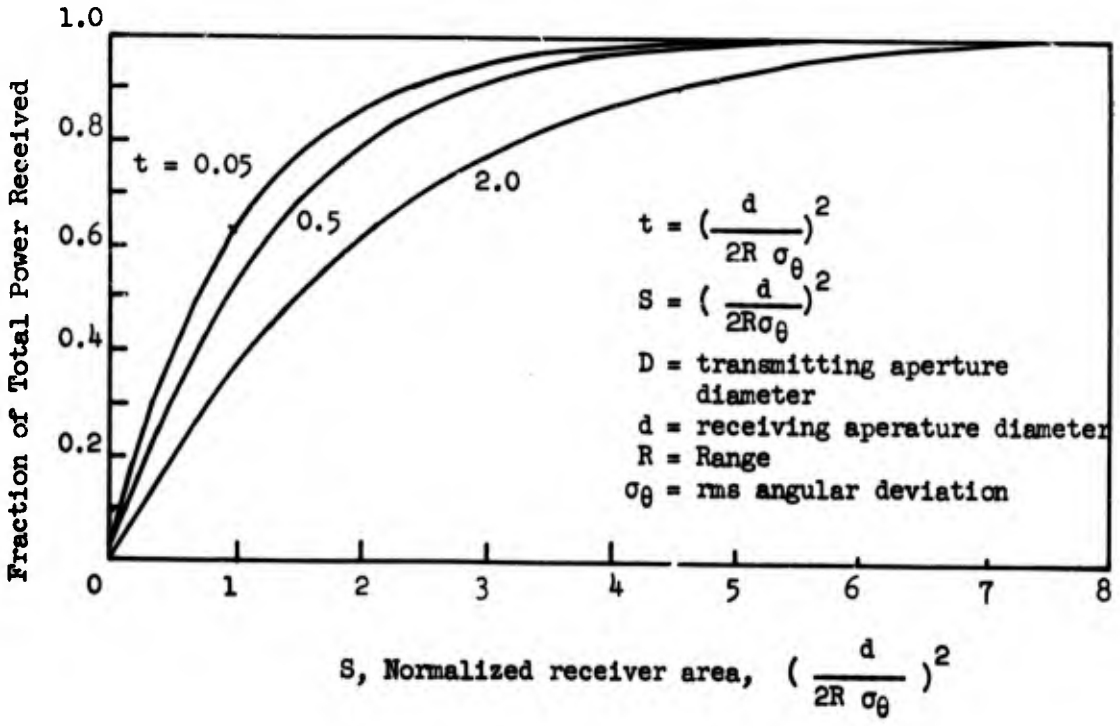

receiver diameter is pre-specified, then power transmitted must be increased by a factor η_b/η times that transmitted in the absence of turbulence. Here η_b is the fraction of total power received in the absence of turbulence.

II.C.2.d. Image Dancing and Blurring

The difference between image dancing and blurring is analogous to that between beam steering and spreading: when the wavefront is not distorted by turbulence, and hence is phase coherent across the receiving aperture, a precise image will be formed. Increasing the turbulence intensity will distort the wavefront and distort the phase coherence. As a consequence the image will become blurred.

As for image dancing, since the rms deviation in angle-of-arrival is generally small, the rms displacement of the image from the focal point of the lens will almost always be negligible. The displacement of the image from the optical axis will, in fact, be less than $3\sigma_\theta f$ where f is the focal length of the lens. As may be seen in Figure 14, for most focal lengths of interest, this displacement will be negligible.

Hufnagel and Stanley have used the results of turbulence theory in deriving an expression for image blurring, and their results show that, with the limitation to small scattering angles, diffraction and scintillation cancel each other in the far-field, so that the problem reduces itself to ray tracing. Consequently, using the arguments based on geometrical optics, we may conclude that the angular blur of a point source is approximately gaussian with mean zero and fluctuation σ_θ^2.

II.C.2.e. Amplitude Fluctuations

Tatarski postulates that the amplitude variations obey a log-normal distribution, and he derives the following expression for the fluctuation in the logarithmic level of the amplitude:

$$X_A^2 = \langle (\log \frac{A}{A_o})^2 \rangle = 0.56K^{7/6} \int_o^R C_N^2 (r)\, Z^{5/6}\, dZ \qquad (32)$$

which holds when $L_o \gg \sqrt{\lambda R} \gg \ell_o$. A_o is the initial amplitude, $K = 2\pi/\lambda$ is the wave number, and R is the range through the turbulence region. The integration is carried out along a ray, Z, from observation point to transmitter, and the argument $\underline{r}$ of the structure constant, $C_n(\underline{r})$, denotes the three space coordinates. This expression holds for a propagation path of varying altitude, and it allows for changes in the turbulence structure along the path. For paths that are nearly horizontal to the earth's surface, along which the turbulence structure does not change appreciably, we have

$$X_A^2 = 0.31\, C_n^2\, K^{7/6}\, R^{11/6} \qquad (33)$$

The fluctuation in the logarithmic level of intensity I (watts/meter^2) is related to that in amplitude by

$$X_I^2 = \langle (\log I/I_o)^2 \rangle = 4\, X_A^2 \qquad (34)$$

This expression can be interpreted as the fluctuation in the logarithmic level of received power for a receiver aperture having a diameter very small compared to $\sqrt{\lambda R}$; but, in general, since the fluctuations in intensity at points separated by distances greater than $\sqrt{\lambda R}$ will not be correlated, compensating fluctuations in opposite directions may occur across an aperture with finite diameter d, and therefore the fluctuation in power will generally

be reduced by this averaging effect. Tatarski calculates a function $G(d/\sqrt{\lambda R})$ which accounts for this averaging, and accordingly the fluctuation in the logarithmic level of power received by an aperture of diameter d from a point source is given by

$$X_P^2 = 1.24\, C_n^2\, K^{7/6}\, R^{11/6}\, G(d/\sqrt{\lambda R}) \tag{35}$$

The expression for the fluctuation in power received by an aperture of diameter d from a point source applies in a reciprocal sense to the power received by a receiver of diameter much less than $\sqrt{\lambda R}$ from a source of diameter D. Thus, when the transmitter and receiver have aperture diameters D and d, respectively, there will be a compound averaging effect, so that fluctuations in logarithmic level of received power will be given approximately by

$$X_P^2 = 1.24\, C_n^2\, K^{7/6}\, R^{11/6}\, G(D\sqrt{\lambda R})\; g(d\sqrt{\lambda R}) \tag{36}$$

Table II-1 lists some values of G for various values of $d/\sqrt{\lambda R}$, and the dependence on X_I should be noted.

Table II-1. Aperture Average Factor, $G[d/(\lambda R)^{1/2}]$[a]

$d/\lambda R$	0	0.2	0.4	0.6	0.8	1.0	1.2	1.4	1.6	1.8
$X_I^2 \ll 1$	1	0.89	0.73	0.57	0.43	0.33	0.25	0.17	0.13	0.1
$G_{XI}^2 = 4$	1	0.94	0.82	0.70	0.61	0.53	0.45	0.38	0.33	0.3

[a]For larger values of $d(\lambda R)^{1/2}$ with $X_I^2 \ll 1$, use the formula $G = 0.39[d/(\lambda R)^{1/2}]^{-7/3}$.

For later use, two important properties of the log-normal distribution are listed. If $u = \log v$ is normally distributed with mean $< u >$ and

fluctuation X_u^2, then the following relationships hold:

$$< v > = \exp (< u > + 1/2\ X_u^2) \tag{37}$$

and

$$\sigma_v^2 = \left\langle \left(\frac{v - v}{v} \right)^2 \right\rangle = \exp (X_u^2) - 1 \tag{38}$$

Thus, for example, in the case of amplitude fluctuations, then

$$\left\langle \frac{A}{A_o} \right\rangle = \exp (1/2\ X_A^2) \tag{39}$$

and

$$\sigma_A^2 = \left\langle \left(\frac{A - < A >}{A} \right)^2 \right\rangle = \exp (X_A^2) - 1 \tag{40}$$

Similar formulas hold for the mean and fluctuation of the intensity and power. But it should be remembered that for sufficiently large apertures ($d \gg \sqrt{\lambda R}$) the distribution of the power is normal.

The maximum scintillation frequency for a receiver with a small aperture $d \ll \sqrt{\lambda R}$ will be approximately equal to $V_N/\sqrt{\lambda R}$ where V_N is the wind speed normal to the line joining the source and receiver. On the other hand, if $d \gg \sqrt{\lambda R}$, the high space frequencies will be discriminated against and the spectrum will be significant up to a frequency of V_N/d.

In order to use the above theory, it is necessary to know the values of C_n which are to be associated with different turbulence conditions. Tatarski has made some estimates of this quantity from astronomical data and from data on the scattering of radio waves in the troposphere; when compared with measurements by Genoud and by Goodwin, order of magnitude agreement for C_n is obtained. It is not possible to give a simple rule for estimating C_n, and consequently we will arbitrarily divide turbulence conditions into three

categories, according to whether the fluctuations are weak, intermediate, or strong. Although this division is somewhat subjective, it provides a basis for estimating quantitatively the various degrees to which turbulence can degrade light signals. Thus, though subject to long interpretation, we will use the following values for C_n in making calculations:

Weak Turbulence: $C_n = 8 \times 10^{-9}\ m^{-1/3}$

Intermediate Turbulence: $C_n = 4 \times 10^{-8}\ m^{-1/3}$

Strong Turbulence: $C_n = 5 \times 10^{-7}\ m^{-1/3}$

When C_n varies with position over the propagation path, it is necessary to perform the integrals for X_A^2 and σ_θ^2. Hufnagel and Stanley have numerically integrated C_n^2 along a vertical path through the atmosphere under conditions corresponding roughly to daytime turbulence. They find:

$$\int_0^\infty C_n^2(Z)\, dZ = 1.3 \times 10^{-11}\ m^{1/3} \tag{41}$$

Their choice for C_n near the ground corresponds approximately to the case of intermediate turbulence.

While beam steering and spreading, image dancing and blurring give rise to a loss of power, the greatest variations in power usually result from amplitude fluctuations. The fluctuation in the logarithmic level of received power is given by

$$X_P^2 = \left\langle \left(\log \frac{P}{P_o}\right)^2 \right\rangle = 1.24\, C_n^2\, K^{7/6}\, R^{11/6}\, G(D/\sqrt{\lambda R})\, G(d/\sqrt{\lambda R}) \tag{42}$$

and the obvious way to keep X_P small is to use large receiver and transmitter apertures. When these dimensions and the wavelength are pre-specified, the

fluctuation in power is unavoidable. The fluctuation in normalized differential power received is given by

$$\sigma_P^2 = \left\langle \left(\frac{P - \langle P \rangle}{P} \right)^2 \right\rangle = \exp\left(X_P^2\right) - 1 \qquad (43)$$

We often want to know what probability can be associated with a certain domain of variation for the received power, and here it is convenient to give the probability that the fractional deviation $\left[\delta P/P_o\right] = \left[(P - P_o)/P_o\right]$ of the received power, P, from that received in the absence of turbulence, P_o, is less than some multiple n of σ_P. Assuming a log-normal distribution, the integration gives

$$\left[\left[\frac{P}{P_o}\right] < n\sigma_P >\right] = \left[\Psi\left[\frac{\log\,(1 + n\sigma_P)}{X_P}\right] - \Psi\left[\frac{\log\,(1 - n\sigma_P)}{X_P}\right]\right] \qquad (44)$$

where Ψ is related to the error function:

$$\Psi(x) = \frac{1}{\sqrt{2\pi}} \int_o^x \exp\left(-t^2/2\right) dt \qquad (45)$$

It should be noticed that, as opposed to the normal distribution, this expression is a function not only of n, but also of σ_P.

In order to plot a graph for the fluctuation in power that is not overspecialized, we compromise by giving a figure for σ_P in which the product $G(D/\sqrt{\lambda R}\,)\,G(d\sqrt{\lambda R}\,)$ is treated as a variable parameter, without specification of the arguments $D/\sqrt{\lambda R}$ R and $D/\sqrt{\lambda R}$ R. In Figure 15 we plot values of σ_P at the wavelengths $\lambda = 0.7$ and 10μ. It should be remembered that the values for σ_P given here are applicable to beams only when the diameter of the beam is large compared to the receiver aperture over most of the propagation path. Furthermore, since the distribution for the received power is asymptotically normal as $d/\sqrt{\lambda R}$ becomes large, the values in the figure will

Figure 15A

Range, R, vs rms deviation in normalized differential power received, σ_P, for intermediate turbulence

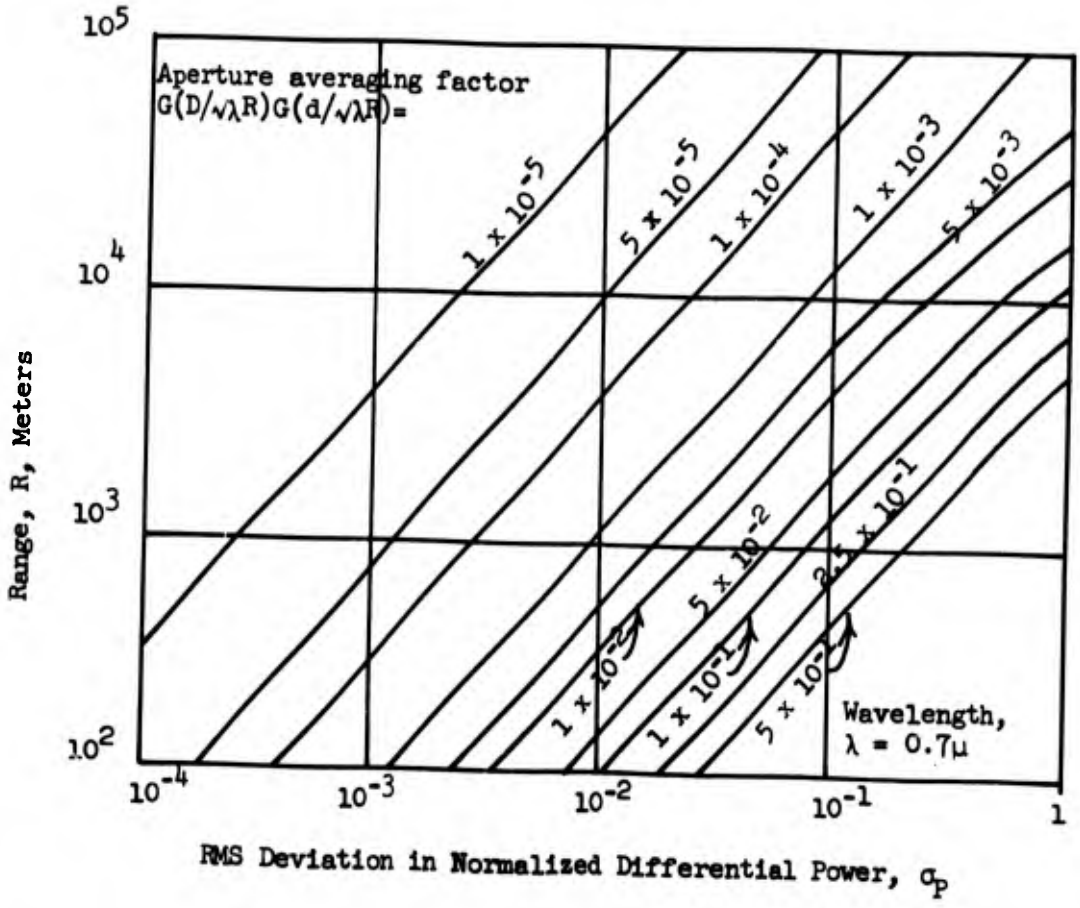

Figure 15B

Range, R, vs rms deviation in normalized differential power received, σ_p, for intermediate turbulence.

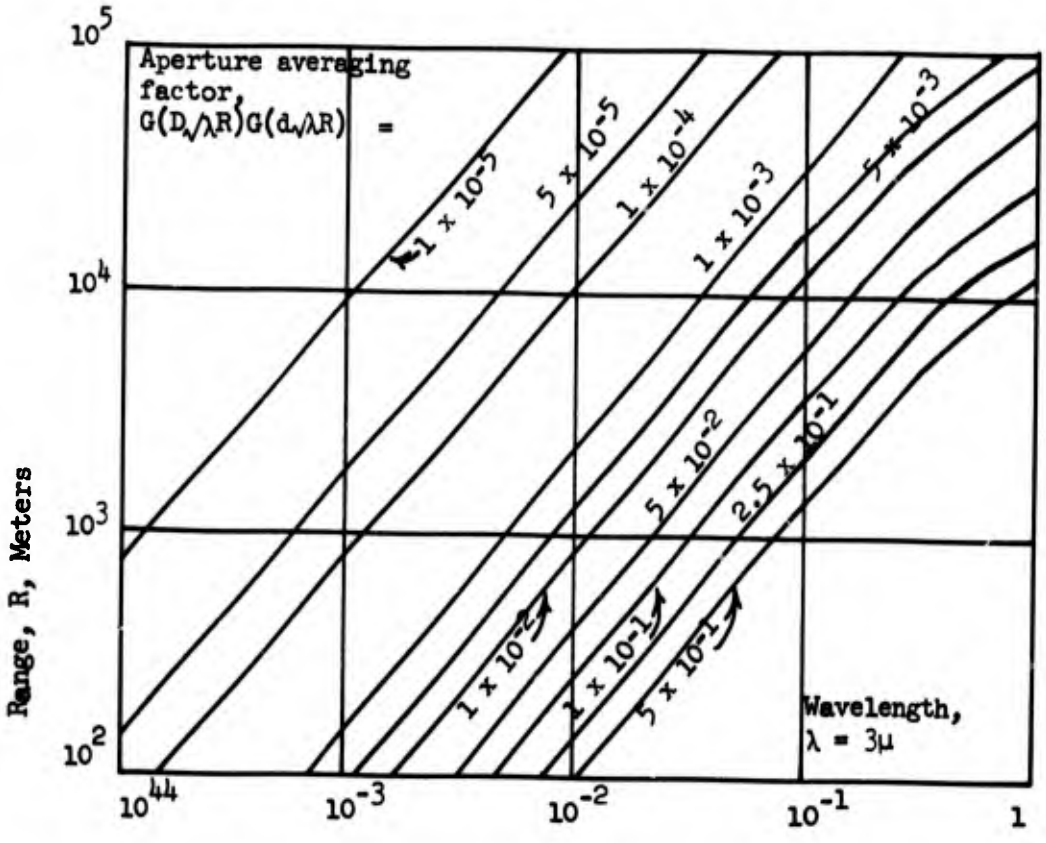

Figure 15C

Range, R, vs rms deviation in normalized differential power received, σ_P, for intermediate turbulence.

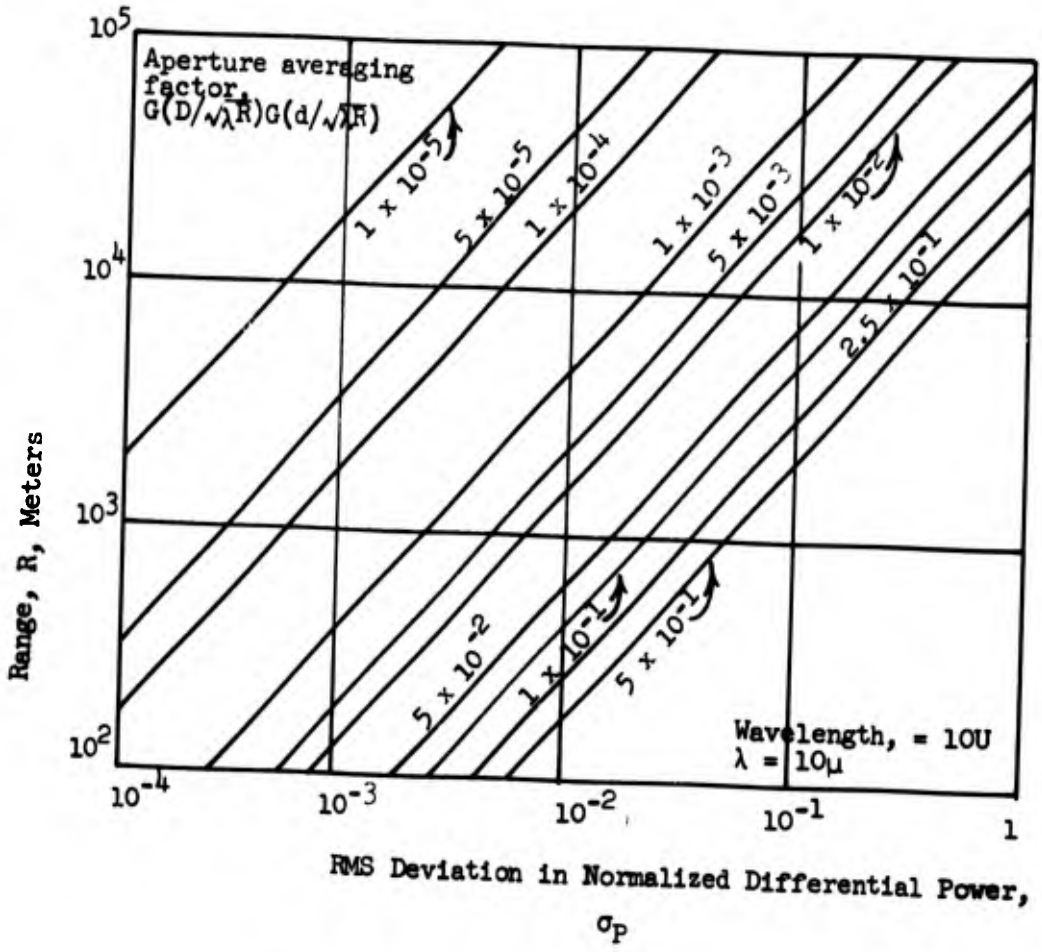

overestimate the rms deviation in this limit.

II.C.2.f. Summary and Conclusions

The earth's turbulent atmosphere can impose certain restrictions on the ability to photograph ground based light signals from high altitude aircraft. A blurred and distorted image can be expected to partially preclude the determining of the center of the image to within the three micron specification. If long exposures were used turbulence induced limitations would not be important (if the exposure is long compared to the rate of fluctuations, the effect of amplitude scintillation will be unimportant). This is because the film integrates across the image and the fluctuations will not be recorded. The loss of phase coherence (i.e., distortion of the wave front), will lead to a blurriness of the image that cannot be corrected. The degree of blurriness due to turbulence depends strongly on the atmospheric meteorlogical conditions, and to predict the reduction in image contrast, climatological data on Casa Grande must be evaluated.

It has been shown that when the wavelength is increased scattering degradation and turbulence induced limitations are reduced. Hence, from the standpoint of atmospheric characteristics as long a wavelength as possible should be used. Operation in the infra-red would be ideal; however, as we shall see in Section IV (Choice of Film) this is not feasible as present film characteristics are such to disallow this.

III. CASA GRANDE CLIMATOLOGICAL CONDITIONS

It is necessary to know the expected climatological conditions for Casa Grande so that estimates of atmospheric turbulence, cloud cover, rain fall, system environmental conditions, and number of days of useful operation per year can be established. Once these conditions have been determined, it is possible to start designing a light system for the photogrammetric test range.

Very little data is available on Casa Grande itself (the Weather Bureau has only a "cooperative observer" in the area); however, the climatological conditions of Phoenix are almost identical. Consequently, the data presented here are taken from the records of Phoenix, with reference to Casa Grande where specific data are available. The data for Phoenix were obtained from the U.S. Department of Commerce and for Casa Grande from private communication with U.S. Weather Bureau personnel in Phoenix.

III.A. Temperature

The normal daily temperatures, recorded over the thirty-year period of 1931-1960, are (^{o}F)

January: (coldest month)	Daily maximum ---	64°
	Daily minimum ---	37.3°
July: (warmest month)	Daily maximum ---	104.6°
	Daily minimum ---	78°

The mean annual temperature is 70.5°.

Knowing the temperature as a function of time of day is important because of thermal gradients giving rise to atmospheric turbulence, which must be

predicted. Weather bureau personnel state that the largest thermal gradients will exist between the hours immediately preceeding and following sunrise and sunset. This means that for best results, the operating hours of the test range should be confined to 2100 to 0400 in the summer months, and 1900 to 0600 in the winter months.

With respect to the system environment, thermal extremes must also be considered. The highest and lowest recorded temperatures in Phoenix have been 114° and 20°, respectively. Hence, it would appear logical to design the system for operation in a 0° to 125° environment.

III.B. Precipitation and Humidity

The following data were obtained on local precipitation and relative humidity for the same thirty-year period (1931-1960):

Normal precipitation:

Wettest month --- 1.12 inches

Driest month --- 0.09 inches

Annual average rainfall --- 7.20 inches

Relative humidity (percent):

January:

0400 -- 59

1000 -- 40

1600 -- 28

July:

0400 -- 43

1000 -- 26

1600 -- 19

In the wettest month and driest month there was 5.56 inches and 0.00 inches of rain respectively and the maximum rainfall recorded in a 24-hour period was 3.07 inches. Figure 16 shows the normal rainfall in Phoenix. The annual mean number of days when the precipitation is 0.01 inches or more is 34. The annual mean number of days where thunderstorms occur is 22 days.

III.C. Cloud Cover Statistics

The only data available on cloud cover is that recorded between sunrise and sunset. The annual mean number of clear days (0.0 to 0.3 sky cover) is 211 days. Eighty-four days have a mean sky cover of 0.4 to 0.7, and 70 days have almost total sky cover. It can most likely be assumed that the same conditions exist at night.

Heavy fog exists on the average of two days per year.

III.D. Wind Conditions

The mean hourly wind speed in January (at ground level) is 4.5 m.p.h. In July it is slightly higher -- 6.3 m.p.h. The highest winds recorded were 75 m.p.h. Approximately 19% of the time the winds were at or below the average.

No data is available for winds above ground level; however, it is expected that they will be sufficiently low as to not cause appreciable turbulence.

III.E. Conclusion

The climatological conditions at Casa Grande can be expected to be reasonably mild. With relatively low temperature gradients in the suggested

Figure 16

Normal rainfall in Phoenix, Arizona

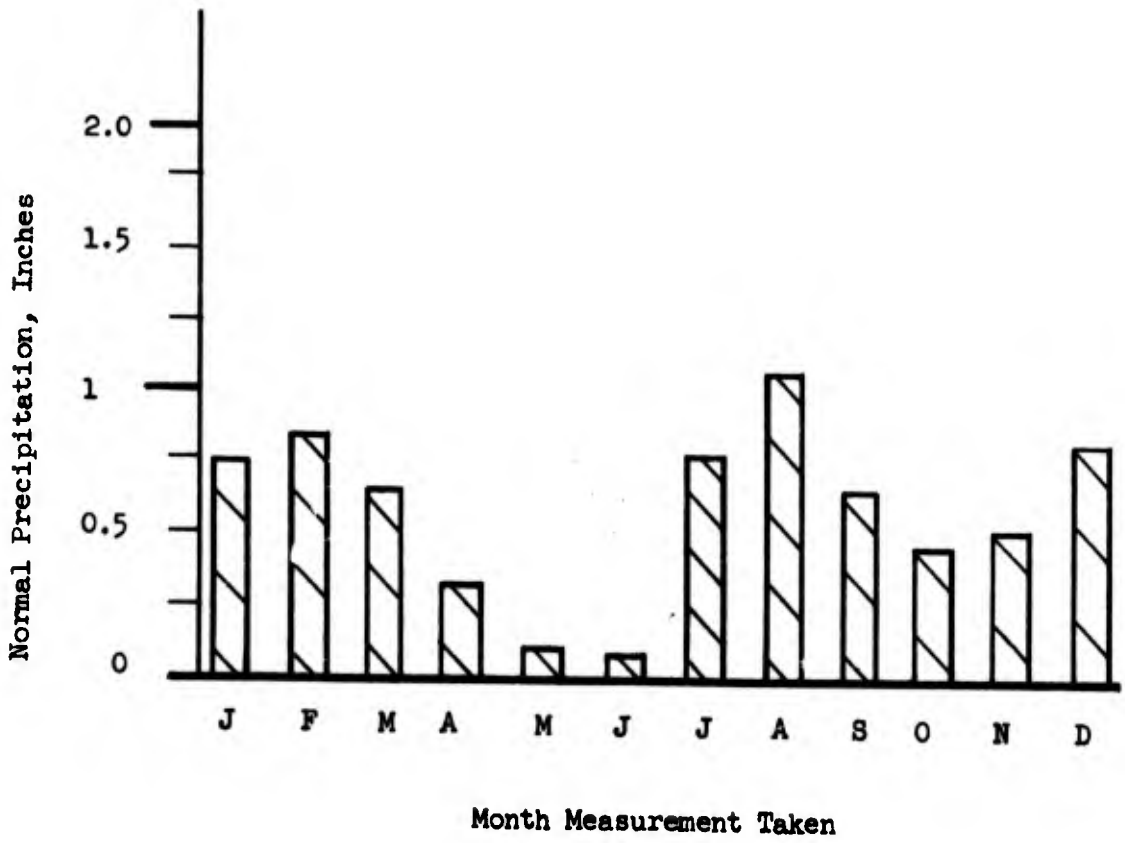

operating hours, low wind speeds, and medium humidity, operation of the photogrammetric test range should be practical during the suggested hours. Operation will be somewhat limited however, due to partial sky cover.

IV. FILM CHARACTERISTICS

The selection of films for use in the test-range must be based upon several factors:

1) spectral characteristics
2) sensitivity
3) graininess
4) contrast
5) availability
6) cost

While each of these factors interrelate to some degree, it is necessary to discuss each separately for clarity and rationalization of choice.

By virtue of the atmospheric characteristics discussed in Section II, the film chosen should be highly sensitive in the red region of the optical spectrum and should display reduced sensitivity in the shorter wavelength region.

The sensitivity of the film should be as high as possible, consistent with the other desired characteristics so that the required source energy (which is directly proportional to film sensitivity) is minimized. In accordance with the image resolution specifications, the graininess of the film must be such as to allow the determination of the image center to within three microns.

Finally, the cost and availability of the film should be kept in mind.

The ideal film for a night photogrammetric test range would be a fast, high contrast (gamma), fine grain, thin emulsion, extended-range panchromatic

(or IR) film. In the following subsections, the various parameters are discussed and the film choice is based upon the film type most closely resembling the ideal one.

IV.A. Spectral Characteristics

A photographic emulsion responds to radiation of certain wavelengths. The spectral range of which an emulsion is sensitive, and the degree of sensitivity at each wavelength, are established during manufacture by the sensitizer and the emulsion. All emulsions are sensitive to radiation in the near ultraviolet and blue regions of the optical spectrum. Emulsions which have only this sensitivity are termed blue sensitive, and most duplicating films fall into this category. When the sensitivity is extended into the red region of the spectrum, the film is called panchromatic. The newer aerial reconnaisance are panchromatic with extended red sensitivity. The sensitivity of these films extends into the near infrared (approximately 0.7 microns). Infrared films are sensitive in the near infrared region to approximately one micron.

A common method for determining the spectral characteristics of an emulsion is to image diffracted light from a continuous spectral (white) source onto the film. A continuous density wedge is placed in front of the film so that the relative sensitivity of each wavelength can be determined from the resultant exposure. This method utilizes an instrument called a wedge spectrograph. Another method employs a spectral sensitometer which exposes known amounts of energy at various wavelength bands thus allowing the determination of the absolute spectral sensitivity. Figure 17 shows the

FIGURE 17a

KODAK DOUBLE-X AEROGRAPHIC Film, Type 2405 (ESTAR Base)

DK-50
D = 1.0 above gross fog

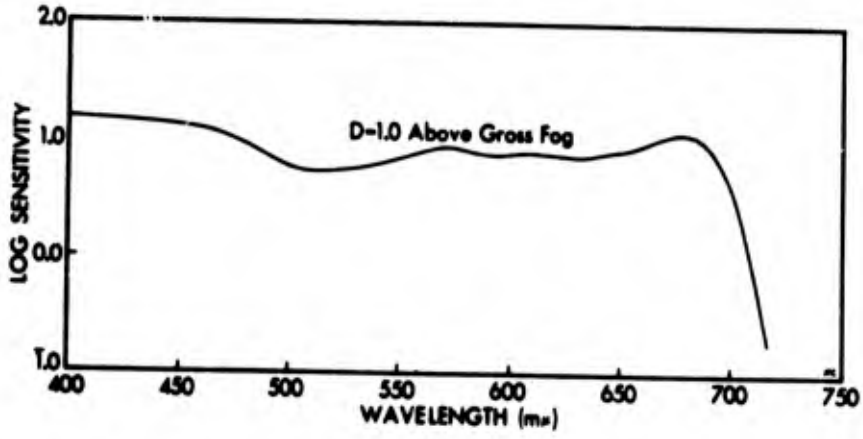

FIGURE 17b

KODAK PLUS-X AEROGRAPHIC Film, Type 2401 (ESTAR Base)

D-19
D = 1.0 above gross fog

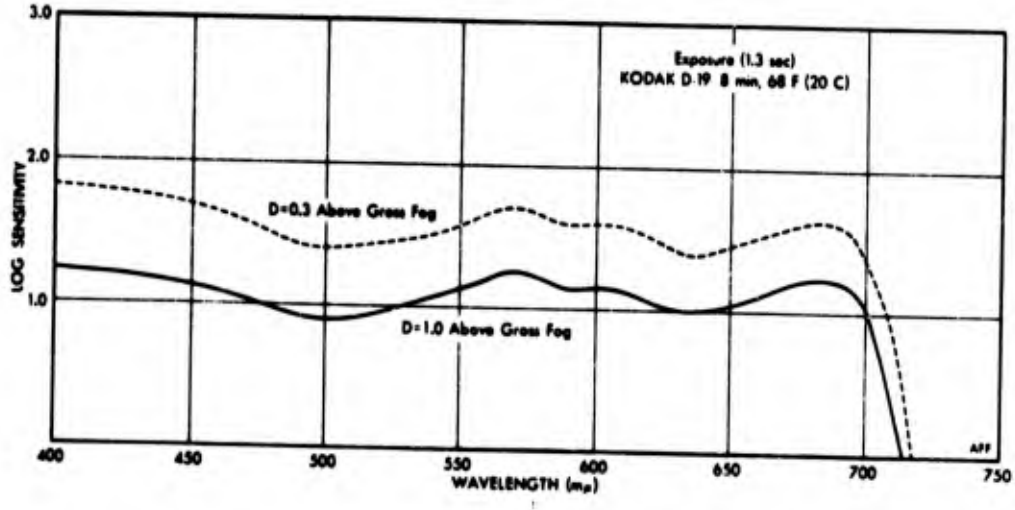

FIGURE 17c

KODAK PLUS-X AEROGRAPHIC Film, Type 5401

D-19
D = 1.0 above gross fog

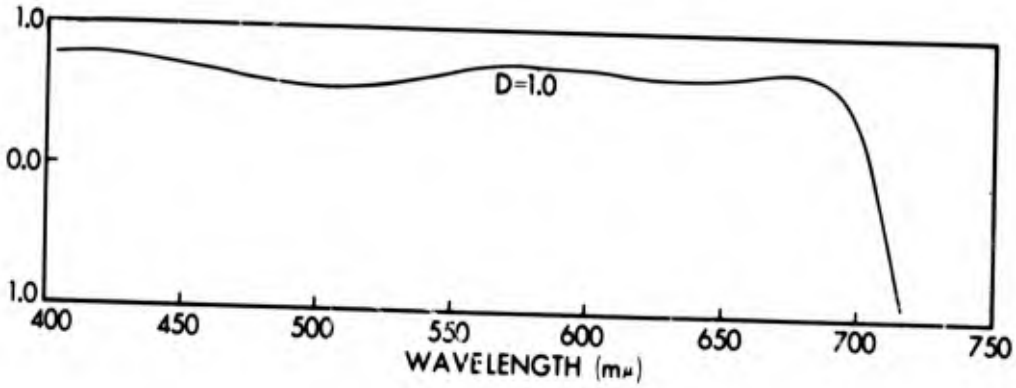

FIGURE 17d

KODAK SUPER-XX AEROGRAPHIC Film, Type 5425

D-19
D = 1.0 above gross fog

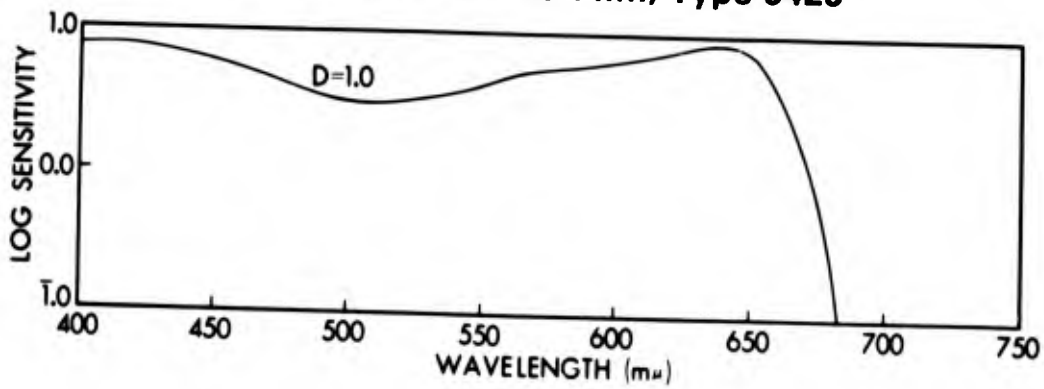

FIGURE 17e

KODAK PLUS-X AERECON Film, Type 8401

D-19
D = 1.0 above gross fog

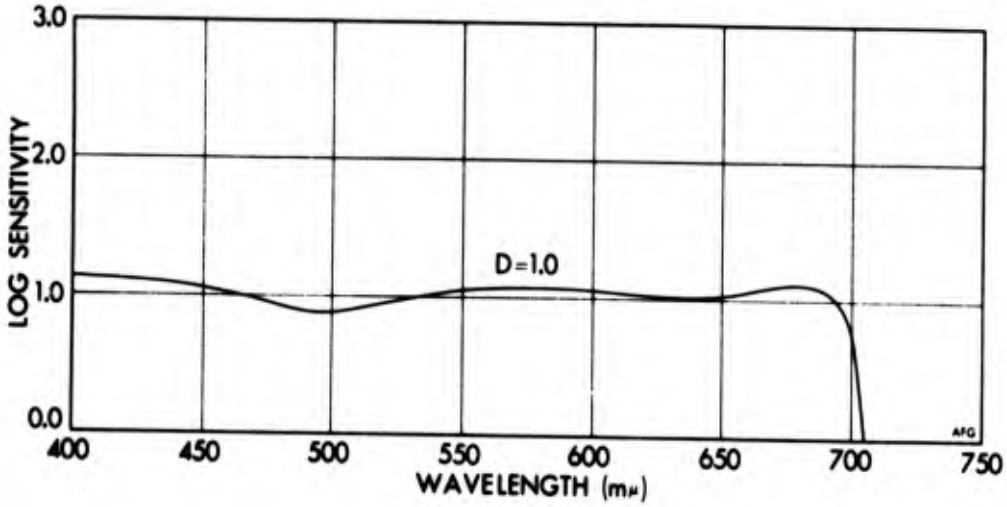

FIGURE 17f

KODAK TRI-X AERECON Film, Type 8403

D-19
D = 1.0 above gross fog

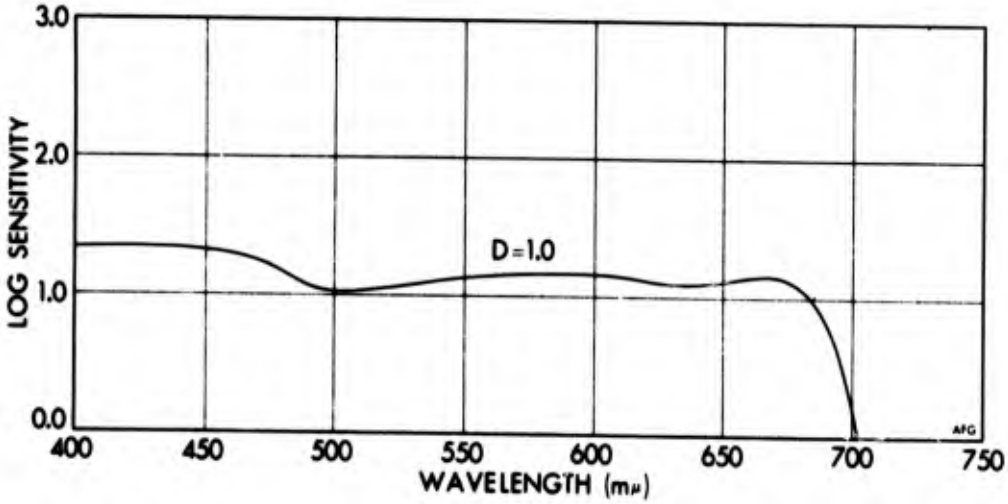

FIGURE 17g

KODAK PANATOMIC-X Aerial Film, Type 3400 (ESTAR Thin Base)

D-19
D = 1.0 above gross fog

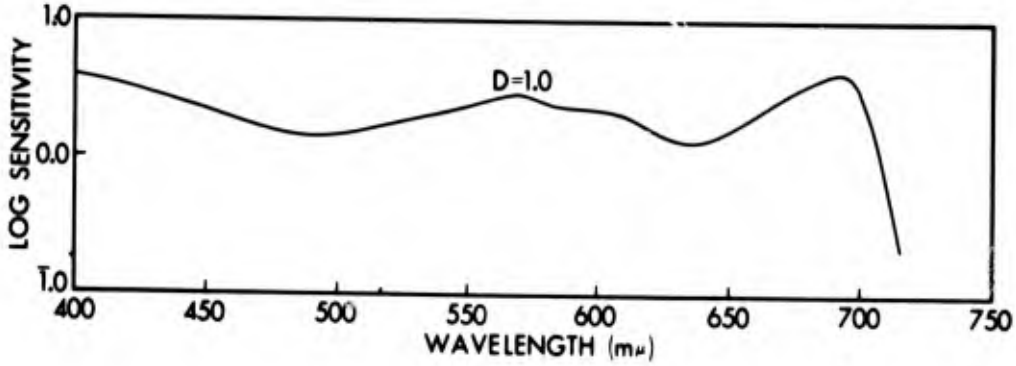

FIGURE 17h

KODAK PLUS-X Aerial Film, Type 3401 (ESTAR Thin Base)

D-19
D = 1.0 above gross fog

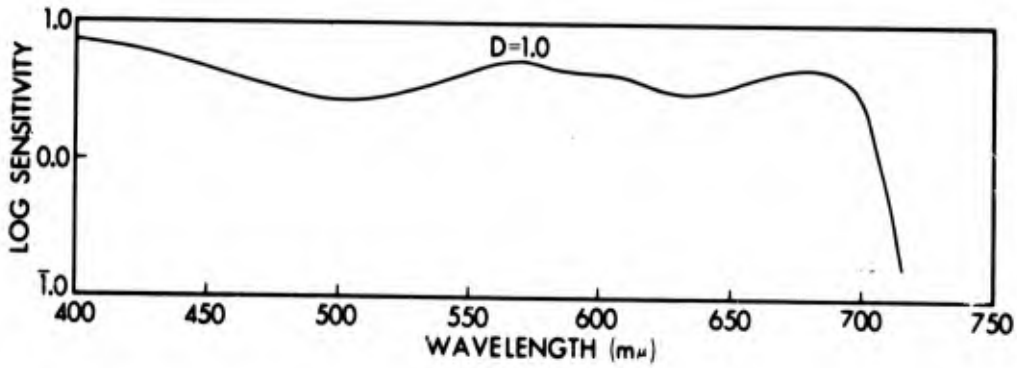

FIGURE 17i

KODAK High Definition Aerial Film, Type 3404 (ESTAR Thin Base)

D-19
D = 1.0 above gross fog

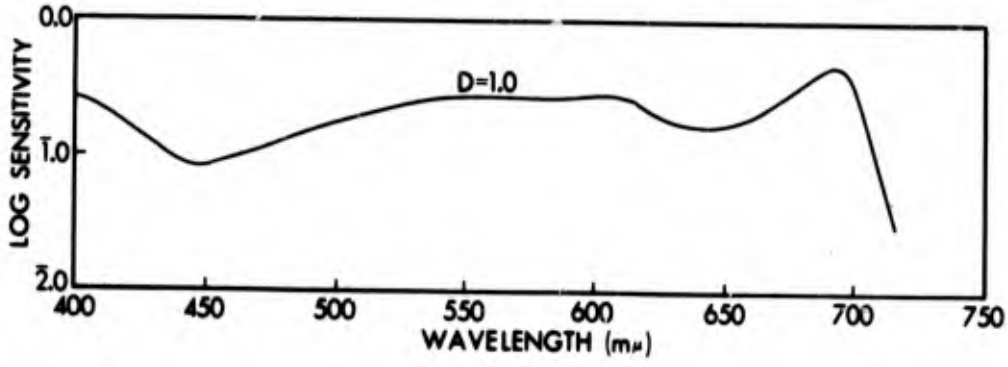

FIGURE 17j

KODAK Infrared AEROGRAPHIC Film, Type 5424

Spectral Sensitivity Curve

D-19
D = 1.0 above gross fog

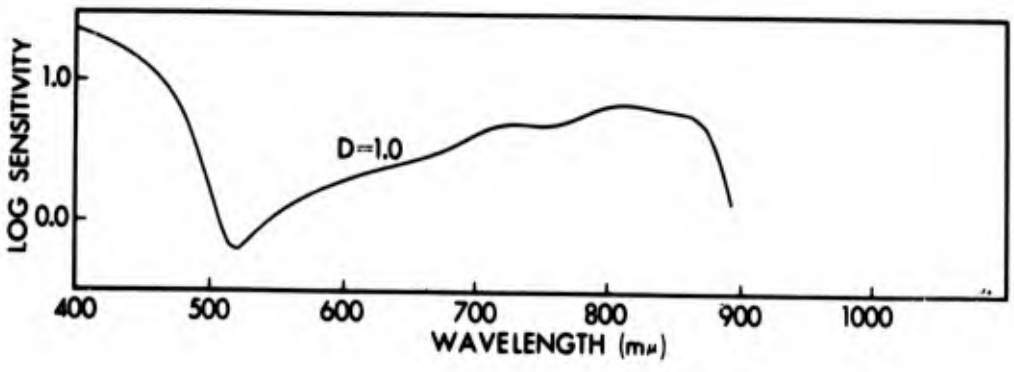

spectral characteristics of various films which may possibly be used in this program. These data were obtained from the Eastman-Kodak company. As may be seen, they each display reasonably good sensitivity to approximately 0.7 microns and thus, conform to the limitations imposed by the atmospheric characteristics.

IV.B. Sensitivity

The sensitometric properties of primary interest are those derived from the characteristic, or D-H, curve. Here the photographic effect is plotted as "output" versus input, which is the density of the negative (density is negative log of transmittance) as a function of the log of exposure. Exposure is customarily expressed as the product of illuminance (meter-candles) and time converted to a logarithm to the base ten. The exposure is plotted logarithmically since this most clearly shows the inflections which occur. While the customary unit of exposure is meter-candle-seconds (mcs), for our purposes in calculating source energy, the exposure is converted to energy density (joules $\cdot$ cm^{-2}).

A characteristic curve has three basic portions: the toe, the straight-line, and the shoulder. The toe is the region of increasing exposure which give rise to an increasing rate of density responses. The shoulder displays just the inverse character. The straight-line portion is the linear response portion of the film and this is the region where operation is desirable. The vertical length of the straight-line portion is called the latitude of the film.

Figure 18 shows characteristic curves of various film which show the possibility of being useful in the Night Photogrammetric Test Range. Two seemingly anomolous characteristics are observed on these curves. One, the density does not decrease to zero as the exposure decreases, and two, several curves are characteristic of a given film. The static level of density is referred to as the fog level of the film and is the result of the chemical reduction of unexposed grains by the developer. The amount of fog produced is a function of the nature of the emulsion and the energy, temperature, and agitation of the developing chemistry. Since an increase in fog level reduces the total contrast range of the film (latitude), every attempt should be made to maintain the lowest fog level possible. The reason several curves are characteristic of a particular film is because the shape of the curve is a function of the development. This is covered in a later section.

IV.C. Graininess

A developed photographic image consists of an aggregate of silver grains suspended in gelatin. The image structure properties of a film depend largely on the size and disposition of these grains, and upon thickness of the emulsion layer. The developed silver grains will occupy approximately the same position as they did when they were silver halide, but are not related to their original shape. The perception of non-uniformity in a photographic image is a function of grain size and disposition and the concentration of the developed silver grains. Maximum graininess occurs at a density of 0.3. If the amount of developed silver increases above 0.3 density, graininess decreases since the grains become considerably more concentrated.

FIGURE 18a

KODAK DOUBLE-X AEROGRAPHIC Film, Type 2405 (ESTAR Base)

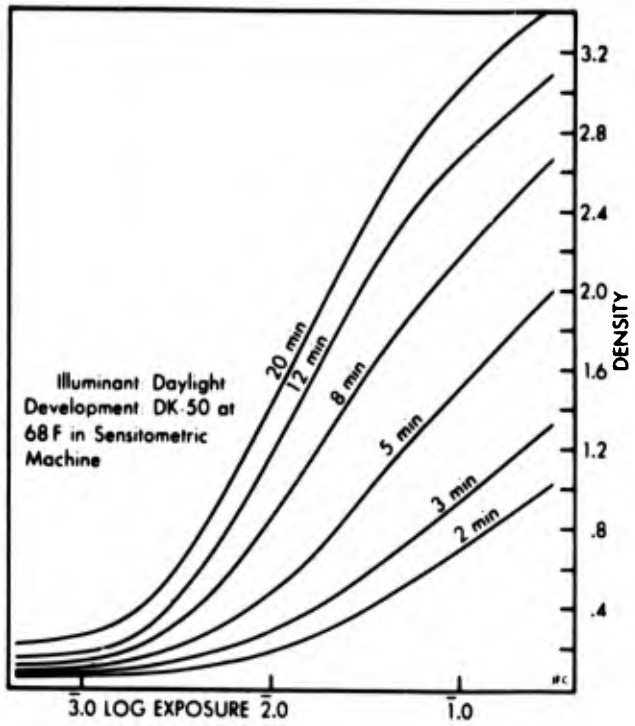

FIGURE 18b

KODAK PLUS-X AEROGRAPHIC Film, Type 2401 (ESTAR Base)

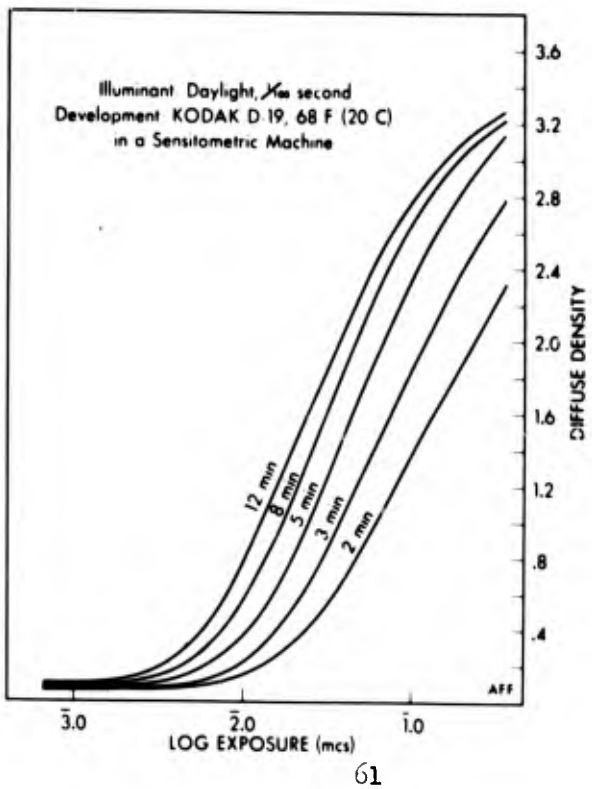

FIGURE 18c

KODAK PLUS-X AEROGRAPHIC Film, Type 5401

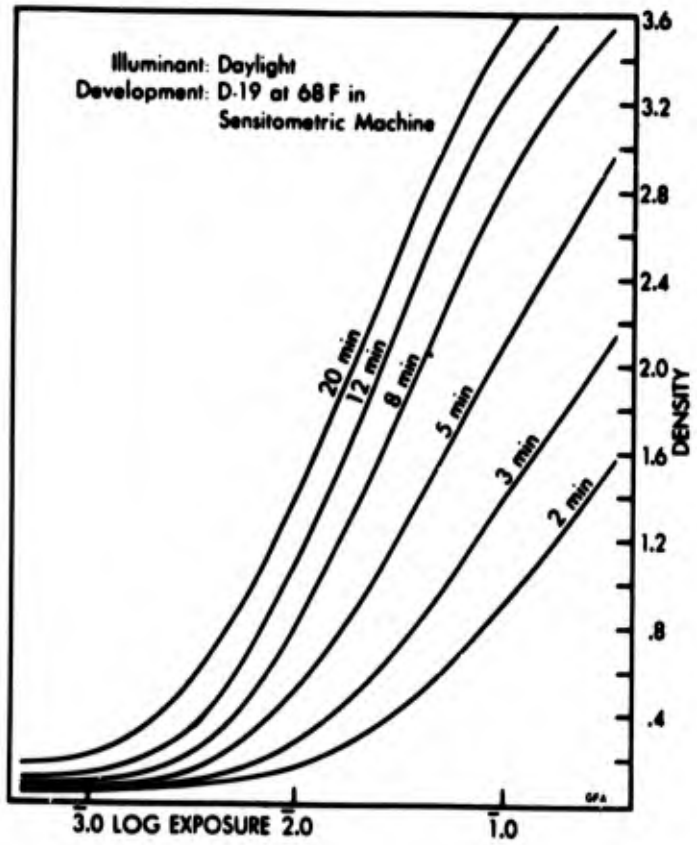

FIGURE 18d

KODAK SUPER-XX AEROGRAPHIC Film, Type 5425

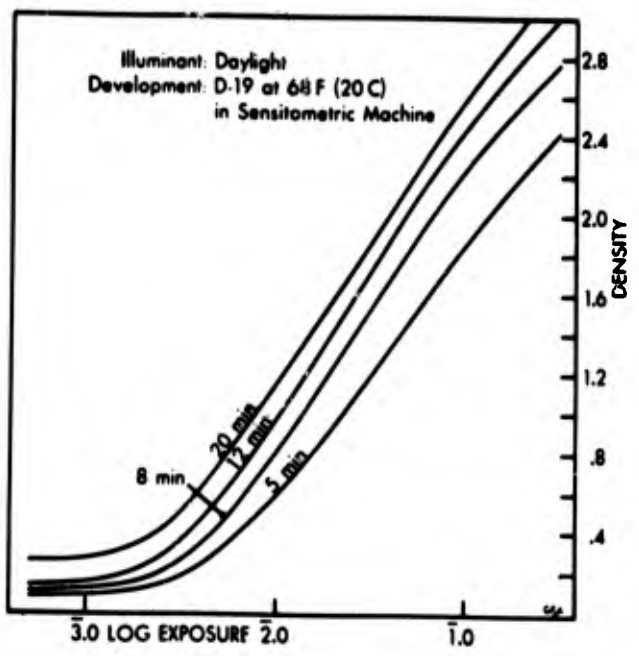

FIGURE 18e

KODAK PLUS-X AERECON Film, Type 8401

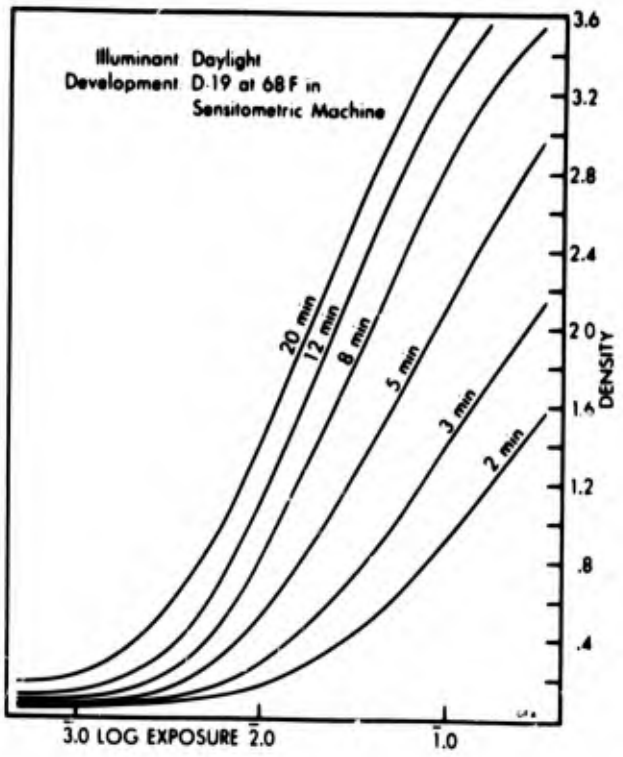

FIGURE 18f

KODAK TRI-X AERECON Film, Type 8403

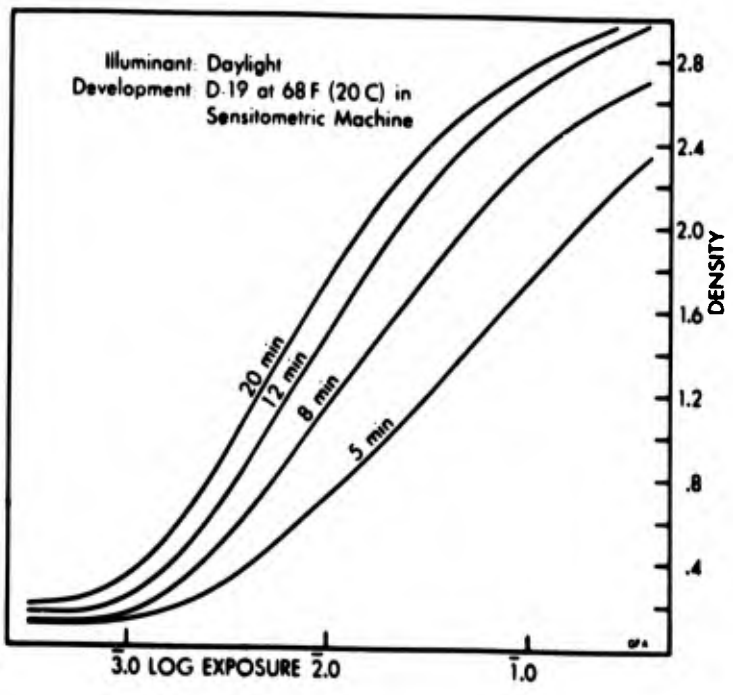

FIGURE 18g

KODAK PANATOMIC-X Aerial Film, Type 3400 (ESTAR Thin Base)

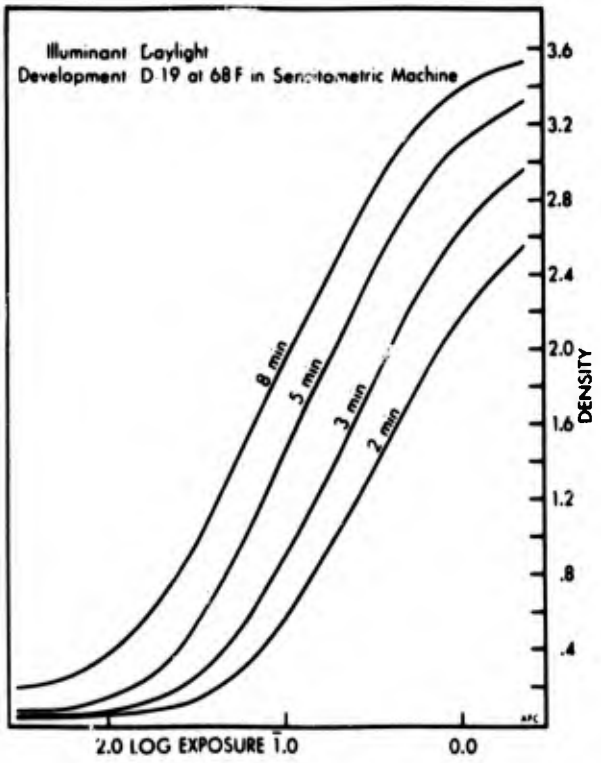

FIGURE 18h

KODAK PLUS-X Aerial Film, Type 3401 (ESTAR Thin Base)

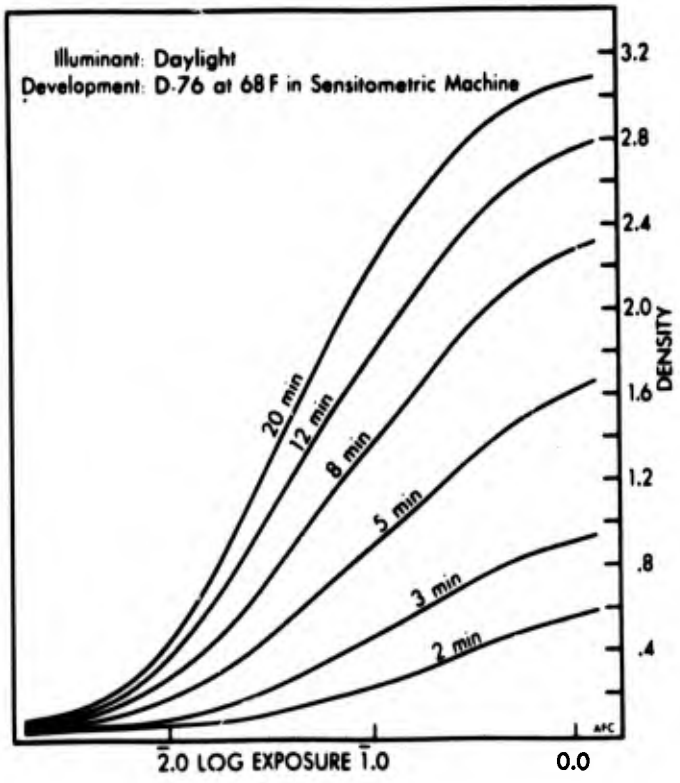

FIGURE 18i

KODAK High Definition Aerial Film, Type 3404 (ESTAR Thin Base)

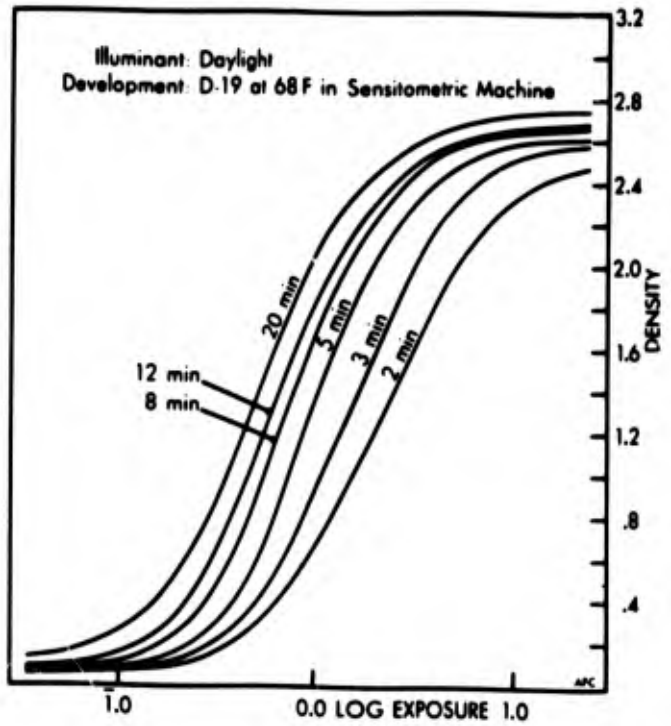

FIGURE 18j

Sensitometric Curves

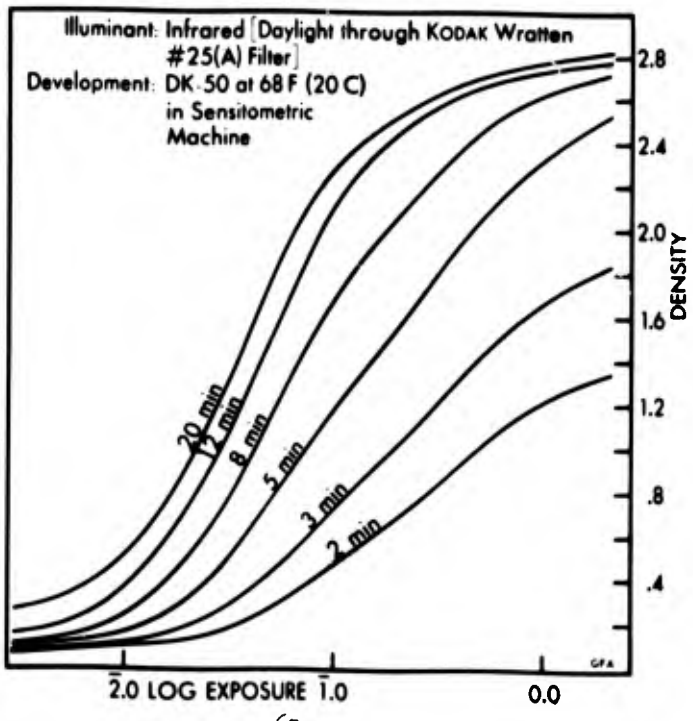

If the developed grains are small, a greater image contrast will be realized. On the basis of resolution then, we would prefer a fine grain film. A problem exists, though, since fine grain films are generally slower than large grain types. This means that a greater exposure is needed for a given density. At the present time advances are being made in producing fast, fine grain films. The film chosen therefore, must have as small a grain size as is consistent with relatively high speed.

The term granularity is an objective measurement that correlates with the subjective appearance of graininess. The root-mean-square (RMS) granularity value represents 1000 times the standard deviation in density produced by the granular structure of the material. It is obtained when a uniformly exposed and developed sample is scanned by a densitometer having an optical-system aperture of f/2.0 and a circular scanning aperture of 48 microns in diameter. The granularity value indicates the magnitude of the impression of graininess that would be produced if the film were examined visually at a magnification of twelve times.

Table IV-1 gives the granularity values for the films previously examined for spectral characteristics and sensitivity. The values shown are for negative films having a net density of 1.0 (excluding the density of the support).

Film Type	2405	2401	5401	5425	8101	8403	3400	3401	3404	5424	8443
RMS Granularity	36	35	34	37	34	48	20	35	9.7	39	22

Table IV-1. RMS Granularity for Different Film Types

The graininess of a print made from a negative of given granularity is also affected by the printing process. Among other things, granularity is changed approximately in proportion to the contrast of the print material. For example, if a negative of granularity ten is printed onto a material of contrast two, the granularity of the resulting print will be approximately doubled to twenty.

IV.D. Contrast

The slope of the straight-line portion of the characteristic curve is called the gamma of the film and is a measure of the contrast capability of that film. Gamma is actually a measure of the amount of density increase for a given increase in exposure. When gamma equals one, a perfect tone reproduction of the photographed scene results. This scene however, is degraded due to atmospheric scattering and turbulence. If a higher gamma, hence higher contrast film is used, a higher contrast image will result. Thus, using a high gamma film somewhat compensates for atmospheric scattering and turbulence. For aerial photography, films having gamma values of two to three are used.

As may be observed from the characteristic curves (c.f. Figure 18), for a given density, the higher a films gamma, the more sensitive it is. Thus, aside from contrast considerations, the higher the gamma the lower the required source energy.

It is also noted that gamma is a function of development time. The effect of development time on gamma is shown in Figure 19 where it is noticed that there is a maximum gamma. Further, the type of developer used gives rise to different gammas as well as different maximum gammas.

Suffice it to say, that the higher the gamma of a film the better the image and the lower the source energy. Consequently, the film and developer chosen should be such to increase gamma to its highest value.

IV.E. Choice of Film

The ideal film for the photogrammetric test range would be a fast, high gamma, fine grain, thin emulsion*, extended-range panchromatic film. In order to choose, or at least rank the various film in their order of preference, a figure-of-merit (FOM) was calculated for each. In this way each of the films can be compared with the others and a logical choice made on the overall characteristics of a particular film.

The FOM can be expressed in terms of the spectral sensitivity, S_λ, energy sensitivity, E_{min}, RMS granularity, G, the contrast or maximum gamma, γ_{max} film speed, s, and availability, A, as

$$FOM = \frac{S_\lambda^{\alpha}\ \gamma_{max}^{\beta}\ s^{\delta}\ A^{\varepsilon}}{G^{\eta}\ E_{min}^{\theta}} \qquad (46)$$

where the exponents are used for weighting of the various parameters. It is necessary now, to assign values to the different parameters and their

---

*If the emulsion is thin there will be less scattering of light between the grains; hence, an image with greater resolution. This phenomenon is called turbidity.

FIGURE 19a

KODAK DOUBLE-X AEROGRAPHIC Film, Type 2405 (ESTAR Base)

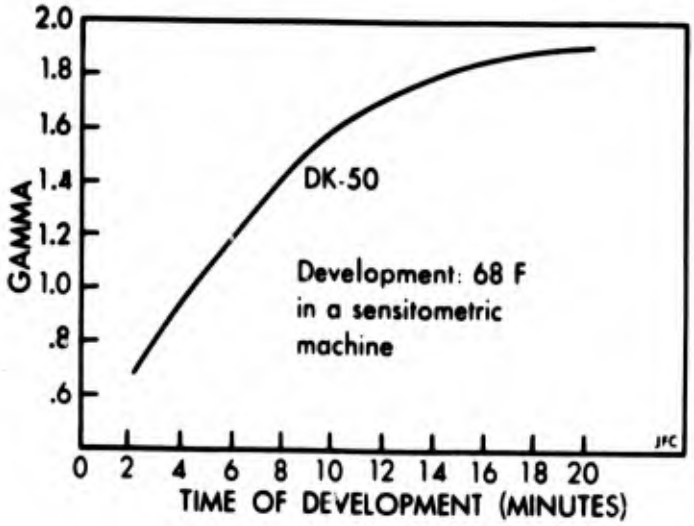

FIGURE 19b

KODAK PLUS-X AEROGRAPHIC Film, Type 2401 (ESTAR Base)

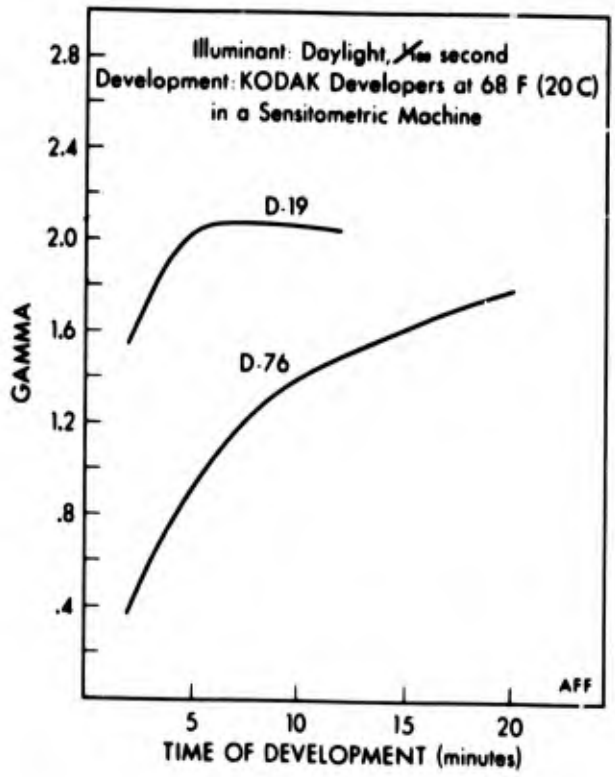

FIGURE 19c

KODAK PLUS-X AEROGRAPHIC Film, Type 5401

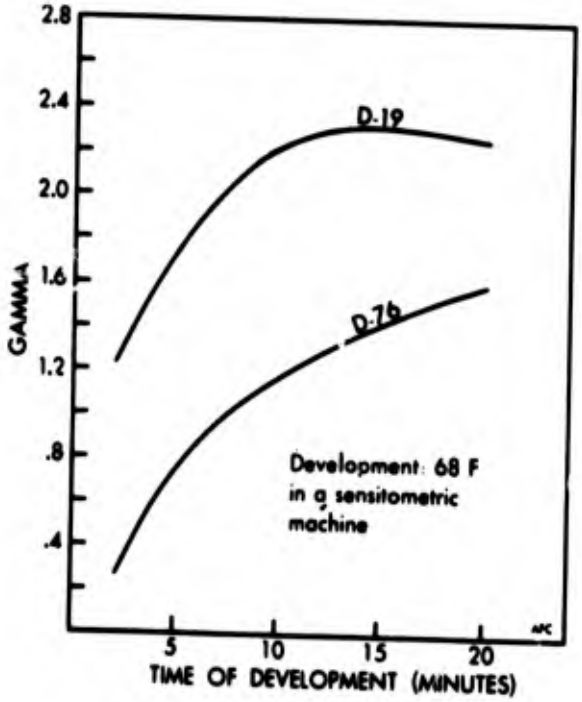

FIGURE 19d

KODAK SUPER-XX AEROGRAPHIC Film, Type 5425

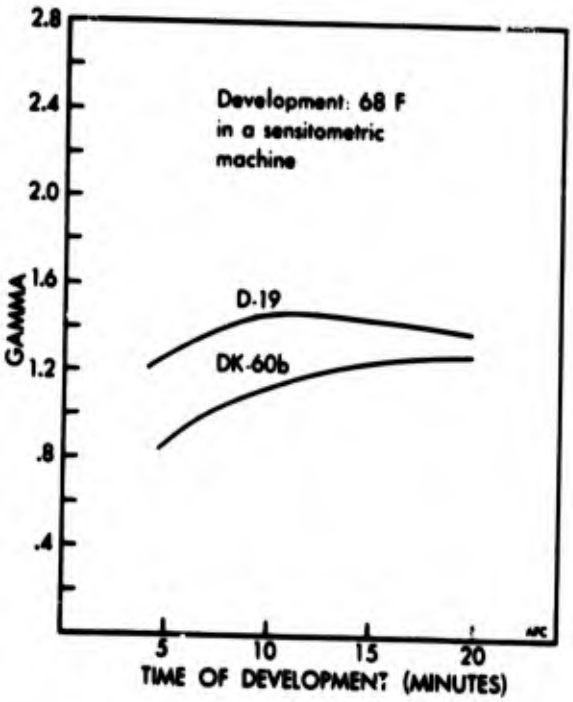

FIGURE 19e

KODAK PLUS-X AERECON Film, Type 8401

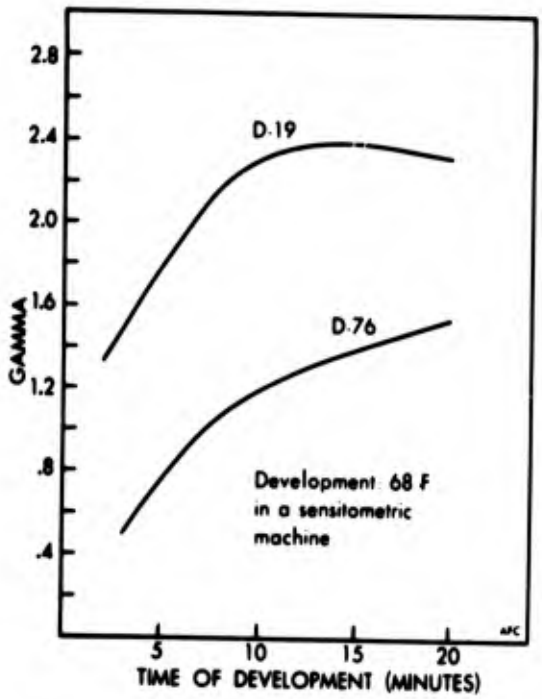

FIGURE 19f

KODAK TRI-X AERECON Film, Type 8403

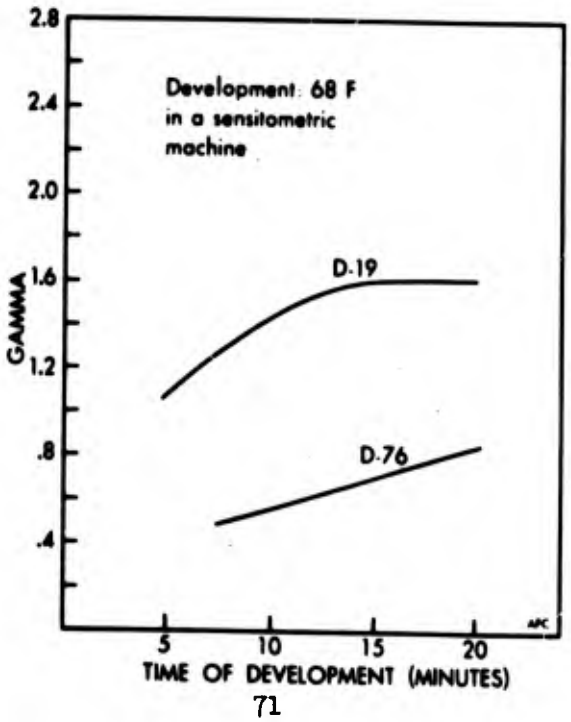

FIGURE 19g

KODAK PANATOMIC-X Aerial Film, Type 3400 (ESTAR Thin Base)

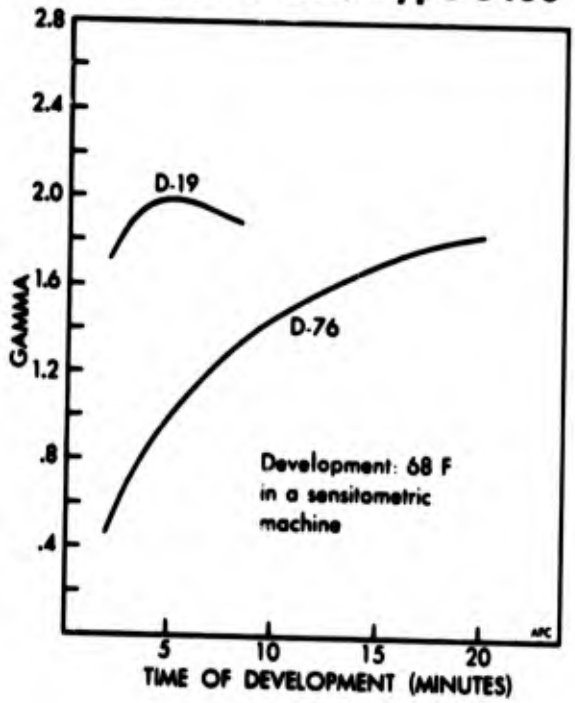

FIGURE 19h

KODAK PLUS-X Aerial Film, Type 3401 (ESTAR Thin Base)

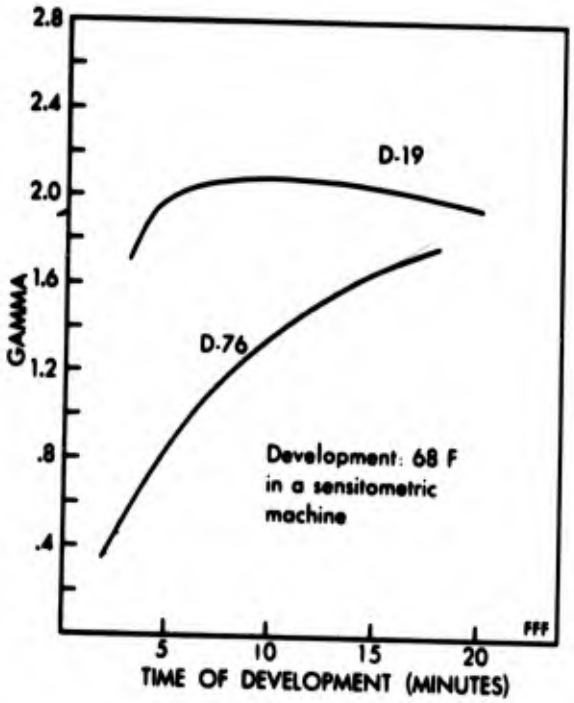

FIGURE 19i

Time-Gamma Curve
Illuminant: Infrared

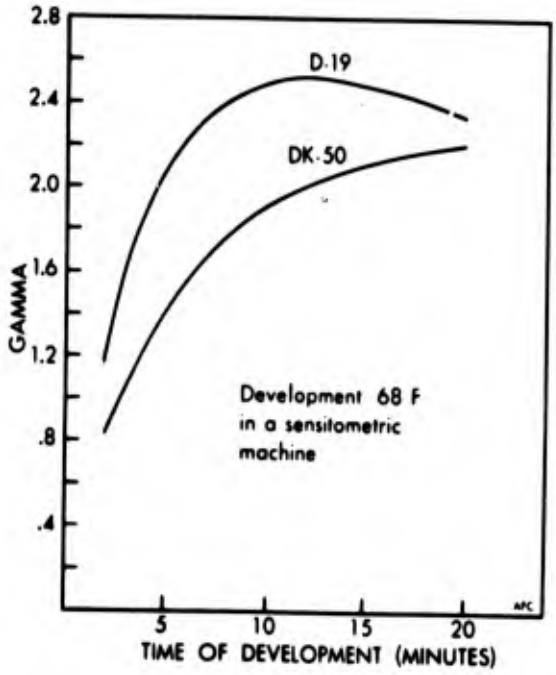

FIGURE 19j

KODAK High Definition Aerial Film, Type 3404 (ESTAR Thin Base)

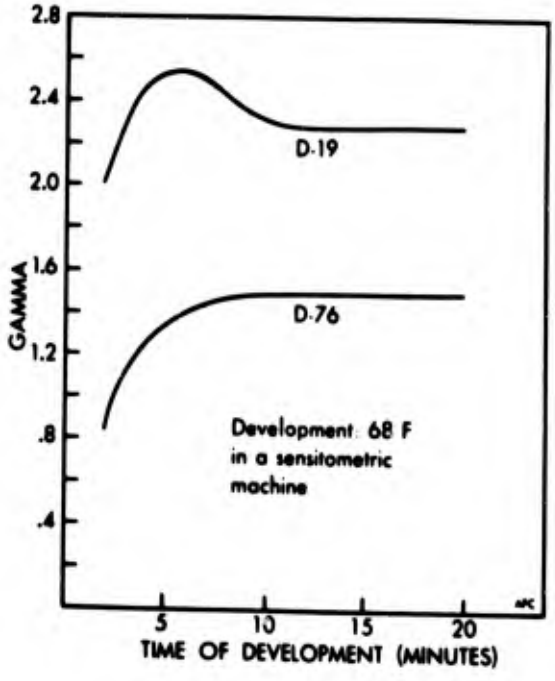

appropriate weighting factors so that the FOM for each film can be calculated. The values, and method of determining them are outlined below:

S_λ -- The spectral sensitivity is considered good if the upper wavelength cutoff is at a high level. That is to say, the higher the cutoff wavelength the better the film. To assign a value to S_λ, the upper cutoff wavelength is compared to a fixed point on the optical spectrum. The fixed point on the spectrum chosen is 0.4 microns, a value consistent with atmospheric limitations. S_λ is taken to be the difference between the upper wavelength cutoff and 0.4 microns. $(280 \leq S_\lambda \leq 500.)$

γ_{max} -- The maximum developed gamma of the particular film being examined is used in the calculation of the FOM.

s -- For the purpose of calculations, the film speed is taken to be the Aerial Exposure Index. This is defined to be the reciprocal of twice the exposure (in meter-candle-seconds) at the point on the toe of the characteristic curve where the slope equals 0.6γ.

A -- Many of the films are factory stocked by the Eastman-Kodak Company while some are available only through special-order purchase. Further, while most of the films can be used in almost all aerial cameras, a few have extremely thin bases and require special cameras (or at least are recommended for use in such cameras). Arbitrarily, factory stocked films are assigned the value ten for A, and special order types are assigned the value three. Further, if the film is recommended for use only in special

cameras, it takes on the value of unity.

E_{min} -- The exposure in meter-candle-seconds which gives rise to a density of 1.0 above gross fog is used.

G -- The RMS granularity as reported by the manufacturer is used in the calculations.

In order to choose the appropriate values of the weighting exponents, the relative importance of each major parameter must be evaluated. Once this has been done, the proper values can be established.

The most important film parameter for this program is the spectral characteristic, S_λ, and this must be reflected in the choice of α. The RMS granularity, maximum gamma, and film speed are approximately equally important. Ranking next in importance is minimum energy, E_{min}. S_λ takes on values between 280 and 500 (millimicrons) while γ_{max} lies between 1.5 and 2.6. The values of α and β must be chosen to show the relative importance of S_λ and γ_{max} but also be such that S_λ does not overpower γ_{max}. Typical values of G for mapping films are 35-45 and so η must be chosen to reduce this value such that

$$S_\lambda^{\alpha} > \gamma_{max}^{\beta} \approx G^{\eta} \approx s^{\delta} \qquad (47)$$

with $80 \leq s^{\delta} \leq 125$ being typical values for mapping films. Finally, the values of minimum exposure lie between 10^{-3} mcs and 0.5 mcs so that θ should be chosen to scale these into proper perspective. From Eq. (47) the following values of weighting factors are obtained:

$\alpha = 0.5$

$\beta = 2.5$

$\delta = 0.6$

$\epsilon = 1$

$\eta = 0.4$

$\theta = 0.5$

Now Eq. (46) can be rewritten as

$$FOM = \frac{S_\lambda^{0.5} \gamma_{max}^{2.5} s^{0.6} A}{G^{0.4} E_{min}^{0.5}} \qquad (48)$$

By substituting the appropriate values for each film the films can be ranked according to their desirability for use. Table IV-2 lists the films in their order of preference.

Film	8401	5401	5424	8403	2405	5425	2401	8443	3401	3400	3404
FOM	$1.07 \cdot 10^5$	$8.5 \cdot 10^4$	$7.79 \cdot 10^4$	$7.77 \cdot 10^4$	$7.5 \cdot 10^4$	$2.34 \cdot 10^4$	$1.51 \cdot 10^4$	$1.22 \cdot 10^4$	$5.33 \cdot 10^3$	$3.3 \cdot 10^2$	$3.14 \cdot 10^2$

Table IV-2. Figure-of-merit for Different Film Types

As may be observed in this table, film type 8401 is very slightly superior to types 5401, 5424, 8403, and 2405. Consequently, any of these films would be logical, and desirable to use in the tests. Film types 5425, 2401, and 8443 are also good; however, they are approaching an order-of-magnitude less in their FOM than the best film. The remaining films (3401, 3400, and 3404) exhibit relatively low figures-of-merit. This is due to the FOM's reflection of their special-order and special camera requirements. Note however, that if these films were factory-stocked and did not require special cameras, only type 3401 would appear desirable. This is due to the low speed of the films which are high-altitude, special reconnaissance films.

V. COMPARISON OF TEST RANGE CONCEPTS

There are basically two methods which may be employed to calibrate aerial cameras -- a passive method and an active method. The passive scheme utilizes an airborne illuminator in conjunction with ground-based reflectors, while the active employs a set of ground-based light sources. Each of the two methods display advantages and disadvantages; however, as will be evident, relative to the aims of this program, the active system is superior to the passive system.

V.A. Passive Test Range

A passive photogrammetric test range using an airborne pulsed source with ground-based reflectors could be utilized in calibrating aerial photography equipment. Such a system is desirable since an inherent property would be almost perfect synchronization between the source, the camera and the ground-based tracking cameras. In addition, it would intuitively appear, from a cost-effectiveness standpoint, that such a system would be quite feasible.

The appropriate method for evaluating the feasibility of any system is to examine the magnitude of important system parameters. One such method of evaluation is the solving of the "energy-range" equation for the system. This equation is essentially the same as the "radar" equation and its solution provides an indication of the required energy (hence the power requirements) of the source for a given set of system parameters.

The amount of source energy and power depends upon several factors:

a) Minimum energy required for exposure (E_{min})

b) Range (R)

c) Beam width of the source (ω_s)

d) Atmospheric transmissivity (T)

e) Camera lens diameter (D)

f) Image diameter (d)

g) Optical cross-section of reflector (σ_r)

h) Optical efficiency of the system (η_S)

The equation analogous to the radar equation for a passive system is

$$E_S = E_{min} \frac{2\pi \omega_s^2 R^4}{\sigma T^2 D^2 \eta_S} \left(\frac{d}{D} \right)^2 \qquad (49)$$

where E_S is the minimum source energy required for exposure of the film. The term $(d/D)^2$ provides a measure of the increase in image intensity due to the magnification of the lens system.

It must be appreciated that the light received by the camera consists of not only light reflected by the reflectors, but also light reflected from the ground, surrounding installations, and clouds. Background irradiation, H_B, at the receiver aperture will give rise within the exposure time (open shutter), τ, to an average number of noise photons at the film given by

$$\bar{N}_B = H_B \tau (\Delta\lambda) (\pi/4) D^2 \eta_C / h\nu \qquad (50)$$

where

N_B = average number of noise photoelectrons

$\Delta\lambda$ = spectral width of energy at the film

η_C = efficiency of the receiving optics

h = Planck's constant

ν = frequency

It is necessary now to determine the background spectral irradiance from

all possible sources. The chief sources of noise will be reflection of light from clouds and the ground and light backscattered from atmospheric particles. To determine the amount of energy scattered from clouds and from the ground, consider the following: If the spectral irradiance of the incident light is H_S watts per unit area per Å normal to the direction of propagation, then the power reflected, P_R, per steradian per Å in the direction θ_T per unit area of the cloud, or ground, is

$$P_R = \frac{H_S}{\pi} \cos \theta_T \cos \phi_T \tag{51}$$

where ϕ_T is the angle between the normal to the reflector (cloud or ground) and a line from the source to that reflector. An expression for the total area, A_R, reflecting light may be written

$$A_R = \frac{\pi}{4} (\omega_R R)^2 \frac{1}{\cos \theta_T} \tag{52}$$

By combining Eq.'s (51) and (52) and by noting that the optical bandwidth of the camera is B_o, the rate at which quanta are received, N_R/t, may be written

$$\frac{N_R}{t} = \frac{\pi}{16} \frac{\eta_C D^2 B_o \omega_R^2}{h\nu} H_S \rho_T \cos \phi_T \tag{53}$$

where ρ is the reflectivity of the reflector. If this result is multiplied by the exposure time, the number of noise photons received is determined.

To estimate the amount of noise photons which arise from atmospheric scattering, a uniform atmosphere is assumed and the extinction theory of Koschmieder is followed. Consider a small element of cone defined by the camera field-of-view. It will have a volume given by

$$\frac{\pi}{4} (\omega_C r)^2 dr \tag{54}$$

where r is the distance from the camera to the scattering element and ω_C is the camera field-of-view. Let σ_S be the integrated scattering coefficient per unit volume, then the power scattered per steradian in the direction of the camera is (assuming isotropic scattering)

$$P_S = \frac{\pi B_o H_S}{16} \sigma_S (\omega_C r)^2 dr \tag{55}$$

Noting that this will be reduced by the atmospheric transmissivity before reaching the camera, the received quanta rate is calculated by integrating over the entire cone,

$$\frac{N_{SA}}{t} = \frac{\pi \eta_C}{64h\nu} \int_o^R B_o T(r) \sigma_S H_S \omega_C^2 D^2 dr \tag{56}$$

$$= \frac{\pi}{64} \left(\frac{\eta_C D^2 B_o \omega_C^2}{h\nu} \right) \left(\frac{\sigma_S}{\alpha} (1-T) H_S \right) \tag{57}$$

with α the atmospheric absorption coefficient.

The total flux of quanta due to scattering is the sum of the individual contributions -- i.e., $\bar{N}_N = N_G + N_{SA} + N_C$. Here $\bar{N}_N$ is the average total number of noise photons, N_G is the number caused by scattering from the ground and N_C is the number due to reflections from clouds. The total flux then can be expressed as

$$\frac{\bar{N}_N}{t} = \frac{\pi}{4} \frac{\eta_C D^2 B_o H_S}{h\nu} \left[\frac{\pi \omega_R^2 T \cos\phi_t (\rho_G + \rho_C)}{4} + \frac{\omega_C^2}{16} \left(\frac{\sigma_S}{\alpha} (1-T) \right) \right] \tag{58}$$

where ρ_G and ρ_C are the reflection coefficients of the ground and clouds, respectively.

If the background noise level is sufficiently high there will be a

reduction in the clarity, or deliniation of target signals relative to the background. Ideally the image would be a black background with a lattice of light spots representing the set of reflectors on the ground. If the background is uniform in intensity, and non-zero in magnitude, then the light spots will be situated on a light background. In the limit of equal intensity of both background and reflected light there is no deliniation of the lights from the background. While this will not be the case, it is expected that the presence of background radiation will degrade the image, the amount of degradation being dependent on the amount of cloud cover, type of clouds, and reflective characteristics of the ground.

V.A.1. Passive Test Range Design

Basically, the design of the test range depends strongly upon the type of reflector used since its optical cross-section determines the minimum required energy for exposure and the image size at the film plane. The other parameters which appear in the range equation are relatively fixed in value and thus cannot be changed to minimize the source energy.

V.A.1.a. Reflector Design and Optical Cross-Section

A reflector used in a passive range must exhibit a maximum optical reflection cross-section for an effective cross-sectional area such that a 100 micron image is obtained at the film plane (using typical cameras) at the maximum slant-range for which the system is designed, and an angular divergence such that the reflected light can be observed at any point in the range by the aerial camera.

There are two reflector configurations which meet these requirements - the Lambertian and the spherical (convex) reflectors. In both cases the image size characteristic requires a reflector diameter of 18 inches and, in order to illuminate the complete range as well as accepting light from any point in the range, the reflected angular divergence should be 80°.

The optical cross-section of a reflector is taken to be the product of the effective cross-sectional area (the area reflecting light) and the coefficient of reflectivity. In the case of a Lambertian reflector however, some of the incident energy is lost. This is due to the characteristics of a diffuse reflector. As a consequence, the optical cross-section must consider this loss. For a plane angular divergence of 80°, the amount of energy lost due to diffusion is $0.587\ E_i$, where E_i is the incident energy. Thus, if ρ is the reflectivity of the Lambertian reflector and A is its cross-sectional area, the amount of energy reflected in an 80° cone, E_R, is

$$E_R = 0.413\ E_i\ \rho A \tag{59}$$

and the ratio E_R/E_i is taken to be the optical cross-section of a Lambertian reflector:

$$\sigma = 0.413\ \rho A \tag{60}$$

For an 18-inch circular reflector with a coefficient of reflectivity of 0.85 (a typical value), the optical cross-section to be used in calculating the required source energy is $\sigma = 88.3\ in^2$.

A spherical reflector whose radiation pattern appears to be an 18-inch

diameter flat-plate emitting energy into an 80° cone* has a higher optical cross-section since it can be made a specular reflector which reflects essentially all of the impingent energy into the cone. Because it appears to be an 18-inch plate, its effective geometrical cross-section is 251.5 in^2, the same as the Lambertian reflector. For the same coefficient of reflectivity as the Lambertian reflector, the optical cross-section is $\sigma \approx 214$ in^2 -- a factor of 2.42 over the Lambertian reflector. As a consequence it is logical to choose the spherical reflector for use in a passive photogrammetric test range.

V.A.1.b. Source Energy Requirements

Having determined the optical cross-section of the reflector, it is now possible to calculate the minimum amount of source energy required to expose the film. The parameter values which are used in the calculations are justified as follows:

a. Minimum required received energy at the film plane, E_{min} -- for the films studied, this value is taken to be the nominal value for the best films, $E_{min} = 2.5 \times 10^{-3}$ mcs (3.75×10^{-10} $J \cdot cm^{-2}$).

b. The slant-range, R -- the maximum slant-range of 100,000 feet is used.

c. Beam-width of source, ω_S -- this is assumed to be 90°.

d. Atmospheric transmissivity, T -- an average value of 0.8.

---

*These characteristics are achieved with a segment of a sphere of radius 14-inches and an interior angle of 66°.

e. Camera lens aperture diameter, D -- the value used for D is nominal value of two inches as was determined by a survey of aerial cameras.

f. Image diameter, d -- from contractual specifications, d = 100 microns (3.94×10^{-5} in).

g. Optical cross-section of reflector, σ -- $\sigma = 214$ in^2.

h. Optical efficiency, η_S -- a typical value is $\eta_S = 0.75$.

Substitution of these values in Eq. (49) provides us with

$$E_S = 4.3 \times 10^3 \text{ J} \tag{61}$$

V.B. Active Test Range

An alternate method of performing airborne camera calibration is to place light sources on the ground and photograph them in a flight pass over the test range. The chief advantages of this type of configuration are lower source energy (one-way transmission only), less atmospheric problems, and the absence of background radiation. The major reasons for lower energy being a factor of prime consideration are less power required - hence less weight - and cost reduction. The other two advantages are extremely desirable since, due to accuracy requirements, the best possible images are required. With no noise background, the photographed image will appear as a lattice of light spots on a black background allowing localization of the image with much greater confidence than that obtained with a passive system. The problems associated with atmospheric scattering and turbulence induced fluctuations are reduced by approximately the square of the range. Consequently, the active system is far more attractive than the passive system.

On the basis if image properties, as well as the reduced cost of the active system, this configuration is chosen for the test range. In the following sections the design of an active test range is developed.

VI. DESIGN OF THE PHOTOGRAMMETRIC TEST RANGE LIGHT MODULE

Having determined that an active test range is required for calibration of aerial cameras, it is now necessary to design the best possible system. In accordance with contractual requirements the light module must satisfy the following conditions:

a) The light source shall be of a size such that it will be imaged as a circle no more than 100 microns in diameter upon the recording film.

b) The system shall be capable of being used with aircraft at altitudes up to 100,000 feet.

c) The light sources shall be of a size, intensity, and spectral value such that the true center point of the photographic images they produce (on selected films) shall be resolvable to an accuracy of three microns RMS or less.

d) The lights shall be remotely controlled and capable of being turned on or off from both the aircraft and the ground.

e) The range shall be self-sustaining, with minimum maintenance requirements. The system shall function trouble-free for a minimum of thirty days (sixty hours of operation) and require minimal maintenance thereafter.

f) The system shall incorporate a regenerative power supply.

g) The individual lights shall be portable enough for one man to remove or install them on a fixed base in minutes. This requires the lights to be light-weight (no movable package must weigh in excess of 100 pounds), and have a modularized (plug-in) construction.

h) Each light shall be both vandal proof and bullet proof.

i) Each light shall be designed such that it will withstand the climatological conditions at Casa Grande, Arizona for a five-year period.

In addition to the above requirements, cost must be considered as an extremely important parameter. It has been assumed that a fixed amount of funds will be available for construction of the test range. Consequently, the lower the cost per light installation, the more installations that can be built. Having a large number of sites is desirable since more accurate results are achieved (locating the true center of the source) with an increasing number of lattice points.

VI.A. Source Energy and Power Requirements

The first step in designing the test range is to determine the source energy required for exposure of the film. To do this an equation similar to the range equation (Eq. 49) is used; however, since this problem is concerned with one-way transmission the equation is somewhat different. The required source energy, E_S, is given by

$$E_S = E_{min} \frac{\pi R^2 \omega_S^2}{\tau_S T D^2} \left(\frac{d}{D}\right)^2 \qquad (62)$$

The differences between this equation and the range equation are the absence of the term σ, the quadratic dependence of range, and the linearity of the equation with respect to the atmospheric transmissivity. The solution of this equation, using the values for the system parameters as in the passive case is

$$E_S = 3.6 \times 10^{-3} \text{ J} \cdot \text{cm}^{-2} \tag{63}$$

If the diameter of the transmitting source is known, the actual lamp energy required is specified. As discussed previously, an 18-inch diameter source is necessary to image a 100 micron light spot on the film; thus, the actual lamp energy, E_L, is

$$E_L = \frac{\pi E_S D_S^2}{4\eta_c} = 2.52 \text{ J} \tag{64}$$

where:

D_S = diameter of transmitting source

η_c = efficiency of transmitting optics (collector)

Compared to the lamp requirements for a passive test range (4300 J), it is easy to see the advantage (from a power standpoint) of using an active system.

The energy value determined above is the amount required for the exposure of one frame of film. The power requirements of the lamp are determined by the frame time of the camera and the duty factor of the system. For most cameras which are expected to be used, the exposure time is one millisecond. This means, in terms of peak power (i.e., the amount of power output per frame), that 2500 watts is required. This is an extremely high value if the system is operated continuously. On this basis it appears that a pulsed light source is considerably more feasible than using a 2500 watt continuously operating lamp. If N frames per second are required for calibration of the camera, the average power output of the lamp required is

$$P_{ave} = N E_L \tag{65}$$

For example, if the system is designed for a lamp pulse repetition frequency, (PRF) of twenty pulses per second, a lamp must be chosen with an average power capability of at least fifty watts. The amount of average power is dependent upon the frame rate of the camera and the number of photographs which are to be taken. In the following section this subject is duscussed in greater detail.

The characteristics of the lamp to be used in the test range are:

1) Capable of 2.5 J output

2) Capable of 2500 watt peak power output

3) The lamp must have spectral characteristics which are consistent with the spectral characteristics of the atmosphere and the film.

The subject of lamp choice is discussed in a later section.

VI.B. Lamp/Camera Synchronization and Source Average Power

Utilization of a pulsed transmitting source requires a method for synchronization of the pulsed light and the camera framing. Apparatus can be manufactured to accomplish this task; however, it would be relatively complex as well as expensive. An alternate method may be utilized -- "self-synchronization" of the system. In this case the light is pulsed at a rate significantly higher than the frame rate of the camera and, due to an inverse "eclipsing" effect caused by the relative motion between light pulses and camera framing, the camera and source will periodically be synchronized.

If ν_c is the frame rate of the camera and ν_L is the pulse-repetition frequency of the source, the period between synchronizations, T_s, is given by

$$T_s = |\nu_c - \nu_L|^{-1} \tag{66}$$

where

$$\nu_c \neq \nu_L$$

and the number of times per second, or the number of photographs per second which may be taken, N, is

$$N = |\nu_c - \nu_L| \tag{67}$$

Once the frame rate of the camera is known, it is possible to determine ν_L (for any value of N) and thus determine the average power requirement of the source. It would be desirable to have pulses transmitted at rates of about ten to forty times per second for compatability with typical cameras. This would result in values of N from approximately ten to forty which would be consistent with the requirements of both reconnaissance and mapping cameras.

If the system is designed to operate at frequencies of forty pulses per second, the lamp chosen must be capable of operating at output power levels of the order of 100 watts. Further, assuming that the narrowest pulse of 10^{-3} seconds in duration, peak powers of 2.5×10^3 watts must be achievable in this lamp. In the following section several types of lamps are evaluated and a choice is made with consideration of the required parameters.

VI.C. Selection of Lamp

Several lamps were studied to determine which ones were best suited to the requirements of this program. Ordinary fluorescent lamps, as well as power

groove fluorescents (circular tube shape) were discounted immediately because of their inability to be flashed at high enough pulse rates. Incandescent lamps are also undesirable because of their flashing characteristics. The types of lamps which appear suitable are of the xenon flash-lamp family. These basically have the desired spectral, power, and energy characteristics necessary to meet the requirements of the program.

Determination of the most logical lamp choice was based upon the figures-of-merit for the lamps under consideration. The factors of importance in choosing a lamp are:

a) Spectral efficiency, $\eta_{DC}(\lambda)$. This represents the total amount of energy in the spectral range of interest as related to the total output energy of the lamp. The spectral efficiency is thus given by

$$\eta_{DC}(\lambda) = \frac{\int_{\lambda_1}^{\lambda_2} E_o(\lambda)\, d\lambda}{\int_0^{\infty} E_o(\lambda)\, d\lambda} \tag{68}$$

b) Average output power capability, $\bar{P}_{out}$. This is primarily a measure of the capability of the lamps to be pulsed at certain rates but also has thermodynamic ramifications.

c) Maximum pulse-repetition frequency, PRF_{max}.

d) The amount of average power required, $\bar{P}_{req}$. This parameter is a measure of the conversion efficiency of the lamps.

The figure-of-merit, M, for a given lamp may be expressed in terms of these parameters as:

$$M = \frac{\eta_{DC}^{\alpha}(\lambda)\ \bar{P}_{out}^{\beta}\ PRF_{max}^{\gamma}}{\bar{P}_{req}^{\delta}} \tag{69}$$

where the exponents are weighting factors for the various parameters. The importance of the parameters is reflected in the choice of these weighting factors and once determined Eq. (69) can be applied to enable the lamp choice. The rank of lamp parameters, in order of importance are: $\eta_{DC}(\lambda)$, $\bar{P}_{out}$, $\bar{P}_{req}$, and PRF_{max}. Then, choosing appropriate values for α, β, γ, and δ, Eq. (69) can be written

$$M = \frac{[\eta_{DC}(\lambda)]^{0.9}\ [\bar{P}_{out}]^{0.8}\ [PRF_{max}]^{0.5}}{[\bar{P}_{req}]^{0.6}} \tag{70}$$

Individual lamps can now be evaluated by solving Eq. (70) with the parameters peculiar to a given lamp.

Xenon flash lamps have the desired characteristics required on this program. These lamps are available in essentially two forms, short-arc and helical construction. Short-arc lamps are characterized by the radiation being produced by an arc discharge between two closely spaced electrodes in a high pressure atmosphere of xenon gas. The lamps are generally manufactured for continuous operation but they can be pulsed. In a pulsed mode however, for greatest conversion efficiency, the lamp requires "simmering", i.e., power must be continuously applied to maintain the voltage slightly below the firing threshold.

Helical flash tubes are manufactured by several companies and are designed to operate at pulse rates of the order of sixty pulses/second. The pulse widths available are of the order of one millisecond, which is consistent with

typical camera frame times. These types of lamps have figures-of-merit of the order of three to five, approximately an order-of-magnitude greater than any other type of lamp (typical values of other lamps are $0.2 \leq M \leq 0.6$). On the basis of the qualities of helical flash lamps, they will be chosen in the design of the test range.

VI.D. Control of System

Remote control turn-on and turn-off as well as the ability to remotely change the pulse-repetition frequency is required. To provide this capability in the least complex and costly way presently used UHF equipment is employed. The remote control system is designed as follows.

VI.D.1. Aircraft System

The standard military UHF (225-400 MHZ) command transmitter aboard the aircraft shall be utilized. A frequency shall be selected in this range which is least used by other operations in the Casa Grande area.

The aircraft radio transmitter shall be equipped with a tone generator connected to the modulator circuit of the UHF command transmitter with an interconnecting switch. When the transmitter and the tone generator are in the standby condition, closing a single switch at the system control panel will perform the dual function of tone generation and transmitter operation. At the time of transmission, the transmitter shall be at the preselected frequency referenced above.

The tone will consist of two or more sequenced tones so as to provide an an address which the receiver will recognize and respond to. As covered

elsewhere in this report, three modes, each representing a discreet flashing rate for the lights, is desired. For simplicity and least cost, the airborne transmitter/tone-generator combination will be energized once to turn on the lights at the lowest pulsing frequency, the second manual switch operation shall increase light pulse rate to the next highest pulsing frequency, and a third energizing shall produce the third highest pulsing frequency. At the fourth operation of the control switch the lights will shut off and the system will be cycled preparatory for turn-on at lowest pulse frequency on receipt of the next energizing signal.

VI.D.2. Ground Control System

In order to control the test range from the ground, transceivers must be utilized to relay control signals from a remote area to each light site. A test measuring the propagation of UHF transmission from ground site to ground site was performed approximately seven years ago. The test showed that satisfactory reception of UHF signals can be obtained at distances in excess of seventy miles from the transmitter provided no obstacles exist between the transmitter and receiver. If the receiving (or transmitting) antenna is placed a short distance behind such obstacles, communications are virtually impossible. The topography of the proposed test range shows the presence of two mountains -- the Casa Grande and the Silver Reef ranges -- with sites located such that certain installations will be shaded regardless of the location of the transmitter. To provide satisfactory communications to all sites it is recommended that the following design be used:

At the highest point of each of the named ranges shall be located a

transceiver combination. The receiver shall be set to the aircraft operating frequency for the system, the transmitter at a second available frequency, sufficiently removed to prevent excessive front-end RF loading of the receiver by the adjacent transmitter. Separate omni-directional antennae shall be used for the receiver and for the transmitter, and antenna locations shall be as far apart as can be conveniently and economically accomodated.

The receivers at the tops of the mountains will receive the signal from any location of the aircraft or the ground control point within line of sight; the receiver output will be used to modulate the transmitter so that all sites shall be energized by the signal relayed from the mountain tops. This system will eliminate the necessity for expensive wire installations and will permit extreme latitude in location of the ground control point as well as the use of a mobile ground control station.

The equipment to be used at the ground control point shall be the same as that used in the airborne system. The same operating technique shall be followed as described for the airborne system. This technique of effecting communications is illustrated in Figure 20. In Figure 21, block diagrams are shown for the airborne, ground, and relay systems.

VI.D.3. Light Site Communications System

Each site shall be equipped with a UHF antenna, a single-channel UHF receiver, a tone receiver, and an electrical system incorporating a four-position stepping switch. The receivers shall be transistorized units with low power consumption and shall operate continuously. Upon receipt of a

Figure 20

Air-ground communications link

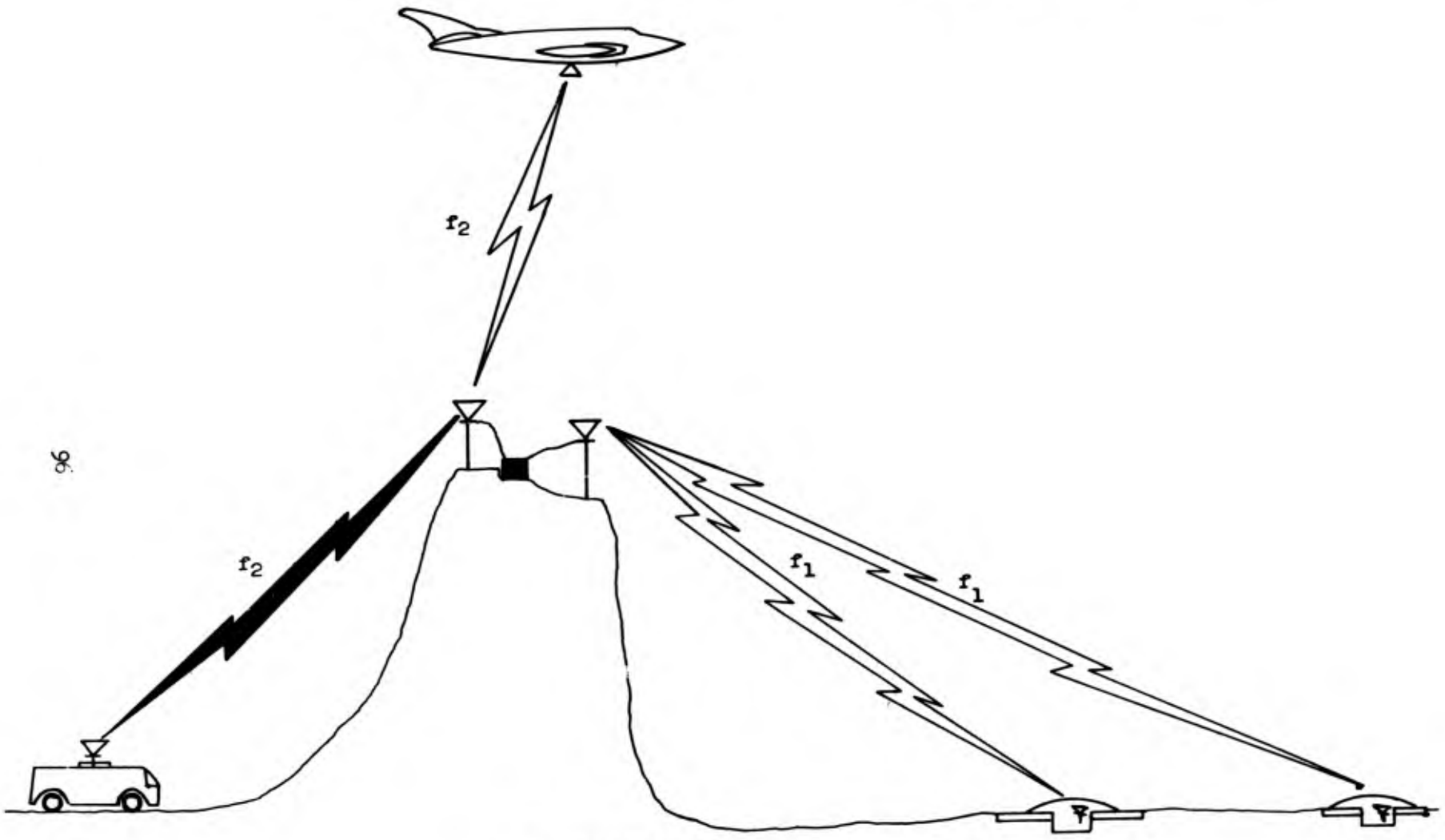

SYSTEM SCHEMATIC

AIRBORNE AND GROUND CONTROL

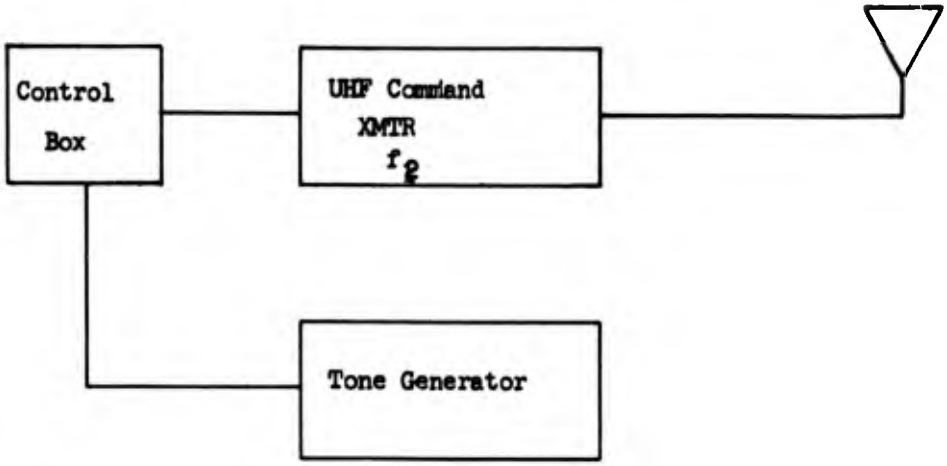

Figure 21A. Block Diagram - Airborne System

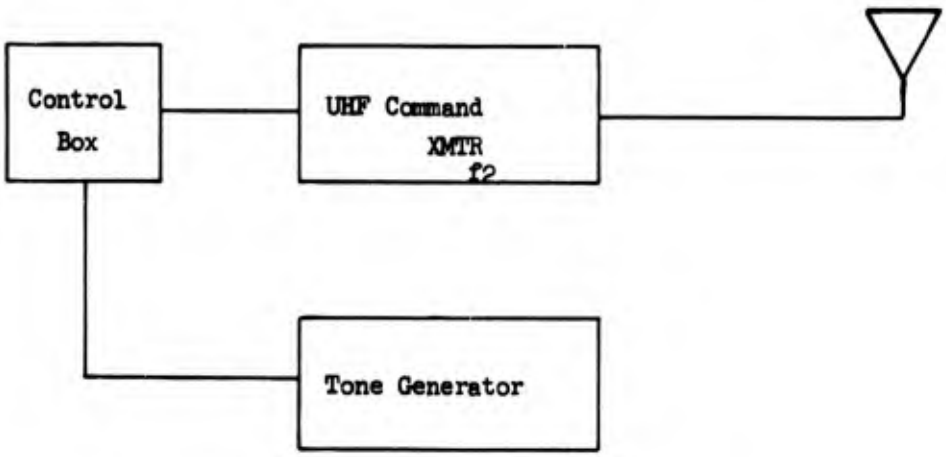

Figure 21B. Block Diagram - Ground Control Station

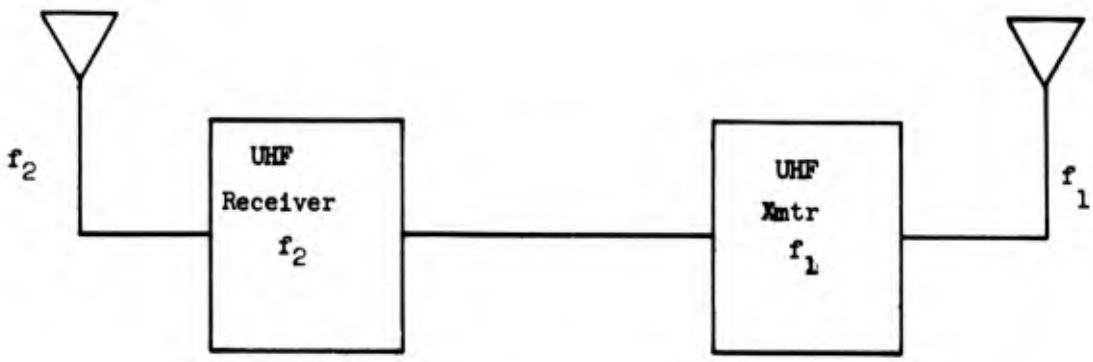

Figure 21C. Block Diagram - Mountaintop Relay Station

signal at the required frequency, the tones (including the address tone(s)) shall cause the receiver to operate a switch which will energize the electrical system and advance the stepping switch one step. At the first step the stepping switch will close an electrical switch to energize the lamp turn-on system and start the system operating at the preset first pulse repetition frequency.

At the second energizing signal the stepping switch shall advance one additional step: the circuit controlling the "light-on" condition shall remain closed, while a second set of contacts will cause the lamp pulse rate to alter to the second preset rate. Like responses will take place for the third energizing signal actuation. At the fourth control signal input the system-on circuit shall be broken and the entire system, except for the receiver, shall be shut off. Figure 22 shows a block diagram of this configuration.

VI.E. Light Collector Design

The image size requirements and shape of the transmitted beam dictate the use of a source collector which appears as an 18-inch circular plate with a beam divergence of 80°. There are four basic types of collectors which can be used to affect such characteristics:

a) Paraboloid

b) Spherical

c) Conical

d) Lambertian

Figure 22

Block diagram of site communications system.

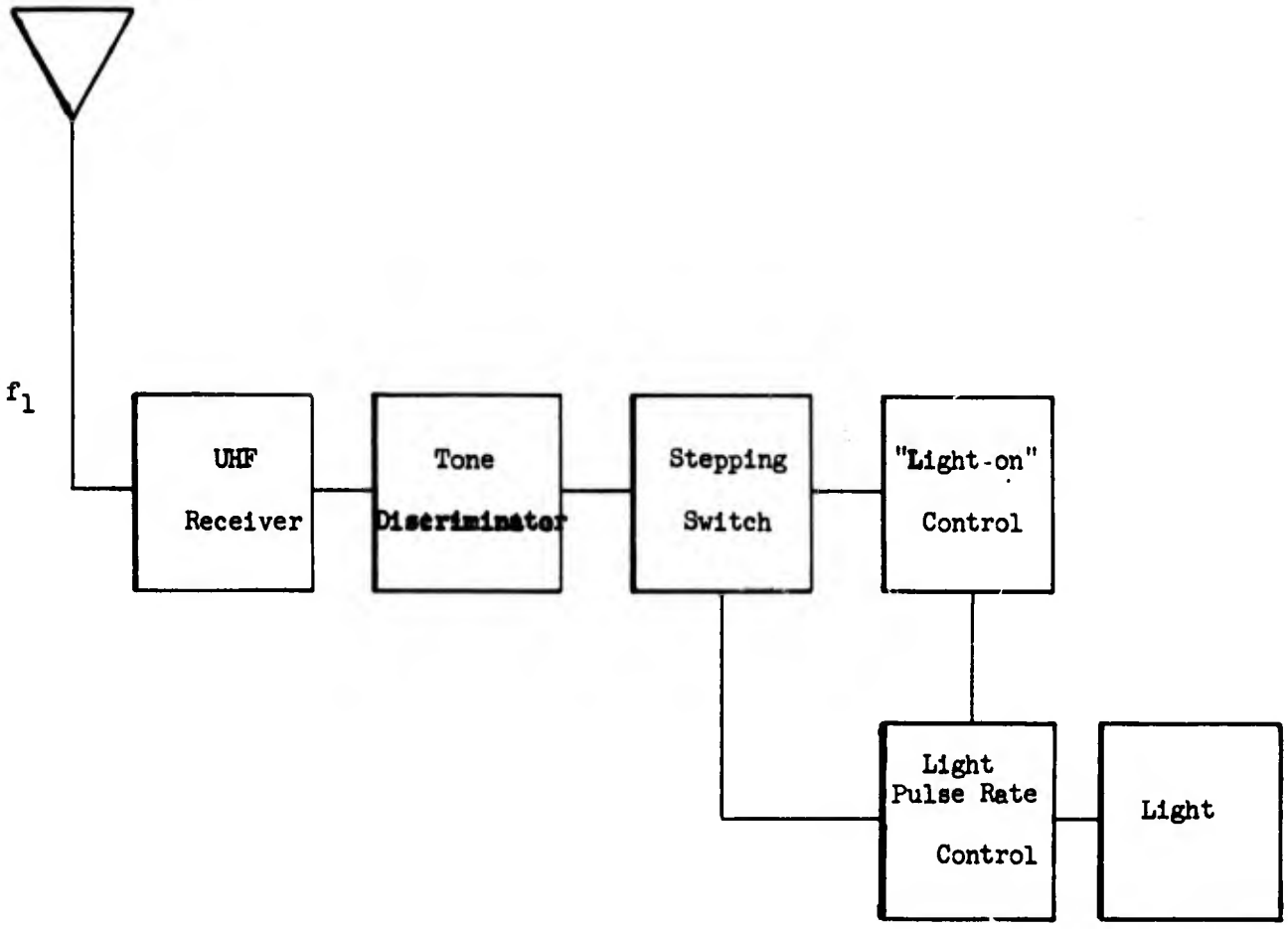

Block Diagram - Light Site

The standard configuration for search-light collectors is a paraboloid of revolution. With a light source at the focus of the paraboloid a virtually parallel beam of light is produced. For the present application however, the beam is not required to be parallel, but rather to diverge with a half-angle of 40°. To produce this beam divergence, a paraboloidal collector could be used if the light source were placed ahead of, or behind the focal point. This would result in an 80° (full angle) spread but there would be a large area in the center of the beam with no illumination (≈ 50 degrees). This is true for both directions defocusing. As a consequence of this absence of illumination, parabolic collectors cannot be used on this program.

An elliptical or spherical collector might also be used to achieve an 80° beam. The problems with this configuration are the presence of a light void in the center of the beam and the lack of an effective 18-inch circular image. For these reasons such a collector would not be desirable.

A third alternative would be the use of a Lambertian emitter. In this configuration a diffuse plate is edge lighted by the source and a Lambertian ($\cos\theta$) intensity distribution results. The major problem which exists here is the relatively low efficiency of the device. Since the Lambertian distribution is spherical (in spherical coordinates) energy is emitted in all directions as viewed from a hemisphere. Thus, if the emitter is shielded so at to produce an 80° cone of radiation a large amount of the energy is lost. The energy which is retained in the 80° cone can be written

$$E = \overline{I(\theta)} \sum_{0}^{\theta} (1 - \cos\theta) \tag{71}$$

where $\overline{I(\theta)} = \bar{I} \cos\theta$, and θ is the angle off the normal. For $\theta = 40^{\circ}$,

$E = 0.413\ E_o$, E_o being the lamp output energy.

A conical, specular reflector appears to be the most desirable configuration for use in this experiment. The reflector consists of an 18-inch diameter 21.5 inch high cone with the lamp at the apex of the cone. The overall efficiency of this collector is 94.6 percent.

VI.F. Pulse Circuitry

The typical xenon flash tube may be considered as a device having a very high impedance until the applied voltage across the tube exceeds a certain value called the self-flash voltage. When this voltage is exceeded, the lamp resistance changes abruptly to a very low value. When the lamp is conducting, the dynamic lamp impedance is determined primarily by lamp geometry, as follows:

$$R = \frac{\rho \ell}{\pi r^2} \tag{72}$$

where:

R = lamp resistance in ohms

ρ = specific resistivity of the ionized gas column, in ohm-centimeters

ℓ = length of gas column between the electrodes in centimeters

r = internal lamp radius in centimeters

The gas column resistivity, ρ, most important of the lamp electrical characteristics, is affected to varying degrees by a variety of lamp parameters. The internal lamp radius and the instantaneous current density in the lamp can critically affect specific resistivity. Smaller effects in R may be made by changes in gas pressure and gas composition. The resistivity

of flash tubes varies considerably with initial voltage gradients, energy input, configuration, and amount of optical damping. Generally it is lowest for a straight flash tube of a large bore used with higher voltage gradients and energy loadings. It is highest for tightly wound, multi-turn helixes of small bore tubing, at low voltage gradients and energy loadings.

Another important lamp characteristic related to pulse circuit design is the deionization time of the lamp plasma. When the current to a flash lamp is interrupted, the lamp requires a finite period to deionize. Electrons are transmitting rapidly to the anode and the ionic drift to the cathode does not balance the space charge at each point along the axis of the lamp. If a pulse is interrupted for so short a period that no appreciable deionization can occur the impedance at turn-on will remain essentially unchanged. Conversely, if the interruption is for a long enough period to allow complete ion diffusion and recombination, a complete reignition cycle must occur and the lamp exhibits the same impedance variations experienced at initial turn-on.

The importance of the deionization characteristic in circuit design is apparent, particularly where high pulse repetition rates are desired.

For peak current densities of 100 amps to 4,000 amps/cm^2, a value of ρ = .01 to .015 ohm centimeters is typical. In practice, the lamp impedance is measured experimentally where precise measurement of resistance is required. This is necessary primarily because lamp manufacturers do not generally hold lamp geometry to the precision tolerances required for accurate analytical determination of dynamic impedance due to the high production costs involved.

Variance in the lamp dynamic impedance from specific design parameters affects both lamp life and electrical conversion efficiency. It is the most important characteristic for consideration in the design of the electrical circuitry for the following reasons:

1) Variations in lamp impedance result in variations in the power applied to the lamp and possible overdriving, which is the major factor in reducing lamp life.

2) Pulsing networks for the lamps are designed for optimum efficiency by critical impedance matching to the lamp. Variations of lamp impedance results in mismatched circuitry and subsequent power loss in order to maintain a given output.

VI.F.1. General Design of Pulsing Circuitry

Generally, the pulsing circuitry is capable of storing DC energy, and applying this energy to the lamp in a characteristic form and at a rate required for maximum utilization of the lamp output and life. The ideal electrical circuit for exciting the flash lamp has lumped inductances and capacitance to ensure smooth current pulses.

Energy storage for flash lamps usually takes the form of a pulse forming network consisting of one or more sections of a lumped constant transmission line in which the characteristic impedance of the line is designed to match the lamp load. The desired pulse shape, repetition rate, and pulse energy may be derived analytically once the lamp load is known subject to the following limitations:

1) Operation with less than a critical value of inductance will

shorten lamp life and increase the danger of lamp failure from the acoustic shock waves associated with rapidly rising current pulses.

2) Operation at higher than recommended pulse energy will reduce lamp life.

3) Large extraneous inductances can result in magnetic plasma pressures which drive the natural mechanical resonances of the quartz tubing and result in eventual failure of the lamp.

4) Specific values of inductance are required to allow the conductivity at the electrode plasma boundary to rise to maximum before full voltage develops across the tube.

The basic advantages of using a pulse forming network are:

1) Relatively high efficiency is inherent since current limiting is accomplished with low resistance inductance.

2) Adjustment of the characteristic impedance is possible to reduce lamp deionization time.

A basic electrical functional diagram is shown in Figure 23 for this application.

The DC-DC converter transforms the comparatively low primary power supply voltage into the required pulse voltage and self-flash trigger voltage. The pulse forming network establishes the pulse width, pulse period and pulse shape. The high voltage trigger applies the required self-flash voltage to the lamp for each pulse or sequence of pulses as desired.

Figure 23

Block diagram of pulse circuitry

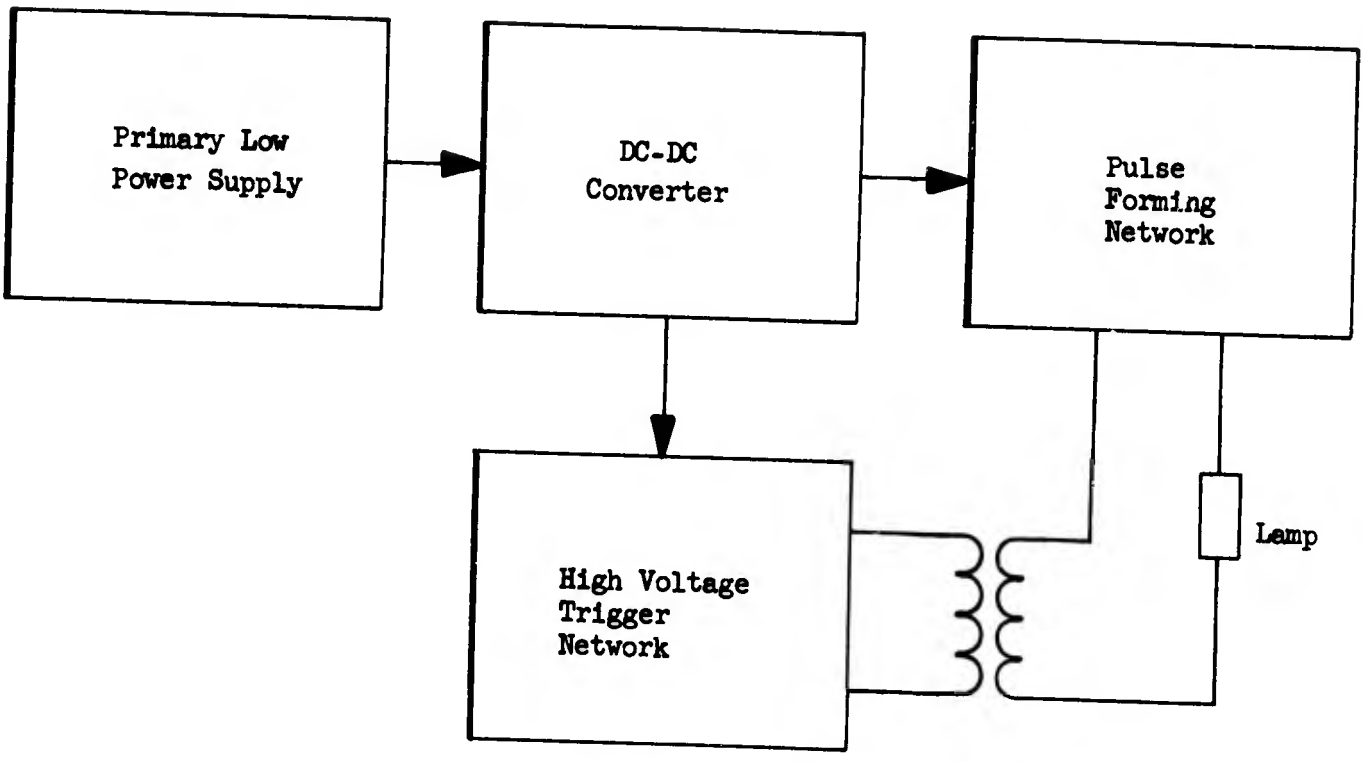

VI.F.1.a. Control and Firing Circuits

1. Resonant Charging

In applications requiring efficient power transfer into the pulse forming network, resonant charging may be considered.

In Figure 24 consider the inductance, L, and the total capacitance, C, of the pulse forming network as a resonant circuit. The resonant frequency, f_o, will be

$$f_o = \frac{1}{2\pi\sqrt{LC}} \tag{73}$$

and the peak voltage appearing across the capacitor will be $2V_o$. The time for the voltage across C to reach a maximum is half the period or $T/2 = \pi\sqrt{LC}$. If L is chosen so that T/2 is less than the desired lamp pulse repetition frequency, the pulse forming network will be charged to $2V_o$ and D_1 will hold this voltage until the stored energy is discharged through the lamp.

2. Lamp Triggering

A convenient trigger design for lamps is illustrated in Figure 25. The trigger transformer, T, has a turn ratio of approximately 3 to 36 with a secondary winding sufficiently heavy to carry the lamp current. Capacitor C_2 is charged and then discharged through the primary of T by spark gap, SG-1. The charging voltage on C_2 is chosen to insure that the positive lamp terminal is raised sufficiently above the lamp self-flash voltage, and the energy stored in C_2 is chosen to insure that the core of transformer T, will be saturated by the trigger pulse. The secondary winding of T, will then present a negligible inductance to the main energy

Figure 24

Pulse forming network

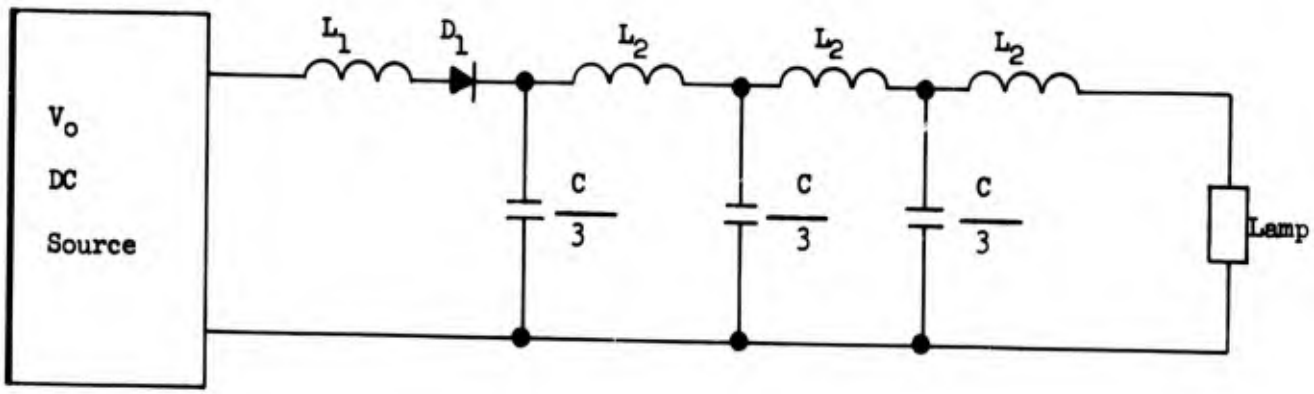

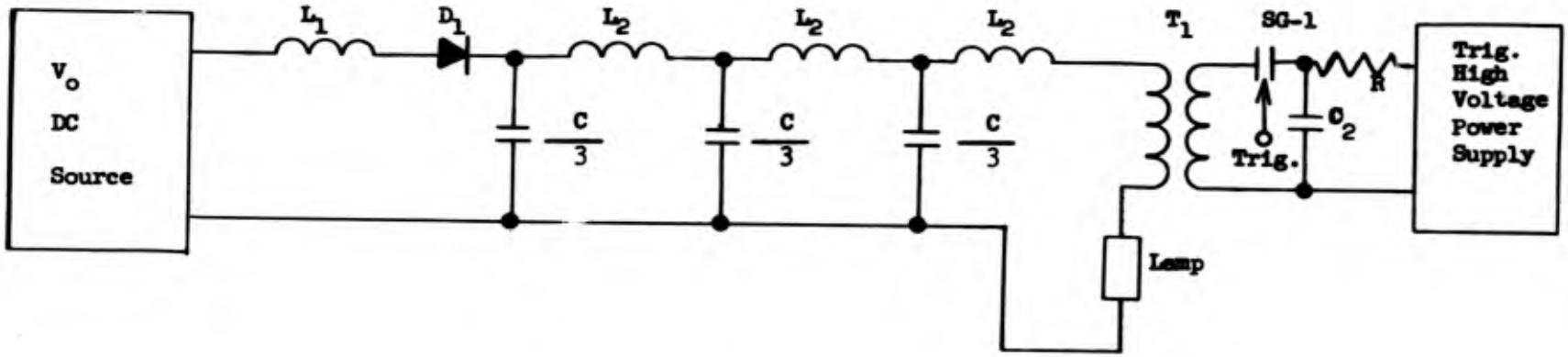

Figure 25

Pulse forming network

pulse. The last inductive section of the network presents a high impedance to the fast rising trigger pulse.

3. Operation with Low Current "Keep-Alive"

Figure 26 illustrates a basically different mode of operation. A low current DC discharge is initially established through the lamp from the "Keep-Alive" high voltage supply, and is maintained at all times during operation. This current is limited by R_1 to a low value, usually less than 20 ma. During the charging cycle, spark gap SG-1 is not conducting. L-3 presents a high impedance to the main current pulse when SG-1 is triggered.

4. High Pulse Repetition Rate

When using the circuit described in Figure 25, the upper limit pulse repetition frequency will be continuous lamp conduction. This will vary over rather wide limits and is heavily dependent on the specific circuit parameters in the pulse forming network. Continuous lamp conduction occurs when residual ionization in the lamp is sufficient to keep lamp impedance at a low value until the charge voltage on the pulse forming network reaches a value equal to the voltage required to maintain a continuous arc.

Substantial improvements in maximum pulse repetition rate may be realized in the following ways:

a. If the characteristic impedance of the network is adjusted such that the current pulse through the lamp is slightly under-clamped, the current will pass through zero more than once

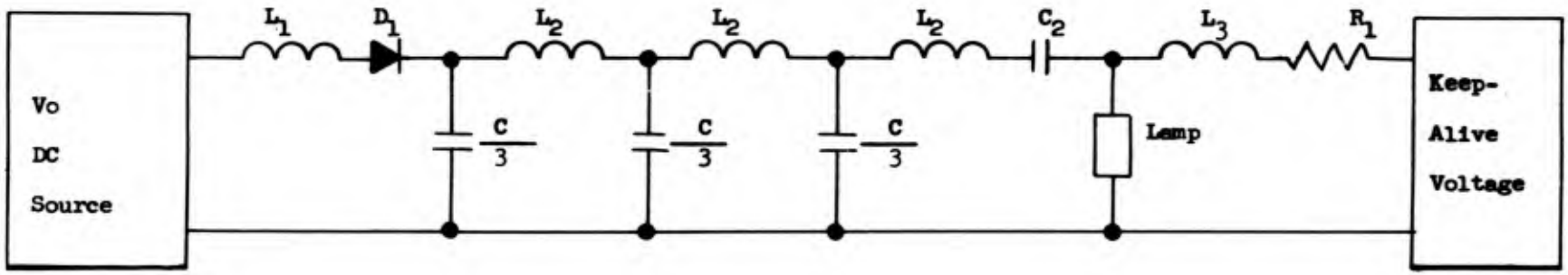

Figure 26

Lamp triggering circuitry

thus reducing the lamp deionization time.

b. Operation of the lamp at less than its rated average power will reduce lamp temperature and thus reduce deionization time.

c. The pulse rate may be increased by adjusting the pulse duration to a minimum consistent with lamp ratings, and adjusting the charging time constant to a maximum consistent with the desired pulse rate.

d. A two electrode spark gap may be inserted between the positive lamp terminal and secondary winding of T in Figure 25. The extinction of the spark gap will be much shorter than the lamp.

e. A high average power Thyratron or Ignitron may be inserted between the voltage source V_o and the charging inductor L_1. The trigger pulse to the Thyratron is then synchronized with the SG-1 trigger pulse and thus delays the recharge cycle until lamp extinction has occured.

5. Injection Triggering

Another approach to excitation of the flash lamp is shown in Figure 27 where a Thyratron tube and pulse transformer is used for so-called series injection triggering. A separate DC source is connected directly to the lamp through a current limiting high resistance (R_3) and a storage capacitor (C_3). The circuit requires a timing pulse to initiate each lamp pulse cycle. Although this approach is generally more economical for lamp triggering, it has the serious disadvantage of inefficiency and is very unreliable when compared to a pulse forming

Figure 27

Thyratron trigger circuit

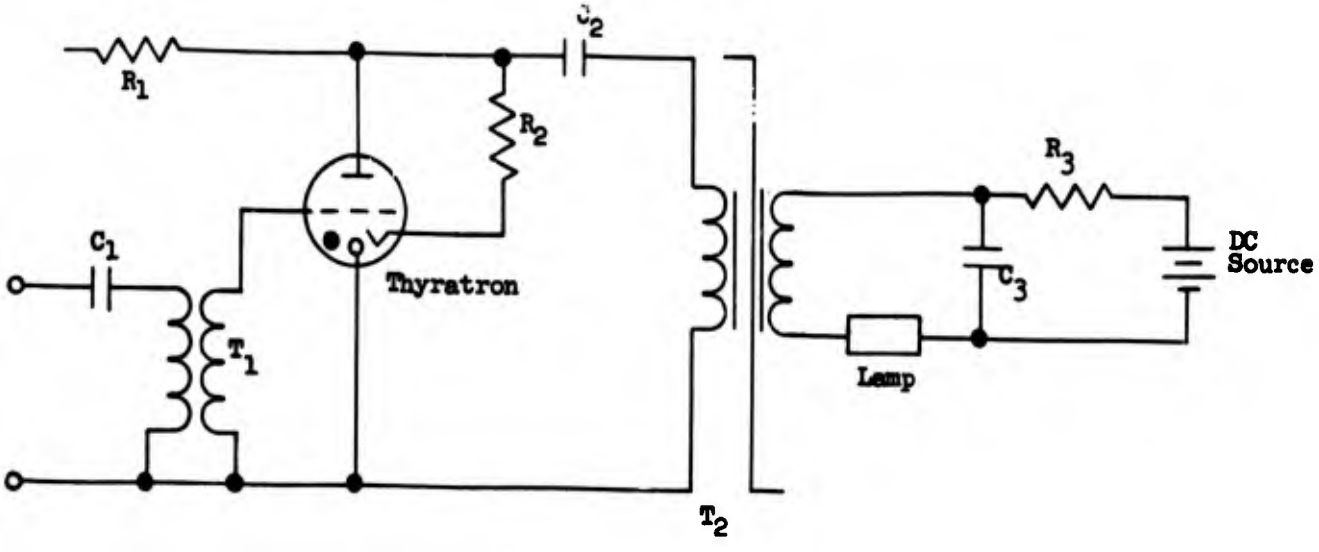

network. Additionally, a separate pulse generator and pulse shaping network is required.

VI.F.1.b. DC - DC Converter Design

The most simple and efficient power converters usually contain two power transistors and a special transformer so connected that a regenerative switching action exists between the two transistors. The transformer, a vital part of the system, has a core material with a hysteresis curve approaching a square loop. The output is almost a perfect square wave, and, when rectified, the resultant voltage contains very little ripple (typically less than 4% at rated load).

The basic circuit for a converter is shown in Figure 28. Its output is magnetically coupled to its input through a square core transformer which has a characteristic hysteresis curve as shown in Figure 29.

To begin the explanation of its operation assume that the circuit is oscillating. If transistor Q_1 is conducting, the supply voltage is dropped across the transformer primary, N_1, and the rate of flux is linear as indicated by the equation

$$\frac{d\theta}{dt} = \frac{V_{cc}}{10^8 N_1} \qquad (74)$$

(Eq. (74) ignores the saturation voltage of the transistor and the resistive drop in N_1 in order to simplify the explanation.) The changing flux in the core induces a voltage in the other coils with polarity as shown by the dots, and magnitude proportional to the turns ratio. Therefore, transistor Q_1 is biased ON with a negative base voltage and transistor Q_2 is

Figure 28

DC-DC Converter

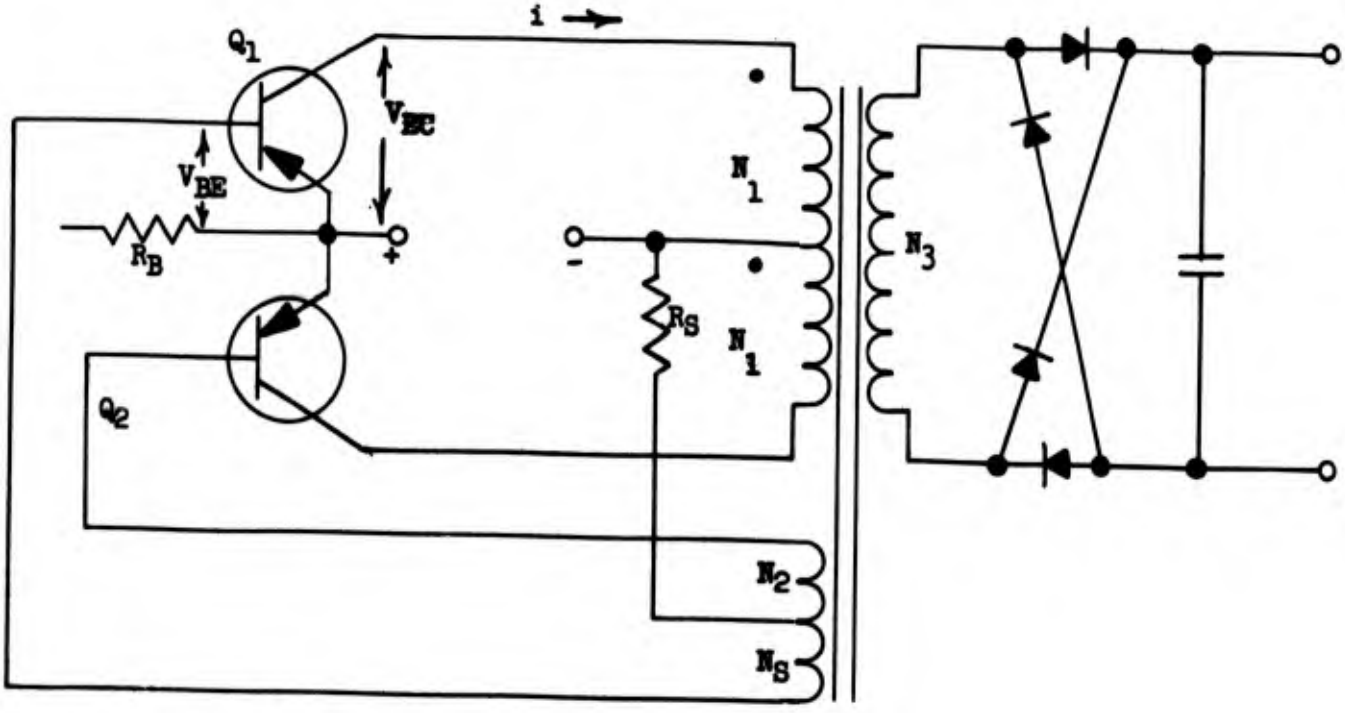

Figure 29

Hysteresis curve of transformer

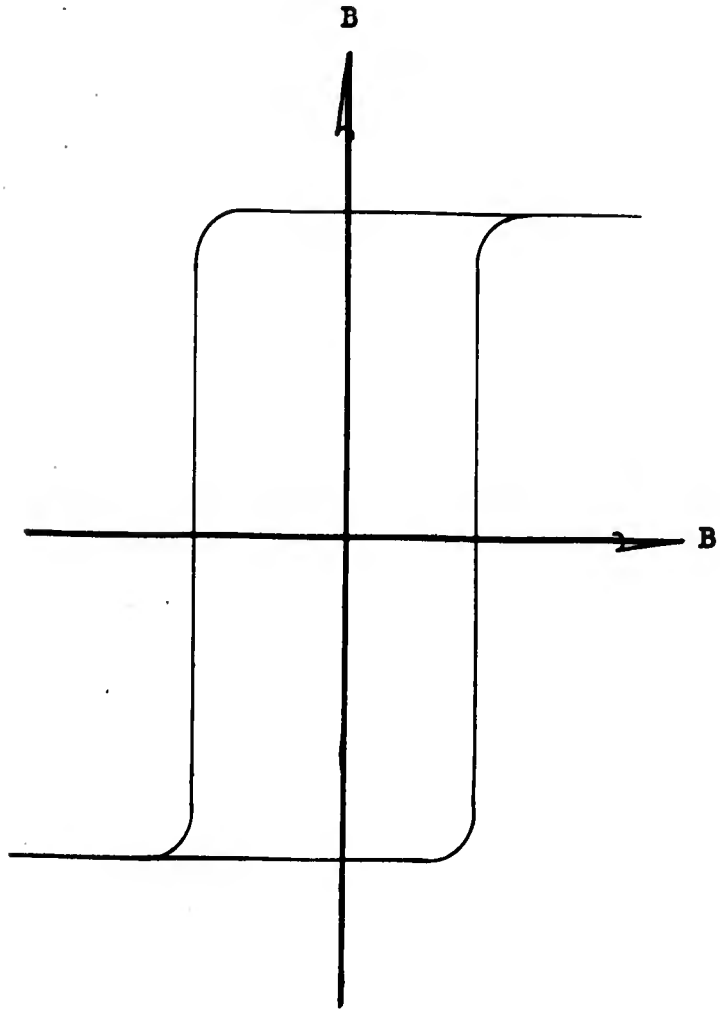

OFF with a positive voltage. Curves B and D of Figure 30 show the collector and base voltages of transistor Q_1. Curve C shows that flux change is linear as indicated by Eq. (74). When the core approaches saturation the induced voltages are reduced, and the base drive is therefore reduced. Since transistor Q_1 is turning OFF, the induced voltage across N_1 is reversed. This causes a reversal of bias, and transistor Q_2 is turned ON as transistor Q_1 is turned OFF. The cycle then continues. It should be noted from Figure 28 that when transistor Q_1 is conducting N_1 of transistor Q_2 has an induced voltage of such polarity as to add to the supply voltage. Therefore, twice the supply voltage appears across each transistor during its OFF time.

The current waveform of the inverter can be explained by the transformer equivalent circuit as given in Figure 31. This is an approximate equivalent of Figure 28 as seen from the input terminals, where R_1 is the effective primary resistance and R_2 is the effective secondary and load resistance referred to the primary. Depending on the sum of R_1 and R_2 the current will rise instantly, as shown by curve A of Figure 30. Then, by the equation

$$\frac{di}{dt} = \frac{V}{L} \tag{75}$$

the current will increase at a constant rate. The current spike at the end of the waveform is due to core saturation since the inductance approaches zero. The current will tend to rise to a vlue governed by the current gain of the transistor.

The basic equation describing converter operation as derived from Eq. (74) is:

$$V = 4B_m f N_1 SA \cdot 10^{-8} \tag{76}$$

Figure 30

Circuit voltage and current waveforms

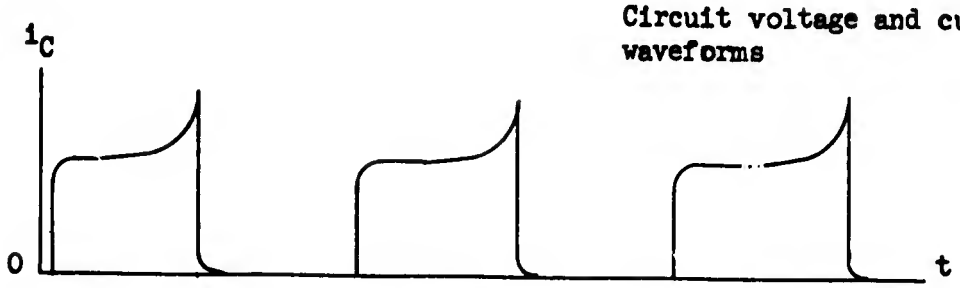

30-A

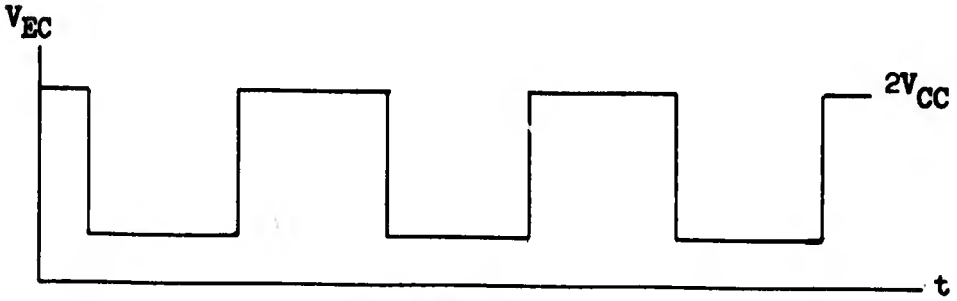

30-B

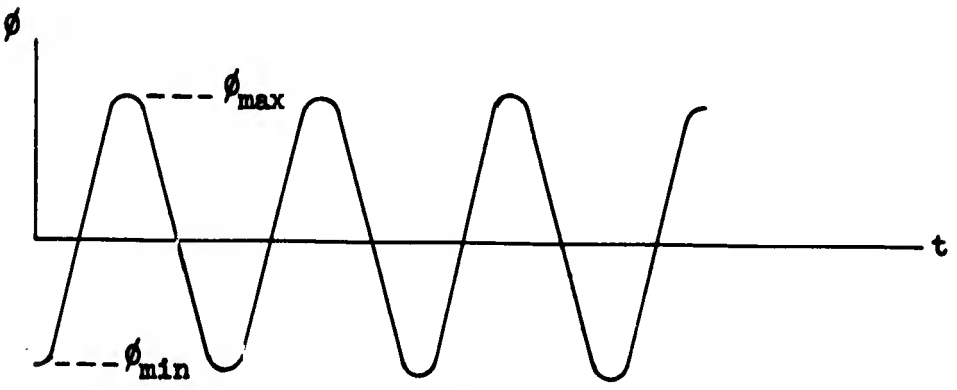

30-C

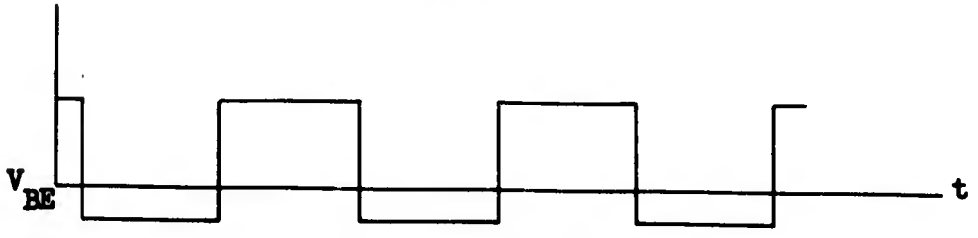

30-D

Figure 31

Transformer equivalent circuit

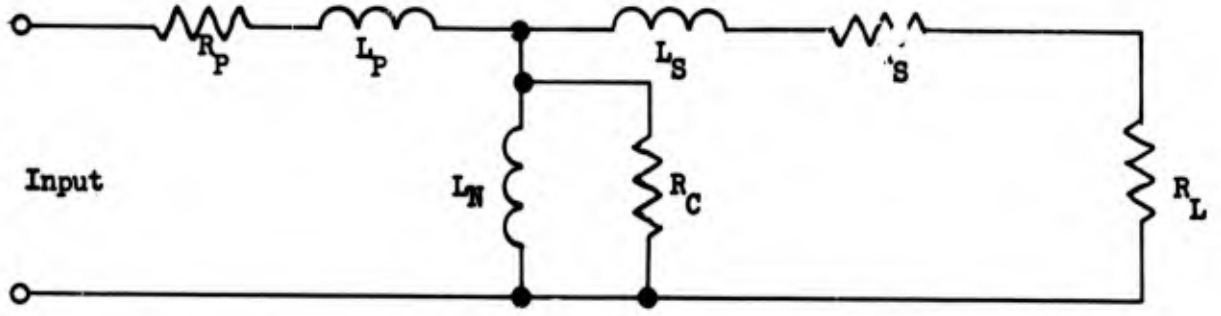

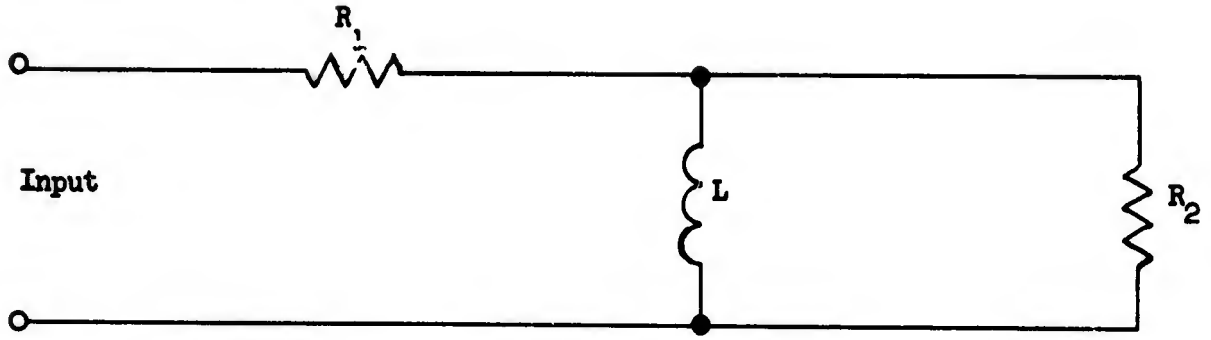

where:

V = peak square wave voltage

B_m = maximum flux density of saturating core

S = stocking factor of core

A = cross-sectional area of the core

It becomes apparent that in the basic converter, i.e., the single-transformer configuration, the transformer performs two functions. It performs the standard function of transformation of power and determines the frequency of oscillation as well. The function of the transistors is simply to switch the DC supply from one-half of the center-tapped primary to the other, thus permitting the resulting square-wave AC voltage to be transformed to the secondary.

The design of the transformer involves the same considerations as that of a standard transformer with respect to amount and type of insulation, wire size, and window area necessary for windings. Eq. (76) is of fundamental importance in determining the relationship among the core size, frequency, and supply voltage.

The transistors for a particular converter must satisfy two basic requirements. They should have a useful h_{FE} at a current level determined by the maximum value of the primary load current, and they must be capable of withstanding the maximum voltage applied to the collector-to-emitter terminals. As previously mentioned, this voltage will be approximately twice the supply voltage (if no voltage spikes are present), and will appear across the OFF transistor terminals. Generally speaking, it is best to limit this maximum

collector-emitter voltage to less than the BV_{CES} rating of the transistor.

The most common type of starting circuit is the resistive voltage-divider type such as shown in Figure 28. A slight forward bias is applied to both transistors through the starting resistor R_S. The required magnitude of R_S is primarily a function of the load and the h_{FE} of the transistors. The worst case for starting will occur with heavy loads and at low temperatures, where h_{FE} is minimum. A filter capacitor on the secondary requires a heavy surge of current during starting as it charges up. Because this initial heavy load can make starting difficult, filter capacitors should be as small as possible.

The value of starting resistance is generally best determined by trial and error, but an approximate value can be determined from

$$V_1 = \frac{V_{cc} R_B}{R_S + R_B} \tag{77}$$

where $V_1 \approx 0.3$ for germanium transistors, and ≈ 0.5 for silicon transistors.

To reduce losses, a diode can be used instead of R_B, being placed such that base current flows in the forward direction. The value of R_S can be increased since the diode appears as an open circuit until the oscillations begin.

The most frequently used circuits are the common-emitter configuration shown in Figure 28 and the common-collector autotransformer configuration shown in Figure 32.

The common-collector autotransformer configuration has an advantage over

Figure 32

Common collector auto transformer configuration

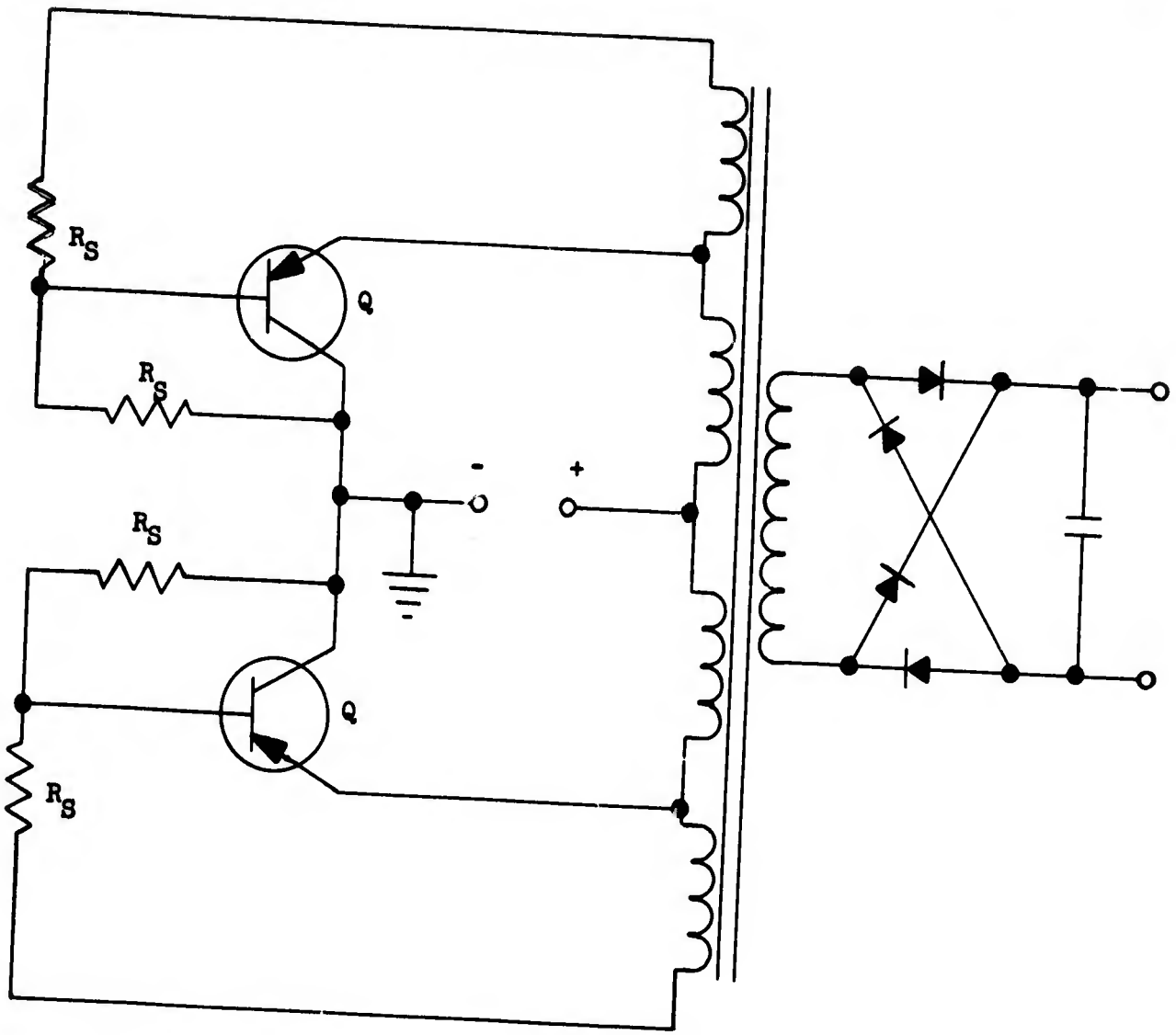

the common-emitter configuration: transistors can be mounted directly on a common heat sink without using insulating washers. A disadvantage is the need for additional base and starting resistors.

The dual-transformer configuration shown in Figure 33 has many advantages over the single-transformer configuration. A comparison of the typical collector currents of both configurations at no load and full load, illustrated in Figures 34 and 35 reveals one of them: since the output transformer of the two-transformer configuration does not saturate its magnetizing current is never large.

In the single-transformer converter, once the transformer saturates, the collector current increases until it tends to exceed $h_{FE}\ I_B$, i.e., pulls the ON transistor out of saturation. Conservative design is usually based upon the minimum value of h_{FE}, i.e.,

$$I_L' \leq h_{FE}\ (\min)\ I_B \tag{78}$$

where I_L' = maximum load current reflected to the primary. Since many transistors exhibit a 3:1 h_{FE} spread, it would be possible for the actual peak collector current to be three times greater than the maximum reflected load current in those transistors with a high h_{FE}.

The dual transformer configuration differs from the conventional converter in that switching is determined by the small saturating tape-wound toroidal transformer, while the larger nonsaturating power transformer handles the feedback and output power transformation. Since the output transformer does not saturate, switching is not determined by the increasing magnetizing

Figure 33

Dual transformer
power converter

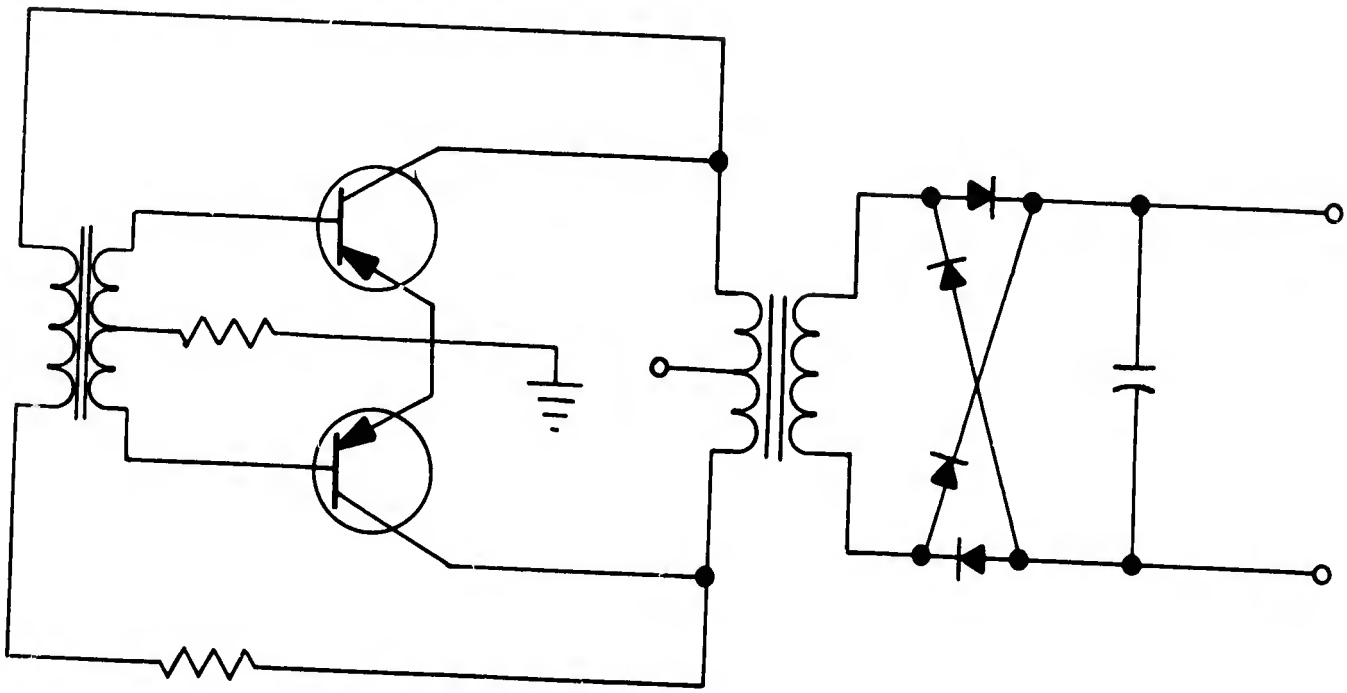

Figure 34

Collector current of single transformer circuit

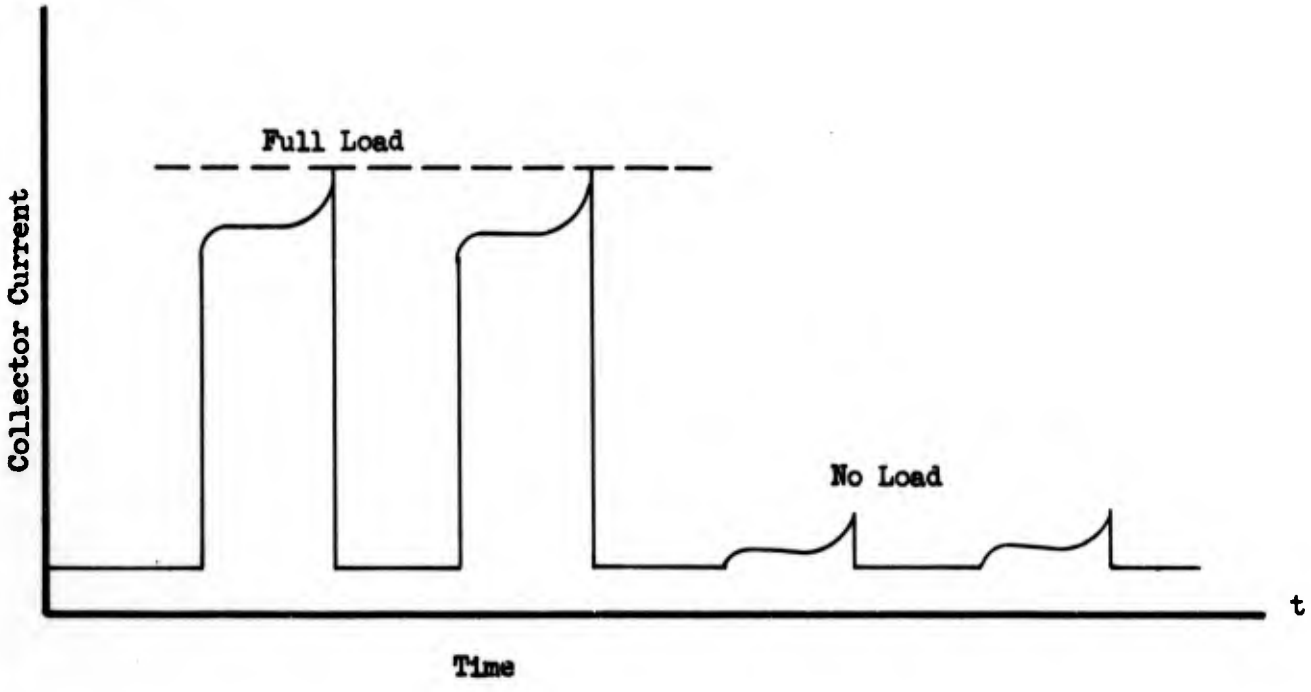

Figure 35

Collector current of V_{Dual} transformer circuit

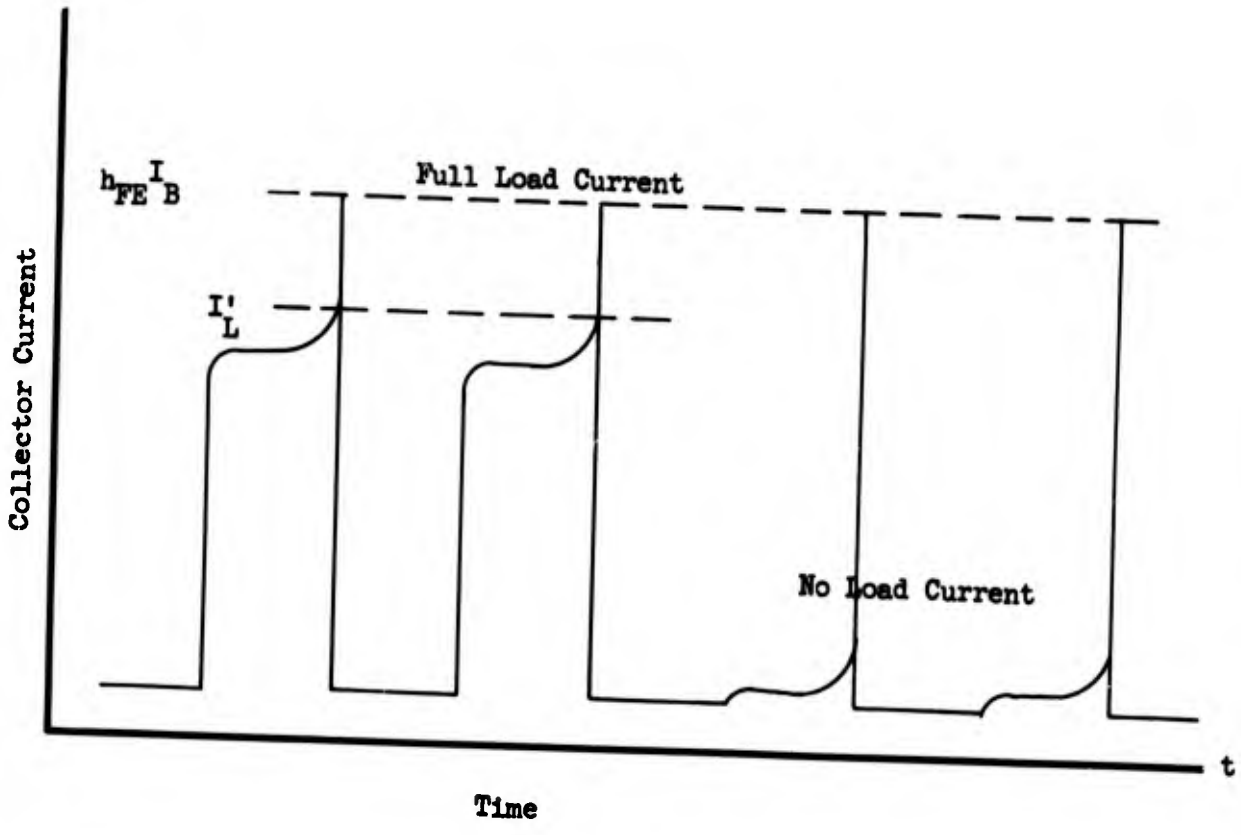

current pulling the ON transistor out of saturation. Instead, the ON transistor is pulled out of saturation by the decrease in base current which occurs when the toroidal transformer saturates. As the core reaches saturation, the increasing magnetizing current causes an additional voltage drop across the feed back resistor R_F. Thus the primary of the saturated transformer has less voltage dropped across it, affecting the decrease in secondary or base-drive voltage.

VI.G. Prime Power Supply

To meet the contractual requirements of being self-sustaining the light fixtures must utilize batteries for prime power. It is suggested that rechargable batteries be used in conjunction with a thirty-day maintenance cycle, i.e., the batteries should be recharged. The units could be totally self-sustaining by using solar panels for the recharging function on a daily basis; however, these would involve a great deal of cost.

The major dry cell battery studied was the ammonium chloride (NH_4Cl) in water electrolyte system utilizing a carbon rod (inactive electrode) and zinc container (active electrode). Although this battery is relatively inexpensive, the system has some inhibiting factors: the terminal emf of a dry cell is on open circuit is approximately 1.5 volts. Further, the dry cell is restricted to a single cycle, inasmuch as the NH_4Cl is disassociated forming NH_4OH and HCl which renders $HCl + Zn \rightarrow ZnCl$ resulting in the perforation of the zinc container. The electrolyte then leaks out of the container and the cell ceases to function.

In surveying the wet charge batteries, the lead-cell, nickel-iron cell and the nickel cadmium cell batteries were investigated.

The lead-cell battery utilizes electrodes of lead peroxide (P_bO_2) and sponge lead (Pb) with an electrolyte of sulfuric acid (H_2SO_4).

It is possible for sulphation to take place, i.e., there are two states of $PbSO_4$ one of which is caused by chemical precipitation and is non-conducting. Discharging such a battery causes this type of sulphation, so it is important that frequent charging maintenance be performed.

The normal cycle life of this type of battery when properly used is approximately 600 cycles. This type of battery can be left standing idle in a charged condition for an average of three months depending on the temperature and design of the battery. Evaporation of the electrolyte should, however, be considered.

The nickel-cadmium (NiCd) the nickel-iron (NiFe) type batteries, utilize nickel dioxide (NiO_2) as the positive plate and either iron or cadmium as the negative plate. The electrolyte for this battery is potassium hydroxide (KOH). Where the lead-cell batteries are often called the lead acid batteries, the nickel-iron cell battery are sometimes called the nickel-base battery.

It is interesting to note that there is no lower limit to the voltage of either NiCd or NiFe batteries since there is nothing equivalent to the sulphation of the lead-cell type battery. Discharge however, cannot be continued below a useful lower limit.

The chief disadvantages of the NiCd and NiFe batteries are their comparative high cost, low efficiency and high internal resistance. Figure 36 shows the relative charge and discharge curves for both lead-acid and NiCd/NiFe batteries.

On the basis of cost and efficiency the lead-acid battery is chosen in preference to the NiCd/NiFe batteries. Table VI-1 gives the basic parameters for some typical lead-acid batteries.

AMPERE-HOUR (20-Hr. Rate)	Weight Cell	Volt Cell	Shelf Life Wet	Shelf Life Dry	Max. Temp.	Cycle Life	Price Cell	Size
50	6.6#	2	3 mo.	5 yr.	150°F	600	$2.88	1.75" x
70	7.0#	2	3 mo.	5 yr.	150°F	600	$4.16	6.875"x
80	7.7#	2	3 mo.	5 yr.	150°F	600	$4.47	9"
130	13.6#	2	3 mo.	5 yr.	150°F	600	$6.86	3.125"x
150	14.3#	2	3 mo.	5 yr.	150°F	600	$7.41	7" x 9"
170	15.0#	2	3 mo.	5 yr.	150°F	600	$7.99	

Table VI-1

Figure 36

Charge and discharge curves of a lead cell and an Edison cell.
c = charge; d = discharge.

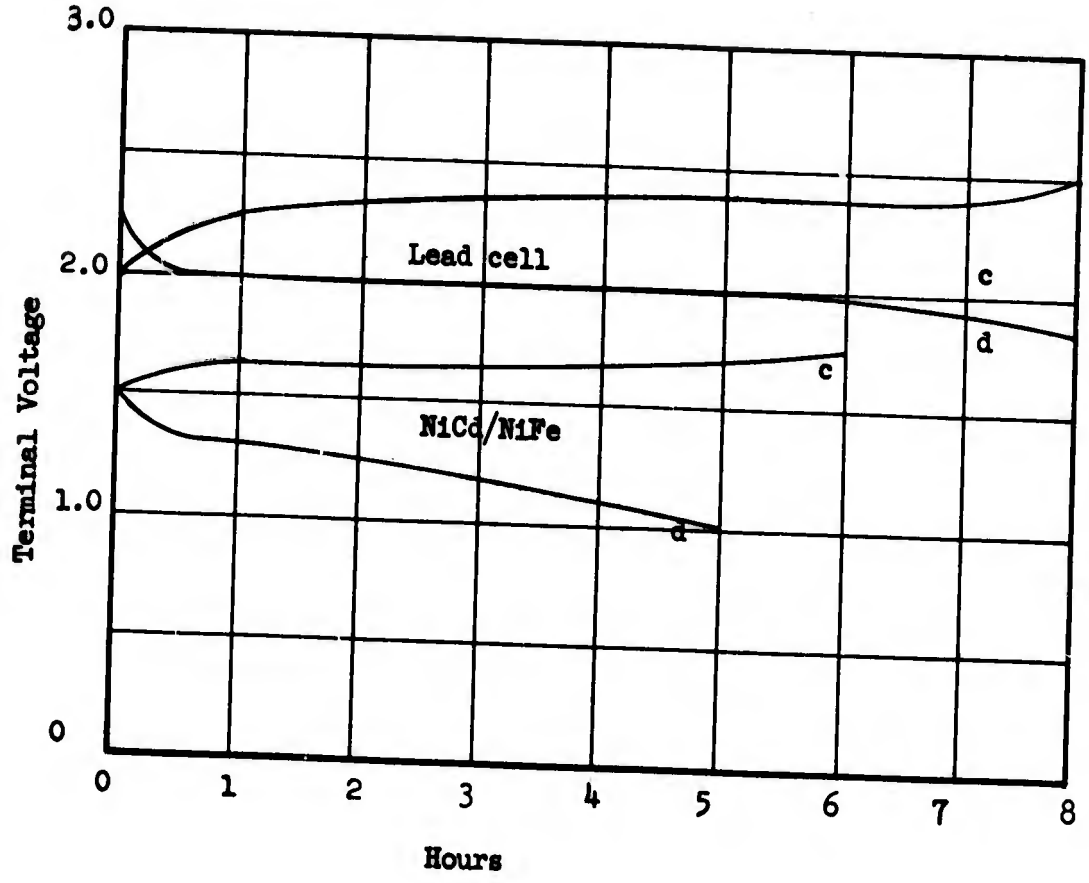

VII. CONCLUDING REMARKS

It has been found that it is feasible to design a photogrammetric test range for the spatial calibration of aerial cameras to accuracies of three microns at the film plane. It is pointed out however, that such accuracies can only be achieved if an active test range (ground-based lights) is used. Atmospheric conditions are such that a passive, or airborne light fixture will not meet the system specifications.

The system which was conceptually designed utilizes a variable pulse repetition frequency, helical, xenon flash lamp as a source with an output energy of approximately 2.5 joules. This lamp is coupled to a conical reflector giving rise to an 80° beam which covers the complete range at 100,000 feet altitude.

The ground-based fixture is remotely controlled by the aircraft, or a ground-based transmitter operating through a UHF relay station. Remote control of system turn-on, turn-off, and variation in pulse rate can be accomplished.

There is nothing critical in the operation of the system with respect to the types of cameras to be calibrated. The different pulse rates have been chosen to be compatible with all cameras, and the system design is based upon utilization of a variety of factory-stocked films.

It is expected that a test range designed to be consistent with this report will enable the accurate calibration of aerial cameras under a variety of different conditions (altitude, speed of aircraft, and weather).

REFERENCES

Section I

1) Statement of Work, PR I-7-4923, R.A.D.C., 24 February 1967

Section II

1) Chapman, R.M. and Carpenter, R., "Effect of Night Sky Backgrounds on Optical Measurements," Technical Report 61-23-A, Geophysics Corporation of America, May 1961.
2) Davis, J.I., "High Energy Laser Systems Analysis, Semi-annual Report, Hughes Aircraft Company Reference Number A 7910, 31 December 1965.
3) Davis, J.I., "Consideration of Atmospheric Turbulence in Laser Systems Design," Applied Optics, Volume 5, Number 1, pp. 139-47.
4) Elterman, L., "Atmospheric Attenuation Model, 1964, in the Ultraviolet, Visible and Infrared Regions for Altitudes to 50 km," Environmental Research Papers No. 46, AFCRL, 1964.
5) Elterman, L., "Aerosol Measurements in the Troposphere and Stratosphere," Environmental Research Papers No. 253, AFCRL, 1967.
6) Fried, D.L., "Optical Heterodyne Detection of an Atmospherically Distorted Wavefront", Conference on Atmospheric Limitations to Optical Propagation, p. 207, Boulder, Colorado, March 1965.
7) Genoud, R.H., "Intensity Scintillation of Terrestrial Radiation Sources," 6th National IRIS, 7-9 November 1961
8) Goodwin, F.E., paper presented at the conference on Atmospheric Limitations to Optical Propagation, Boulder, Colorado, 17-19 March 1965.

9) Goodwin, F.E., Hughes Research Laboratories, private communication with H. Hodara.

10) Henry, H.E., "Laser Space Communications Study," North American Aviation, Inc., (SID), Report No. SID 65-1084, 1965.

11) Hodara, H., "Laser Wave Propagation through the Atmosphere, Proceedings of the IEEE, Volume 54, Number 3, pp. 374, 375, March 1966.

12) Hogg, D.C., "Effect of the Troposphere on the Propagation of Coherent Optical Waves," Proceedings of the IEEE PT-GAP International Symposium, pp. 102-108, 1965.

13) Hufnagel, R.E., "Understanding the Physics of Seeing Through Turbulent Atmospheres," abstracted from Advanced Range Instrumentation presentation made by Perkin Elmer Corporation at Patrick A.F.B., Florida, 20 November 1963.

14) Lawrence, J.D., Crownfield, F.R., and McCormick, M.P., "Optical Radar Measurements of the Atmosphere," NASA Report CR-729, 1967.

15) Long, R.K. and Boehnker, C.H., "Measured Atmospheric Absorption at Ruby Optical Maser Wavelengths," Ohio State University Report 1641-10, June 1965.

16) Middleton, W.E.K., Vision Through the Atmosphere, University of Toronto Press, 1958.

17) Tatarski, V.I., Wave Propagation in a Turbulent Medium, McGraw-Hill Book Company, Inc., New York, 1961.

Section III

1) Selected Climatic Maps of the United States, U.S. Department of Commerce Report.

Section IV

1) Barkas, W.H., Nuclear Research Emulsions, Academic Press, New York, 1963.

2) Boucher, P.E., Fundamentals of Photography, D. Van Nostrand Company, Inc., New Jersey, 1963.

3) Carroll, J.S., Photo-Lab-Index, Morgan and Morgan, New York, 1962.

4) Kodak Data for Aerial Photography, Kodak Publication No. M-29, 1967.

5) Neblette, C.B., Editor, Photography, D. Van Nostrand, New Jersey, 1962.

Section V

1) Middleton, W.E.K., (Koschmieder), Vision Through the Atmosphere, University of Toronto Press, 1958.

Section VI

1) Alexander, T.A., et.al., "High DC Power Solid State Switch for Pulsing an Arc Lamp," Rev. of Scientific Instruments, Vol. 36, No. 12, 1965.

2) Boume, H.K., Discharge Lamps for Photography and Projection, London, Chapman and Hall, Ltd., 1948.

3) Johnson, H.E., "An Investigation of Waves in a Pulsed Discharge," DDC No. AD 618-683, 1965.

4) Kerns, Q.A., and Cox, G.G., "A Triggered Nanosecond Light Source," Lawrence Radiation Laboratory Report UCRL 9269, 1960.

5) Marshak, I.S., "Stong-Current Pulse Discharges in Gas Used in Pulsed Light Sources", Soviet Physics USPEKHI, Vol. 5, No. 3., 1962.

6) McDaniel, E.W., Collision Phenomena in Ionized Gases, John Wiley and Sons, Inc., New York, 1964.

7) Nowicki, J.R., "New High Power Converter Circuits," Mullard Tech. Pub., Vol. 5, No. 43, 1961.

8) RCA Transistor Manual, Technical Series SC-12, 1966.

General References

1) Livingston, R.G. and Berndsen, C.E., "The Aerial Camera," U.S. Army Engineer Geodesy, Intelligence and Mapping R & D Agency Technical Note 64-1, Wright-Patterson A.F.B., Ohio, 1964.

2) Mannen, M.L., "Photographic Visibility of Light Images on Aerial Film," Final Report for U.S. Army Engineers, Ft. Belvoir, Virginia, 1966.

UNCLASSIFIED

Security Classification

DOCUMENT CONTROL DATA - R & D

(Security classification of title, body of abstract and indexing annotation must be entered when the overall report is classified)

1. ORIGINATING ACTIVITY (Corporate author)

Aerospace Controls Corporation
215 West 131 St.
Los Angeles, CA 90061

2a. REPORT SECURITY CLASSIFICATION

Unclassified

2b. GROUP

3. REPORT TITLE

DESIGN STUDY OF A LIGHT MODULE FOR A PHOTOGRAMMETRIC CAMERA CALIBRATION RANGE

4. DESCRIPTIVE NOTES (Type of report and inclusive dates)

Final Technical Report June 1967 - January 1968

5. AUTHOR(S) (First name, middle initial, last name)

Edward B. Jay

6. REPORT DATE	7a. TOTAL NO. OF PAGES	7b. NO. OF REFS
July 1968	145	35

8a. CONTRACT OR GRANT NO.	9a. ORIGINATOR'S REPORT NUMBER(S)
F30602-67-C-0350	
b. PROJECT NO. 698DB	P-575
c. Task No. 698DB00	9b. OTHER REPORT NO(S) (Any other numbers that may be assigned this report) RADC-TR-68-49

10. DISTRIBUTION STATEMENT

This document is subject to special export controls and each transmittal to foreign governments, foreign nationals or representatives thereto may be made only with prior approval of RADC (EMIRA), GAFB, N.Y. 13440.

11. SUPPLEMENTARY NOTES	12. SPONSORING MILITARY ACTIVITY
PROJECT ENGINEER Frank A. Scarano AC 315 330-4203	Rome Air Development Center (EMIRA) Griffiss Air Force Base, New York 13440

13. ABSTRACT

A design study of a light module for a night photogrammetric camera calibration range was performed. It was determined that a ground-based light could be developed to serve as a near pin-point-size object that would be imaged upon the film of an overflying aerial camera and be measurable to an accuracy of 3 microns r.m.s. Such a light would be installed at each grid point of a camera calibration range at Casa Grande, Arizona, and would provide the DOD with a night capability for camera calibration with an expected improvement in accuracy.

It was determined that the light source would be a low energy (2.5 joule), pulsed, xenon flash lamp with provisions for synchronization, and remote control from either the aircraft or a ground station.

DD FORM 1 NOV 65 1473

UNCLASSIFIED

Security Classification

14. KEY WORDS	LINK A		LINK B		LINK C	
	ROLE	WT	ROLE	WT	ROLE	WT
Aerial Cameras Aerial Camera Calibration Photogrammetry						